Studies on development of novel modified RNAs by use of D-threoninol and their biological application.

(D-threoninol を用いた新規修飾 RNA の開発と、その生体への応用に関する研究)

ITO Hiroshi
伊藤　浩
2012

Table of contents

Chapter 1. General Introduction

1-1 Properties and functions of RNA[1]

Ribonucleic acid, RNA, is a well-known biological molecule transcribed from DNA and it is composed of four types of nucleotides which contain ribose sugar attached with a nucleobase; Adenosine (A), Cytosine (C), Guanine (G) or Uracil (U). Therefore, the chemical structure of RNA is very similar to that of DNA, however, they are completely different in some points (Figure 1-1). The most significant difference is that RNA has hydroxyl groups at 2′-position of sugar ring in ribose. Because of these hydroxyl groups, RNA is very easy to be degraded by hydrolysis than DNA. Namely, RNA is less stable than DNA. In addition, the hydroxyl group of ribose sugar also affects duplex structure.

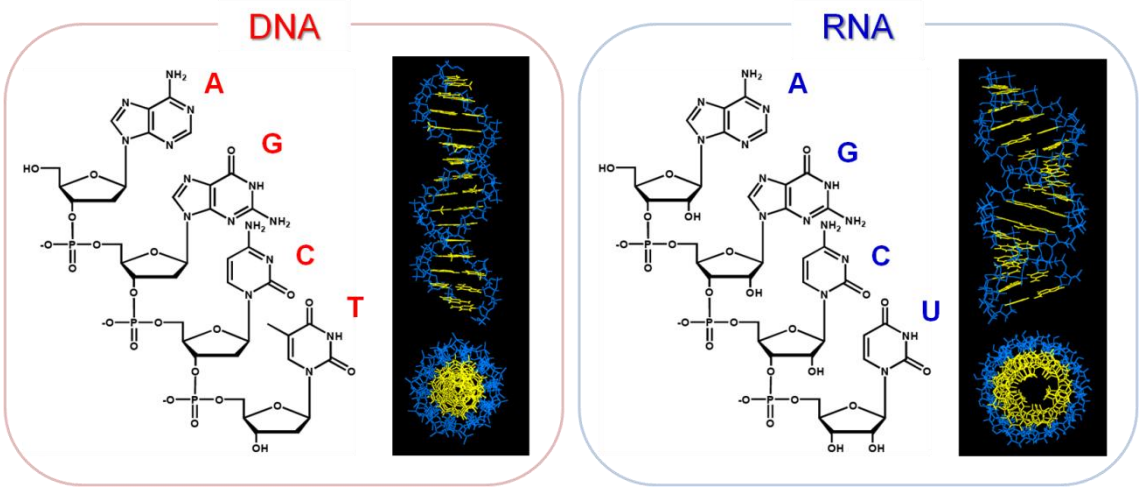

Figure 1-1. The chemical structures and the images of duplex structures of DNA and RNA.

Although most of RNAs existed in organisms are single strand, RNA also forms duplex with complementary strand. However, differed from B-from structure of DNA duplex, RNA forms A-form duplex which has rigid structure compared to B-from duplex. This is because all ribose sugars in RNA duplex hold C2′-endo puckering due to the steric hindrance of hydroxyl group at 2′-position, whereas nucleotides in DNA duplex exhibits C3′-endo sugar puckering. These differences in chemical and structural properties between DNA and RNA are also concerned with the difference in each role in organisms.

Various RNA molecules are involved in several biological functions such as gene expression (Figure 1-2). For instance, like DNA, RNA is also essential for protein synthesis, especially, messenger RNA (mRNA) plays a crucial role as a carrier of genetic information copied from DNA. The information of mRNA forms series of three nucleotides sequences, called codons, and each codon corresponds with a certain amino acid, hence, mRNA is used as a template for translation. In the process of translation, other types of RNA, such as transfer RNA (tRNA) and ribosomal RNA (rRNA), are also very important for protein synthesis. tRNA contains each sort of amino acid and an anticodon sequence which can form base-pair with its complementary codon sequence in mRNA. Thereby, tRNA plays a role of decoding codons in mRNA by using its

anticodon and delivering accurate amino acids to the active center of protein synthesis, called ribosome. rRNA is the main component of ribosome. Numerous proteins associate with several rRNAs to form a large and a small subunit of ribosome which works as the aid of mRNA-tRNA association and the catalyst for protein synthesis. Like these three types of RNAs, each RNA molecule has its own role in several biological processes.

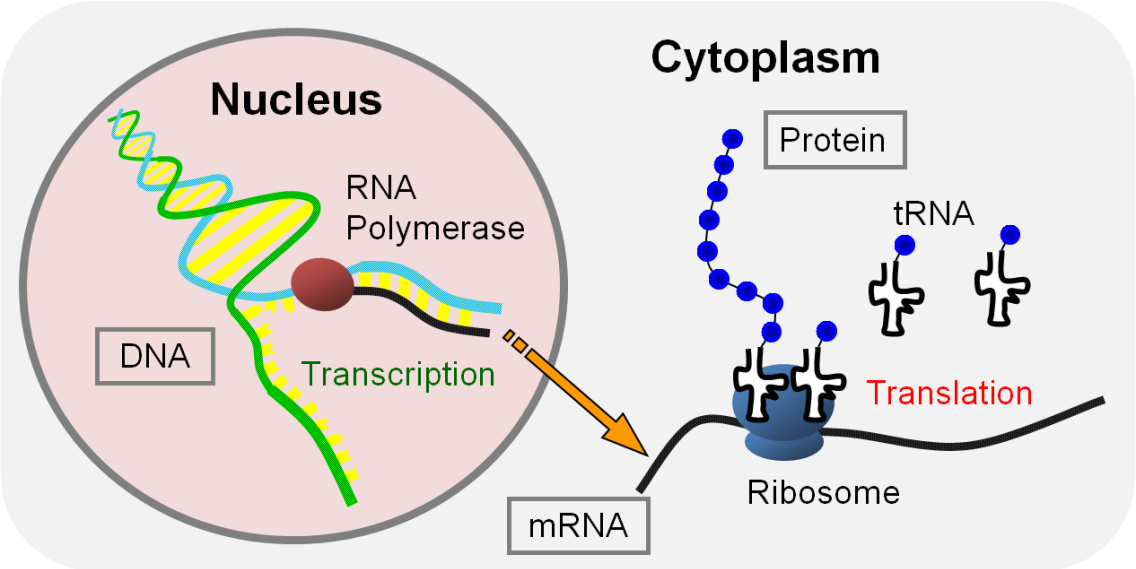

Figure 1-2. Illustration of gene expression involving mRNA, tRNA and ribosome composed of rRNAs.

1-2 Non-coding RNAs and their functions

As described above, both tRNA and rRNA play key roles in translation, however, they are quite different from mRNA because they are not translated to a protein. These RNAs are called non-coding RNA (ncRNA), which can exhibit biological functionality

without translation.[2] Although tRNA and rRNA are the most famous and abundant ncRNA in cells, recently a number of novel ncRNAs were continuously discovered and they received much attention as functional RNAs due to their diverse functions and importance in biological systems.

One of the most important advances in RNA biology is the discovery of ribozyme.[3] Thomas R. Cech and Sidney Altman found out that some RNA molecules can catalyze the cleavage of phosphodiester bonds of RNA chain and these catalytic RNAs were regarded as "RNA enzyme", then named as ribozyme (Figure 1-3). Before the discovery of ribozyme, it had been accepted that only enzymes composed of proteins exhibit catalytic activity in any biological reactions, however, this new finding proved that RNA molecules can not only carry genetic information but also catalyze enzymatic reactions. Hence, the discovery of ribozyme became the trigger of "RNA world hypothesis".[4]

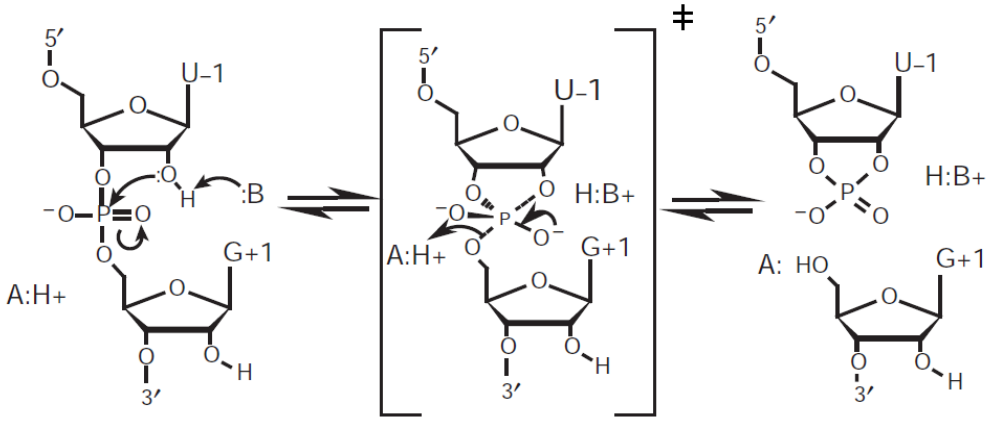

Figure 1-3. Mechanism of the RNA-catalyzed self-cleavage.[3]

Meanwhile, some RNA molecules can regulate gene expression. For example, micro RNA (miRNA), which is a short (approximately 20 nt) single-stranded RNA participates in post-transcriptional regulation.[5, 6] miRNA is initially generated as precursor miRNA (pre-miRNA), which is hairpin RNA with central mismatches, then pre-miRNA is finally processed to mature single-stranded miRNA (Figure 1-4). The mature miRNA is a component of RNA-induced silencing complex (RISC), which can bind target mRNA and inhibit gene expression by using miRNA strand as a "guide" strand.

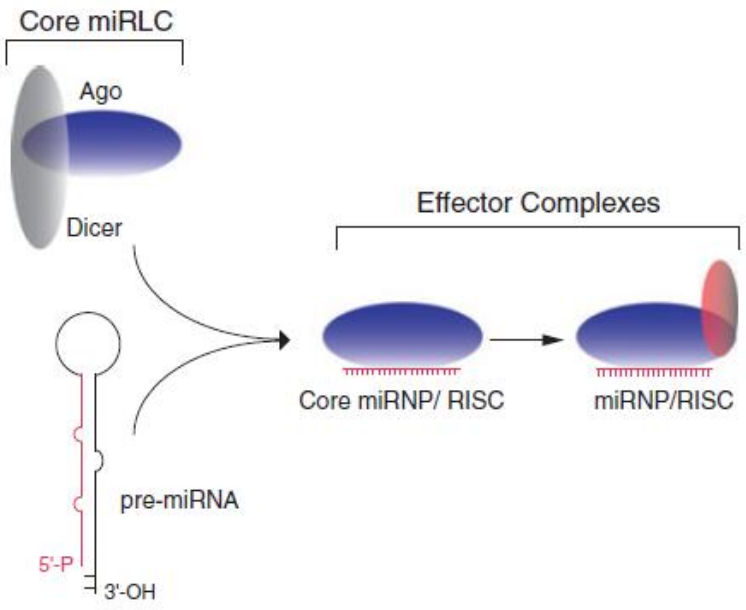

Figure 1-4. Processing of pre-miRNA and formation of RISC with mature miRNA.[5]

On the other hand, small interfering RNA (siRNA) is also a regulator of gene expression.[6, 7] siRNA forms 21-23 nt double-strand and can initiate RNA interference (RNAi); the regulatory system retained in living cells. RNA interference is quite similar

to the miRNA process, however, while RISC with miRNA can only bind target miRNA for inhibition of translation, RNAi can induce the cleavage of target mRNA, thus RNAi is the much more powerful for the regulation of expression.

In this study, we focused on this RNAi and attempted to apply this system to the new biotechnology.

1-3 RNA interference; its mechanism and applications

In 1998, RNAi was discovered by Andrew Fire and Craig C. Mello found out that introduction of a pair of RNA strands; antisense strand (complementary to target mRNA) and sense strand (complementary to antisense strand), could efficiently suppress the target gene expression, that is the first discovery of RNAi. [8] Then, it was also found that short double-stranded RNA with 3′-overhangs was generated by Dicer, an RNase III enzyme, as siRNA to initiate RNAi (Figure 1-5 and 1-6). In RNAi pathway, antisense strand of siRNA is loaded into RISC assembly as a guide strand, and then sense strand, regarded as a passenger strand, will be degraded, thus only one strand of siRNA is used for RNAi (Figure 1-6). This mature RISC can recognize the target mRNA by sequence-specific manner and can suppress gene expression by target mRNA digestion.

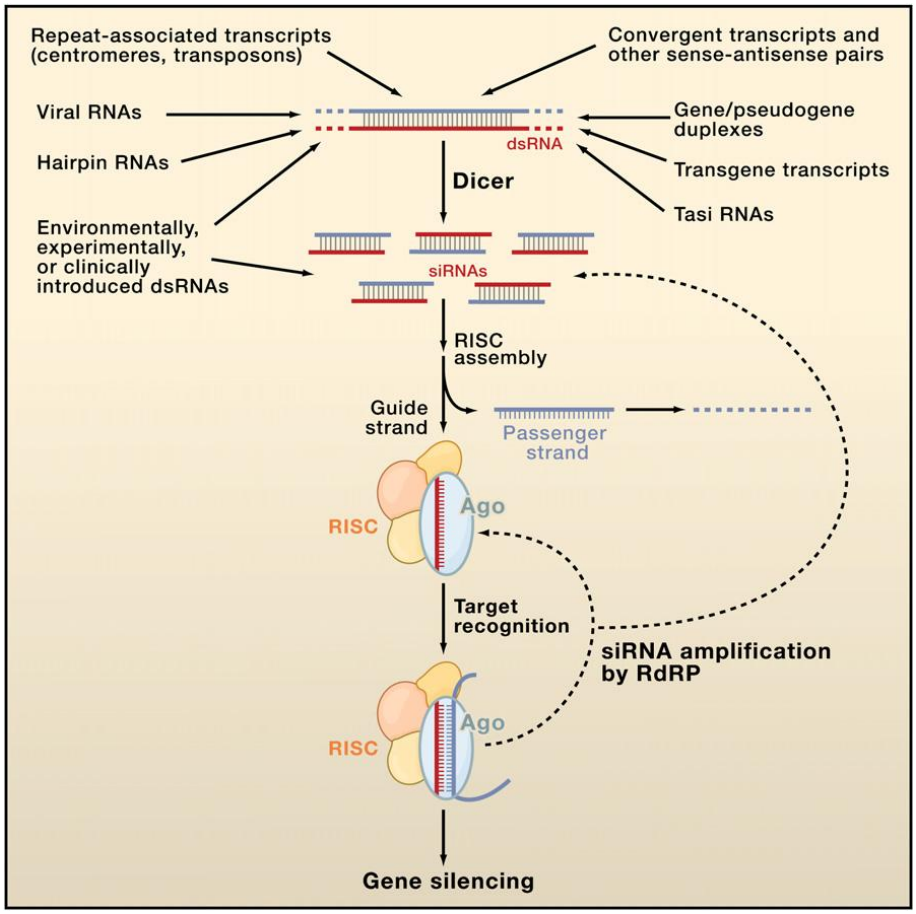

Figure 1-5. Generation of siRNAs for RNAi induction. [6]

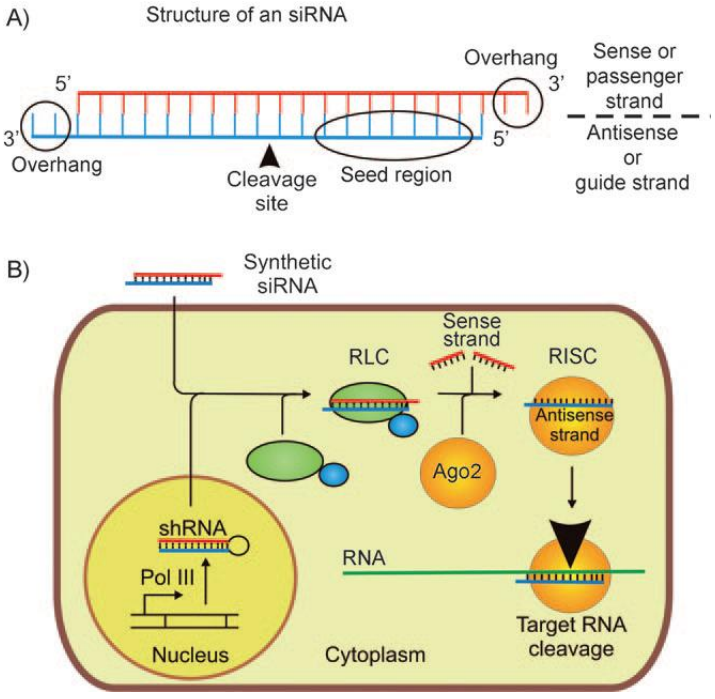

Figure 1-6. Illustration of A) siRNA structure and B) RNAi machinery.[9]

As described above, both endogenous and exogenous siRNA can induce RNAi in living cells. To make things better, exogenous siRNA can easily be constructed by chemical synthesis due to its approximately short length of nucleotides. Therefore, RNAi is now commonly used as a useful tool for knockdown of a specific target gene for many researches, moreover, it is also expected to apply to therapeutic use due to its powerful silencing effect. [10]

However, RNAi is not perfect. For instance, the RNAi effect of exogenous siRNA should be limited to transient gene silencing because siRNA is easy to be degraded by any kinds of ribonuclease existed in cells, due to instability of RNA itself. For this reason, it seems difficult to expect long-term gene regulation by a single introduction of siRNA. In addition, construction of appropriate delivery system of siRNA is also necessary for therapeutic application. For experimental use, several methods such as transfection, electroporation and microinjection, can be used for siRNA introduction. However, intact siRNA is unfavorable for transportation across hydrophobic cellular membranes because of abundant negative charges on phosphodiesters, besides it is also highly unstable in the blood. Therefore, it should be difficult to use general methods such as intravenous injection or oral administration for siRNA medication to human bodies.

Furthermore, the biggest problems in RNAi is a non-specific gene silencing, called "Off-target effect". As shown in Figure 1-7, one of possible causes of off-target effect should be the unexpected RISC formation with passenger (sense) strand. This kind of off-target effect can be improved by appropriate design of siRNA sequence. At the step of strand selection in RISC formation, which strand of siRNA is loaded to RISC is determined based on the relative thermodynamic stability at each end, namely, lower stability at 5′-end of antisense strand promotes antisense strand loading into RISC (Figure 1-8).[11] However, it is difficult to completely avoid sense strand loading by this principle. In addition, to make matters worse, details of RNAi mechanism, especially RISC loading machinery, are still unknown,[12] hence, which should also be significant obstacle to realize effective and precise RNAi initiation. Therefore, another challenge must be needed to solve these problems in RNAi, and then we thought that chemical approaches should be effective for improving RNAi ability.

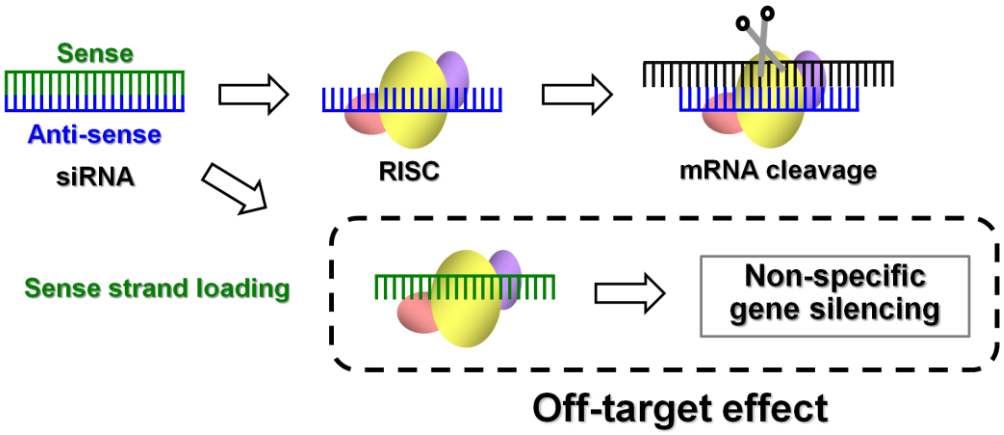

Figure 1-7. Mechanism of off-target effect caused by unexpected RISC formation.

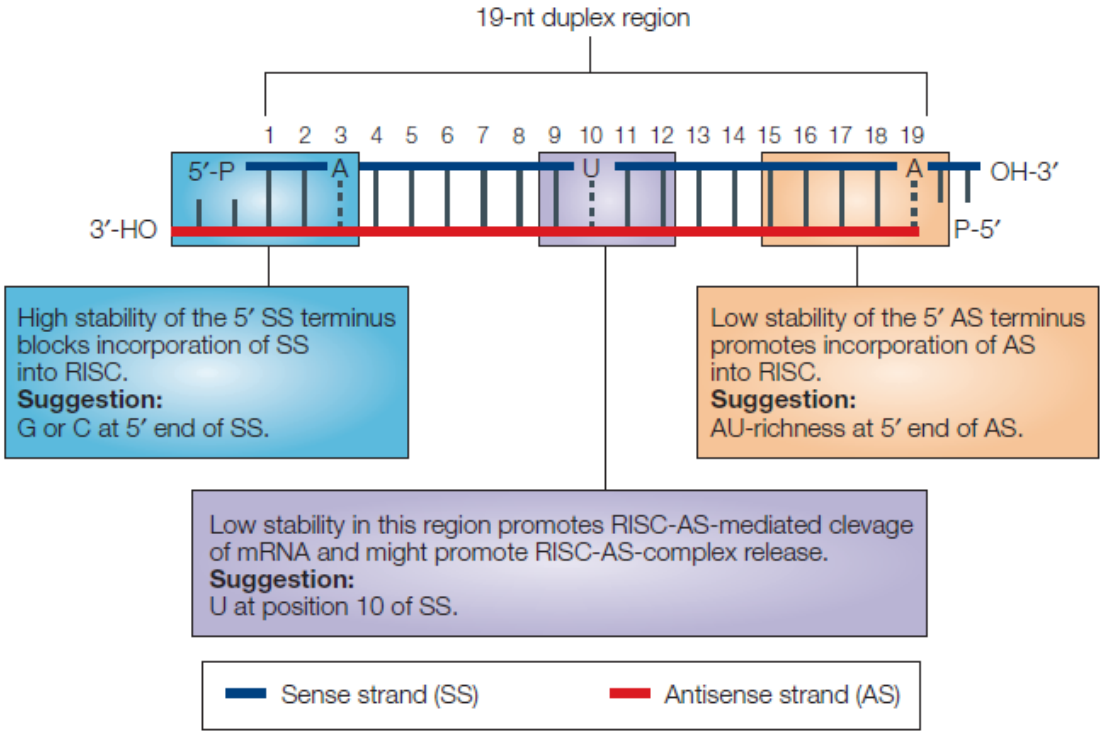

Figure 1-8. The principle of siRNA design for effective induction of RNAi. [11]

1-4 Development of chemically modified siRNA

For the improvement of RNAi, many biochemists have applied chemical modification to more effective siRNA construction. In order to increase the nuclease resistance of siRNA, phosphorothioates are commonly used for substitution of phosphate backbone of RNA strand (Figure 1-9). That is because backbone substitutions can inhibit nuclease recognition of RNA substrates. Similarly, modifications at 2′-OH of ribose ring, such as 2′-*O*-methyl and 2′-fluoro substitution, are also effective to increase siRNA stability (Figure 1-9). These modifications can stabilize siRNA against nuclease but also enhance

RNA stability itself by preventing intermolecular hydrolysis. Furthermore, introduction of locked nucleic acid (LNA) is also successful for improving siRNA property. Another advantage of LNA other than high nuclease resistance is enhanced affinity for the target sequence due to its fixed conformation which can form preorganized tertiary structure appropriate for hybridization. In all cases, these small substitutions can be tolerated by RNAi machinery, however, a large number of modified nucleotides in siRNA are likely to decrease RNAi efficiency and exhibit toxic side effects.[9, 13, 14]

On the other hand, conjugation of functional molecules to siRNA is applied to construct proper Drug-Delivery System (DDS) for RNAi-based therapy (Figure 1-10).

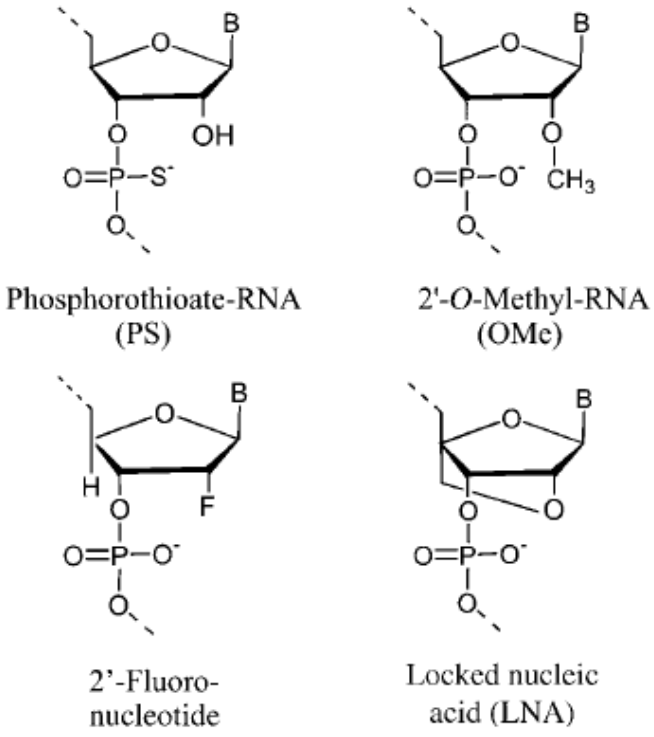

Figure 1-9. The several types of modified nucleotides effective for siRNA. [9]

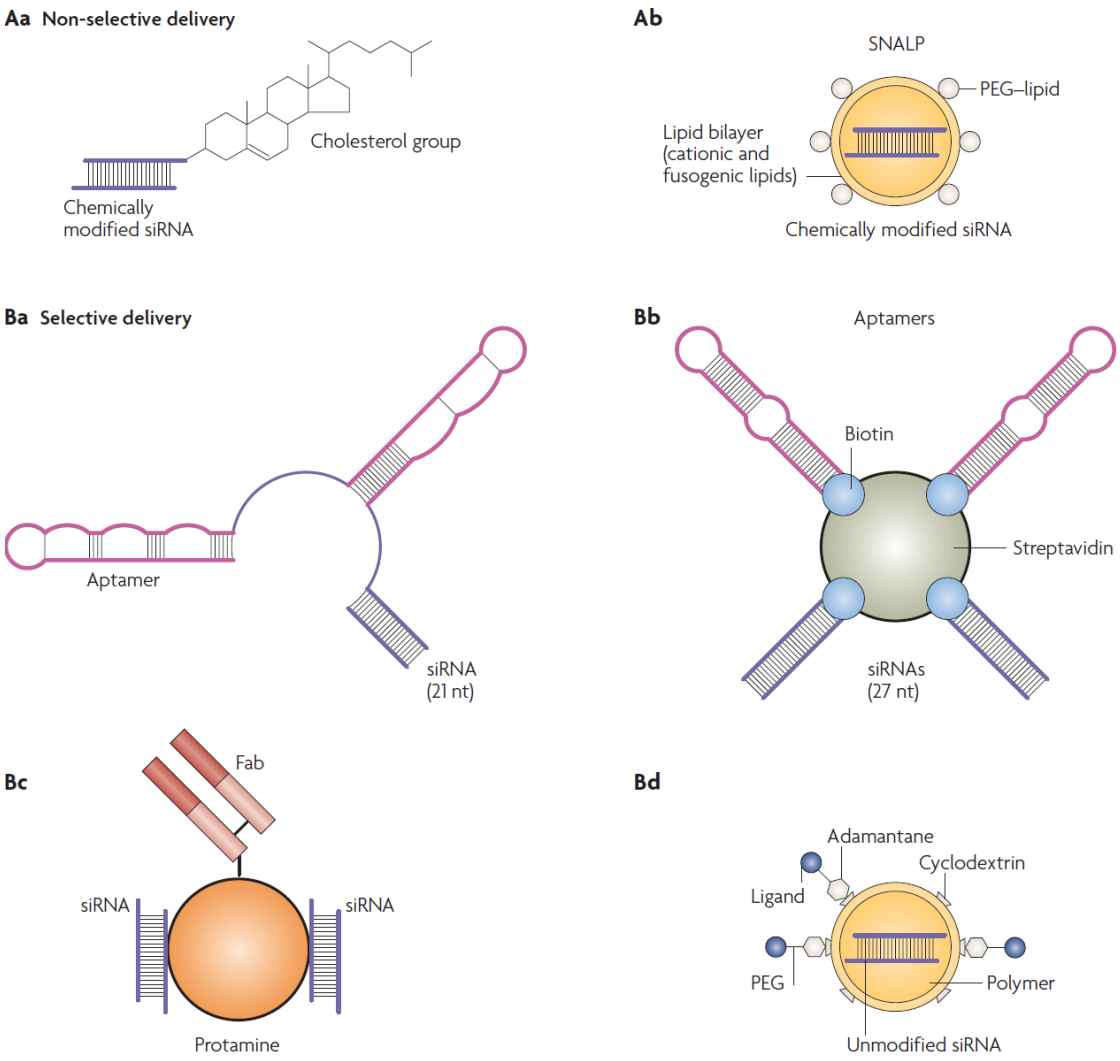

Figure 1-10. Efficient delivery of siRNA by chemical modifications. [14]

For non-cell specific delivery, siRNA conjugated to cholesterol groups (Aa) or packed to liposomal particle (Ab) are effective. These modifications can facilitate cellular uptake of the conjugated siRNA into certain tissue types, such as the liver and jejunum. By contrast, for delivering siRNA to some specific cell types, selective targeting can be realized by using receptor-ligand interaction. As shown in Figure 1-10, aptamer

fragments can be covalently (Ba) or non-covalently, by using biotin-streptavidin binding (Bb), linked to siRNA, then the conjugated aptamer facilitate siRNA incorporation through endocytosis by recognizing a certain receptor expressed on cellular surface. Heavy-chain antibody fragments (Fabs) that are specific for the HIV-1 envelope glycoprotein is also available to achieve selective siRNA delivery to HIV-infected cells (Bc). Sophisticated nanoparticles with cell-type-specific ligands on their surface enable more efficient and selective delivery of siRNA like vehicles (Bd).

Other intriguing challenges in chemical approaches are to regulate RNAi itself by using external stimuli, such as light irradiation. As shown in Figure 1-11, some groups

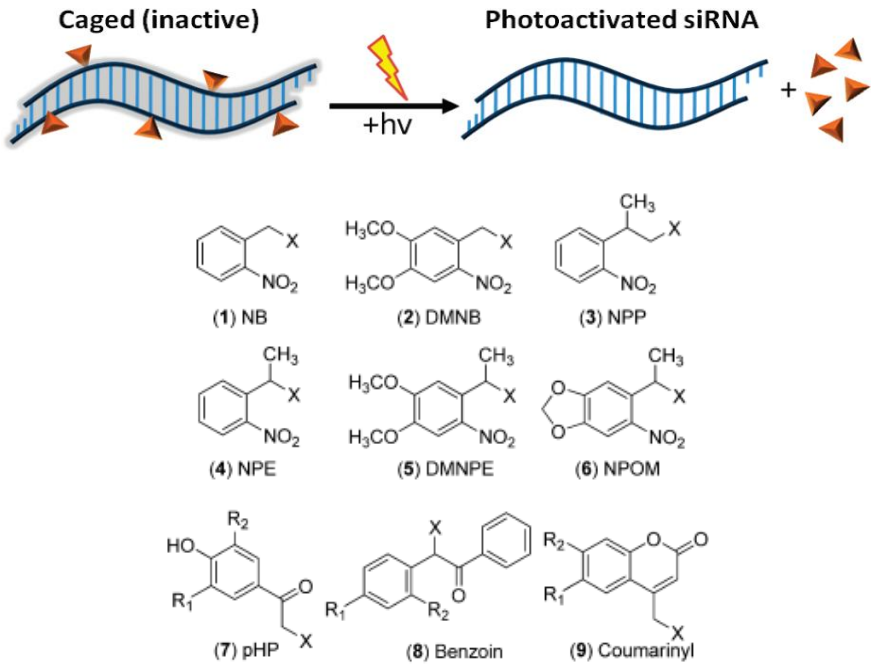

Figure 1-11. Illustration of photoregulation of RNAi by using caged siRNA and chemical structures of various caging compounds. [15]

some groups tried to apply caging groups to the artificial control of RNAi. Caged siRNA is inactive because the attached caging compounds block any biochemical interaction, then only when UV light expose to caged siRNA, caging groups are released from siRNA and RNAi activity is restored. This kind of approach is expected to enable spatial and temporal targeting of gene silencing. Moreover, this caging approach is also applied to other types of regulation. For example, Deiters *et al*. succeeded in photoregulation of gene expression in mammalian cells by using caged T7 polymerase (Figure 1-12).

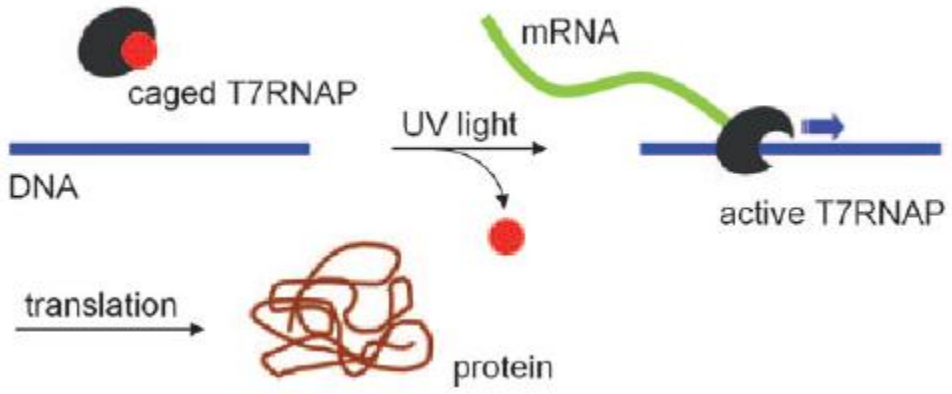

Figure 1-12. Photoregulation of gene expression by using caged T7 polymerase. [16]

As described above, application of chemically modified oligonucleotides to bioreactions should be effective to improve biochemical property and activity in each reaction, thus this approach should also be beneficial for the invention of new biotechnology and therapeutic treatments.

1-5 Present study

The preceding sections mainly described that utility of RNA molecules as regulators; especially siRNA can initiate RNA interference. For the further application of RNAi, some chemically modified siRNA were proposed and they greatly improved the efficiency of RNAi by making up its defects. However, inhibition of off-target effect, one of the most serious problems in RNAi, is still insufficient.

Therefore, in the present study, we tried to suppress the off-target effect by using a novel strategy of RNA modification; the use of base-surrogates with D-threoninol as a scaffold to introduce functional molecules into siRNA.

Moreover, we also made another challenge to uncover the mystery of RNAi. As we mentioned above, details of RNAi machinery are still unclear. Therefore, we also tried to invent siRNA probe, which can realize real-time monitoring of RNAi pathway in living cells.

In chapter 2, we first construct new methodology of RNA modification. Azobenzene has been introduced into RNA duplex to construct modified RNA duplex tethering an intercalator. By structural and thermodynamic analysis, it was found that azobenzene was intercalated into RNA duplex and modified RNA duplex possessed stable duplex structure. Furthermore, the photoreactivity of azobenzene-modified RNA

was also investigated.

In chapter 3, we used azobenzene-modified to reduce the off-target effect. We initially investigated RNAi activity of azobenzene-modified siRNA. When azobenzene moiety was introduced near the 5′-end of sense strand, RNAi activity was drastically increased compared to that of unmodified native siRNA. It was also found out that this sense strand modification could efficiently reduce off-target effect.

In chapter 4, we tried to construct siRNA probe for real-time monitoring of RISC formation. Quencher-fluorophore conjugates were introduced into siRNA, and the fluorescence was efficiently quenched when siRNA formed duplex. Then, changes in the fluorescence intensity in living cells were observed after transfection of siRNA probe.

In chapter 5, additionally, we tried photoregulation of gene expression by using azobenzene modified DNA.

1-6 Notes and References

[1] H. Lodish, A. Berk, P, Matsudaira, C. A. Kaiser, M. Krieger, M. P. Scott, S. L. Zipursky and J. Darnell, Molecular Cell Biology Fifth Edition, **2006**, Chapter 4, 101-131.

[2] J. S. Mattick, I. V. Makunin, *Hum. Mol. Genet.*, **2006**, *15*, R17-R29.

[3] a) K. Kruger *et al*, *Cell*, **1982**, *31*, 147–157. b) J. A. Doudna, T.R. Cech, *Nature.* **2002**, *418*, 222-228.

[4] S. R. Eddy, *Nat. Rev. Genet.*, **2001**, *2*, 919–929.

[5] a) X. Liu, K, Fortin, Z. Mourelatos, *Brain Pathol.*, **2008**, *18*, 113–121. b) D. P. Bartel, *Cell*, **2009**, *136*, 215-233

[6] R. W. Carthew, E. J. Sontheimer, *Cell*, **2009**, *136*, 642–655.

[7] a) S. M. Elbashir, J. Martinez, A. Patkaniowska, W. Lendeckel, T. Tuschl, *EMBO J.* **2001**, *20*, 6877-6888. b)Y. Tomari, P. D. Zamore, *Genes Dev.*, **2005**, *19*, 517–529.

[8] A. Fire, S. Xu, M. K. Montgomery, S. A. Kostas, S. E. Driver, C.C. Mello, *Nature* **1998**, *391*, 806-811.

[9] J. Kurreck, *Angew. Chem., Int. Ed.* **2009**, *48*, 1378-1398.

[10] a) L. Aagaard. J. J. Rossi, *Drug Deliv. Rev.* **2007**, *59*, 75-86. b) P. Gonzalez-Alegre, H. L. Paulson, *Nat. Clin. Pract. Neurol Rev.* **2007**, *3*, 394-404.

[11] V. Mittal, *Nat. Rev. Genet.* **2004**, *5*, 355-365.

[12] T. Kawamata, Y. Tomari, *Trends Biochem. Sci.* **2010**, *35*, 368-376.

[13] a) Y. L. Chiu, T. M. Rana, *RNA* **2003**, *9*, 1034-1048. b) N. M. Bell, J. Micklefield, *ChemBioChem* **2009**, *10*, 2691-2703. c) M. Amarzguioui, T. Holen, E. Babaie, H. Prydz, *Nucleic Acids Res.***2003**, *31*, 589-595.

[14] D. H. Kim, J. J. Rossi, *Nat. Rev. Genet.* **2007**, *8*, 173-184.

[15] a) J. P. Casey, R. A. Blidner, W. T. Monroe, *Mol. Pharmaceutics* **2009**, *6*, 669-685. b) V. Mikat, A. Heckel, *RNA* **2007**, *13*, 2341-2347.

[16] C. Chou, D. D. Young, A. Deiters, *ChemBioChem.* **2010**, *11*, 972-977.

David P. Bartel[1]

Chapter 2. Property of chemically modified RNA duplex with an intercalator

2-1 Abstract

In order to create novel modified RNAs for improving RNAi, we initially constructed RNA duplex involving an intercalator by introducing azobenzenes into RNA using D-threoninol as a scaffold. Structural analysis by circular dichroism (CD) spectroscopy, NMR and molecular modeling indicated that the planar *trans*-azobenzene could intercalate between adjacent base pairs. However, unlike the corresponding azobenzene-modified DNA, the RNA/RNA duplex was not stabilized by base stacking due to a rigid A-form structure. Meanwhile, the large steric hindrance caused by nonplanar *cis*-azobenzene was quite effective to distort and destabilize the duplex structure, and consequently the difference in melting temperature (T_m) between the *trans* and *cis* forms in RNA duplex was much larger than that in DNA. These results indicated that efficient photoregulation of RNA hybridization became possible by *trans-cis* photoisomerization of azobenzene. For further investigation on photoregulatory efficiency of the azobenzene-modified RNA, we also discuss the sequence dependency and the effect of methylation of azobenzene at the *ortho* positions on photoregulation of

RNA/RNA duplex formation.

2-2 Introduction

As described in Chapter 1, the biological roles of small RNA molecules[1] have attracted much attention due to continued discoveries of various functional RNAs such as ribozymes,[2] microRNA (miRNA),[3] and short interfering RNA (siRNA).[4] These functional RNAs, also called non-coding RNAs, are well conserved in many species and are involved in many important bioreactions, especially for the regulation of gene expression.

In our previous work, we have developed a novel methodology of DNA by the use of base-surrogates with D-threoninol as a scaffold for functional molecules. According to this methodology, for instance, we synthesized azobenzene-tethered DNA with D-threoninol as a scaffold and the covalently attached azobenzene was intercalated between base pairs of DNA duplex. Azobenzene is a typical photoresponsible material and commonly used not only as an intercalator but also for photoregulation. Hence, we could demonstrate reversible photoregulation of the formation and dissociation of DNA duplexes by using azobenzene-modified DNA.[5] The mechanism of photoregulation can be described as follows: the planar *trans*-azobenzene intercalates between the two adjacent base pairs and stabilizes the DNA duplex by stacking interactions, whereas the

nonplanar *cis*-azobenzene destabilizes the duplex by steric hindrance. Based on this photoregulation strategy, the photoswitching of various DNA functions such as DNA primer extension,[5b] hybridization for driving DNA nanomachines,[6] and other enzymatic reactions[5b] has been achieved.

From these results, an attractive feature of azobenzene-modified DNA is that the intercalator can inhibit protein recognition of target DNA duplex. Thus, we thought that introduction of intercalator should be effective for improving RNA functions.

In this chapter, we synthesized azobenzene-modified RNA and investigated its structural and thermodynamic properties comparing with the modified DNA. Additionally, we also photoregulated RNA hybridization and examined its photoregulatory efficiency.

2-3 Results and Discussions

2-3-1 Structural analysis of RNA/RNA duplexes involving azobenzene

In order to confirm the intercalation of introduced *trans*-formed azobenzene into RNA duplex, several modified RNAs were synthesized by introducing azobenzene via D-threoninol using standard phosphoramidite chemistry as reported previously,[5a] and the sequences of azobenzene-modified RNA are shown in Figure 2-1. For obtaining

structural information on azobenzene-modified RNA/RNA duplexes, circular dichroism (CD) spectroscopy, ^{1}H-NMR analysis, and molecular modeling were carried out. First, CD spectra of $\mathbf{R_XG/R_cC}$ were measured to investigate the induced CD of the *trans*-azobenzene moiety. As shown in Figure 2-2, a typical CD pattern of an A-form duplex structure was observed at the region of absorption of nucleobases (200-260 nm), demonstrating the introduction of azobenzene did not cause a big change in the RNA/RNA duplex structure. At the region of azobenzene absorption (300-500 nm), a very weak induced CD (positive for π-π∗ transition and negative for n-π∗ transition) appeared after the duplex formed at 0 °C. This result shows that the corresponding π-π∗ transition moment on the plane of *trans*-azobenzene was parallel to the plane of the base pairs.[7]

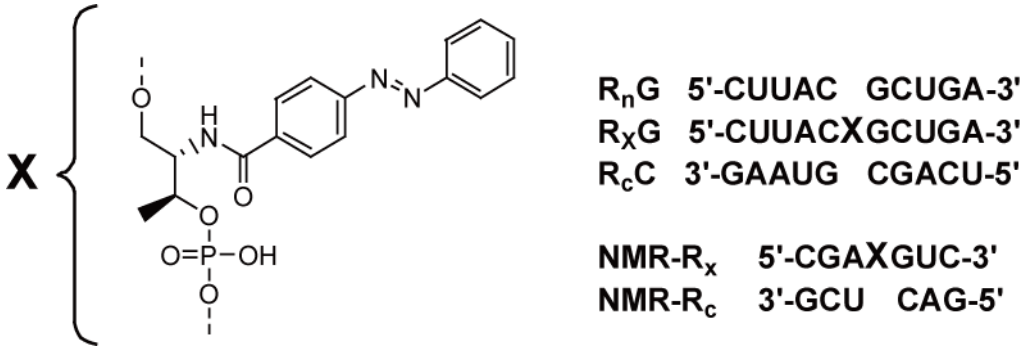

Figure 2-1. Sequences of RNA and the structure of an azobenzene. **X** indicates the position of azobenzene.

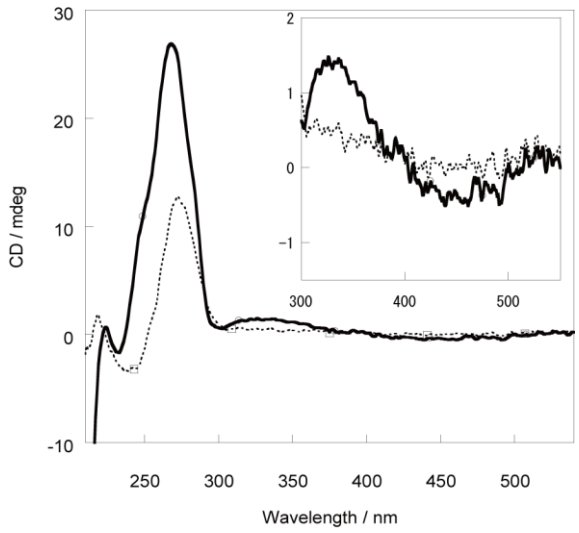

Figure 2-2. CD spectra of the *trans*-**R_XG/R_cC** duplex at 0 °C (solid lines) and 60 °C (dotted lines).

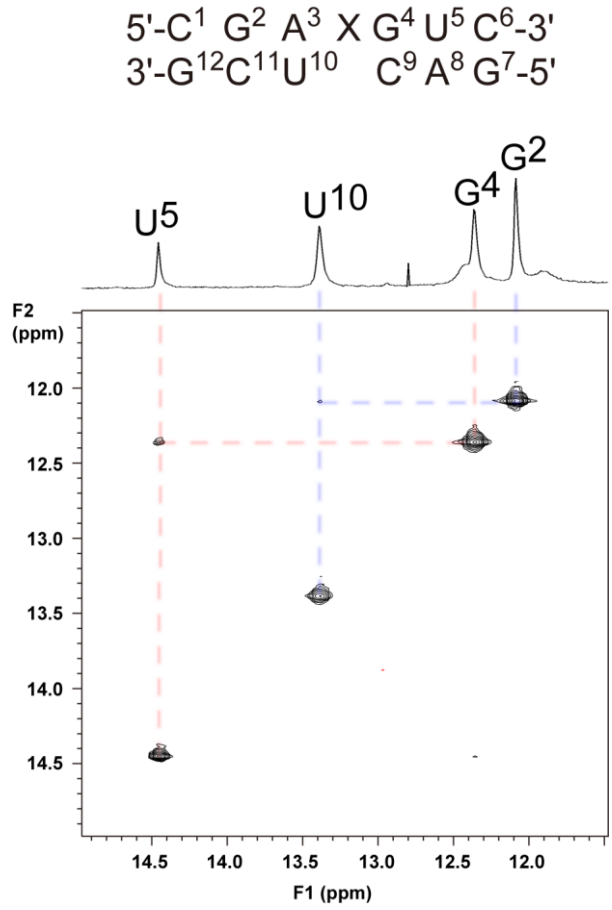

Figure 2-3. 2D NOESY spectra of duplex **NMR-R_X/NMR-R_c** at the imino proton region (12-15 ppm). Conditions: 1.0 mM RNA, H_2O/D_2O 9:1 at 278 K (mixing time = 150 ms), 200 mM NaCl, 20 mM phosphate buffer (pH 7.0).

To obtain more information about the position of *trans*-azobenzene in RNA/RNA duplexes, 1D and 2D ^{1}H-NMR spectra of a 6-bp long duplex, **NMR-R_X/NMR-R_c**, were measured. The above sequence was used because the NMR structure of an azobenzene-modified DNA duplex with the same sequence was determined previously.[8] From the NMR signals of NOESY, DQF-COSY, and TOCSY, most of the protons in the duplex were assigned. As shown in Figure 2-3, the assignment of imino protons (11-15 ppm) could be verified from the 1D and NOESY spectra measured in H_2O (H_2O/D_2O = 9:1). Only four strong signals of imino protons were observed because the two imino protons (G^7 and G^{12}) at both ends are usually very weak and broad due to rapid exchange with water. From the NOEs between imino protons, the four individual signals were assigned (Figure 2-3). The fact that all four peaks are sharp indicates that the introduced azobenzene moiety did not interfere with the base pairing in the RNA/RNA duplex. Furthermore, an NOE between U^{10} and G^4 was not observed, probably because the intercalated azobenzene separates the two base pairs.

Figure 2-4 also depicts the NOESY between the imino proton and aromatic proton regions. Compared to U^5, the signal of the imino proton in U^{10} shifted greatly to a higher magnetic field, indicating that one benzene ring of azobenzene was located above or below the imino proton of U^{10}. NOEs signals between the imino proton of U^{10}

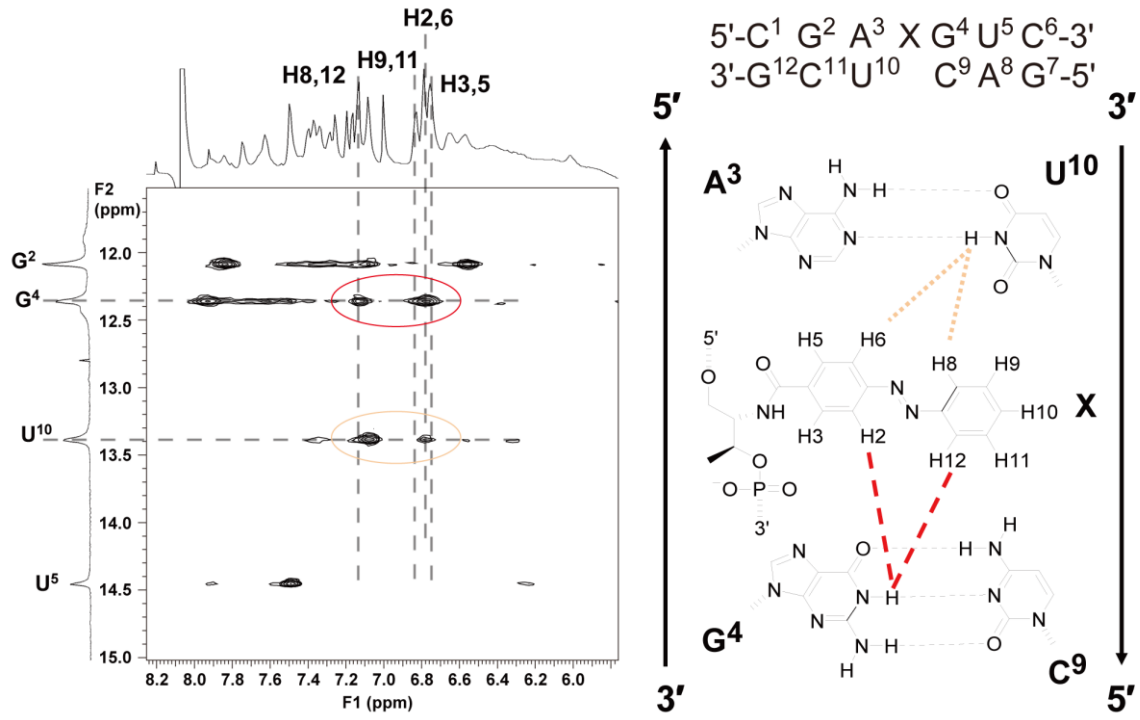

Figure 2-4. 2D NOESY spectra of duplex **NMR-R$_X$/NMR-R$_c$** between signals of aromatic protons (6.0-8.0 ppm) and those of imino protons (12-15 ppm).

and aromatic protons on azobenzene were also observed, although they were not as strong. On the other hand, the signal of G^4 did not shift to a higher magnetic field compared to that of G^2, although strong NOE signals between the imino proton of G^4 and H2 (H6) and H8 (H12) protons on azobenzene were observed. This indicated that the N=N double bond of azobenzene is located close to the imino proton of G^4.

Finally, we performed molecular modeling to obtain an energy-minimized structure of RNA/RNA duplexes involving azobenzene (Figure 2-5, see also Appendix Figure 2-1). Compared to the native RNA/RNA duplex, the *trans*-azobenzene distorted the duplex to some extent, although it partially intercalated between adjacent base pairs. All

of the above results demonstrate that *trans*-azobenzene is located between two adjacent base pairs but is not flipped out completely from the duplex. However, because of a rigid A-form structure of RNA duplex, complete intercalation cannot be obtained because it might cause too much stress in the backbone due to the insertion of the azobenzene residue via D-threoninol.[9]

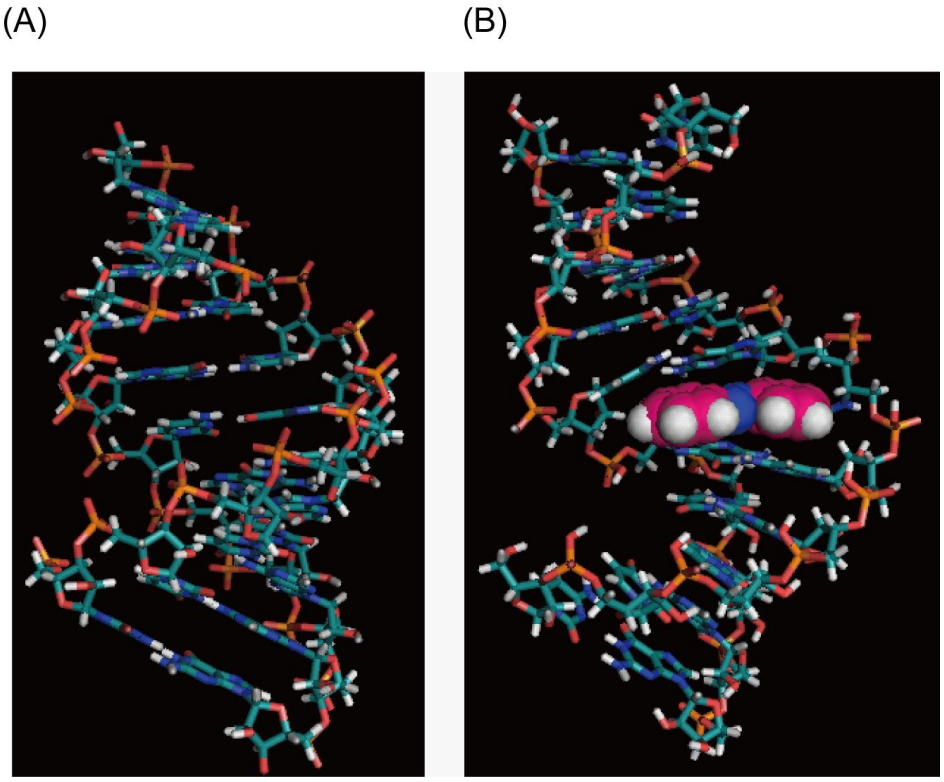

Figure 2-5. Energy-minimized structure of native RNA/RNA duplex **R_nG/R_cC** (A), *trans*-**R_XG/R_cC** (B). The azobenzene moieties are shown as a space-filled model.

2-3-2 Thermodynamic stability and photoregulatory efficiency of azobenzene-modified RNA duplex

As described in previous section, intercalation of azobenzene into RNA duplex was verified, however, stacking interaction between azobenzene and the base pairs should be incomplete. These results raised another concern that this incomplete interacalation of azobenzene could destabilize RNA duplex. In the case of the azobenzene-modified DNA duplex, azobenzene could stack well with the adjacent base pairs, which was also confirmed by NMR analysis and molecular modeling,[8] and this stacking interaction resulted in obvious stabilization of DNA duplex.[5] Therefore, in this section, the effect of the introduced azobenzene on RNA duplex stability was investigated by measuring melting temperature (T_m). Both RNA and DNA sequences with azobenzene moieties were synthesized to compare DNA/DNA, RNA/DNA and RNA/RNA duplex (Figure 2-6). Additionally, T_m was also measured in the case of non-planar *cis*-azobenzene to investigate whether photoregulation of RNA/RNA hybridization could be realized.

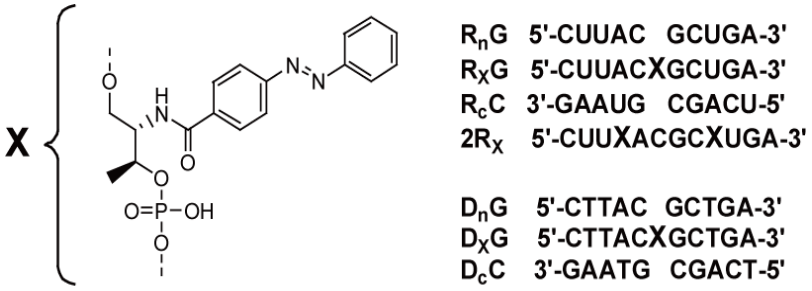

Figure 2-6. Sequences of azobenzene-modified RNA and DNA sequences for T_m measurement.

First, the UV/Vis spectroscopy was measured to investigate photoisomerization (*trans-cis* isomerization by irradiation with visible and UV light respectively) of introduced azobenzene. As shown in Figure 2-7A, upon irradiation with visible light (λ > 400 nm), the introduced azobenzene had a strong absorption around 340 nm (π-π* transition) indicating that most of the azobenzenes (more than 90%) were in the *trans* form (solid line in Figure 2-7A). After irradiation with UV light (320-380 nm), the absorbance at 340 nm remarkably decreased (dotted line in Fig. 2-7A) indicating that *trans*-azobenzene was promptly isomerized to the *cis*-form (about 80%). These changes in UV/Vis spectra are quite similar to those of the corresponding DNA/DNA duplex (**D_XG/D_cC**) shown in Figure 2-7B.

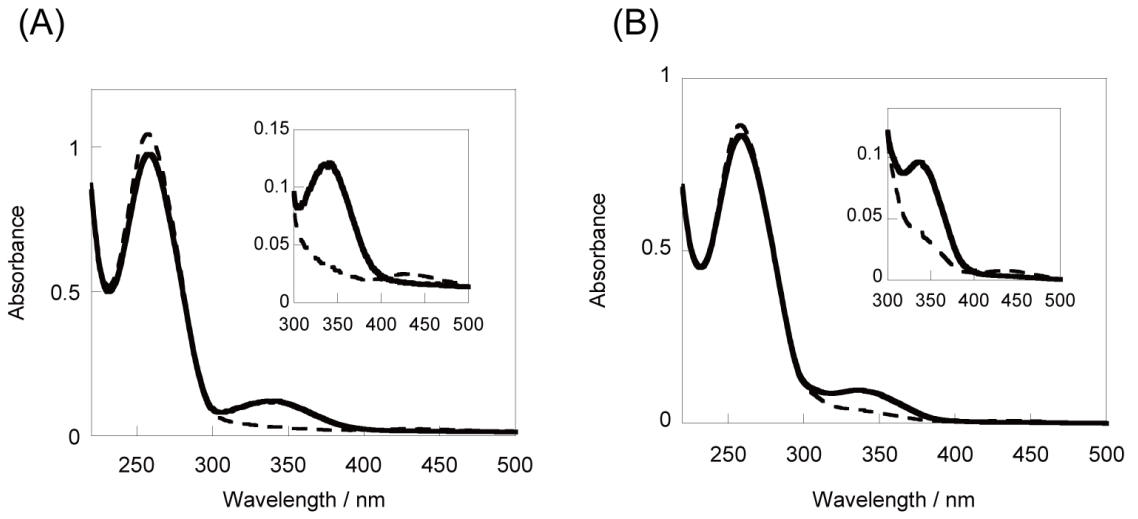

Figure 2-7. UV/Vis spectra of **R_XG/R_cC** (A) and **D_XG/D_cC** (B) with *trans*-azobenzene (solid line) and *cis*-azobenzene (dotted line). Conditions: 5 μM dsRNA, 100 mM NaCl, 10 mM phosphate buffer (pH7.0). The introduced azobenzene was isomerized to *trans*-form with visible light (λ > 440 nm), and to *cis*-form with UV light (320 – 380 nm), respectively.

Then, we investigated the thermodynamic stability of RNA/RNA duplex with both *trans*- and *cis*-azobenzene by comparing T_m values of native (**R_nG/R_cC**) and modified RNA (**R_XG/R_cC**). For duplex **R_XG/R_cC**, the T_m for the *trans*-form was 48.8 °C as determined from its melting curve (solid line in Figure 2-8A.).

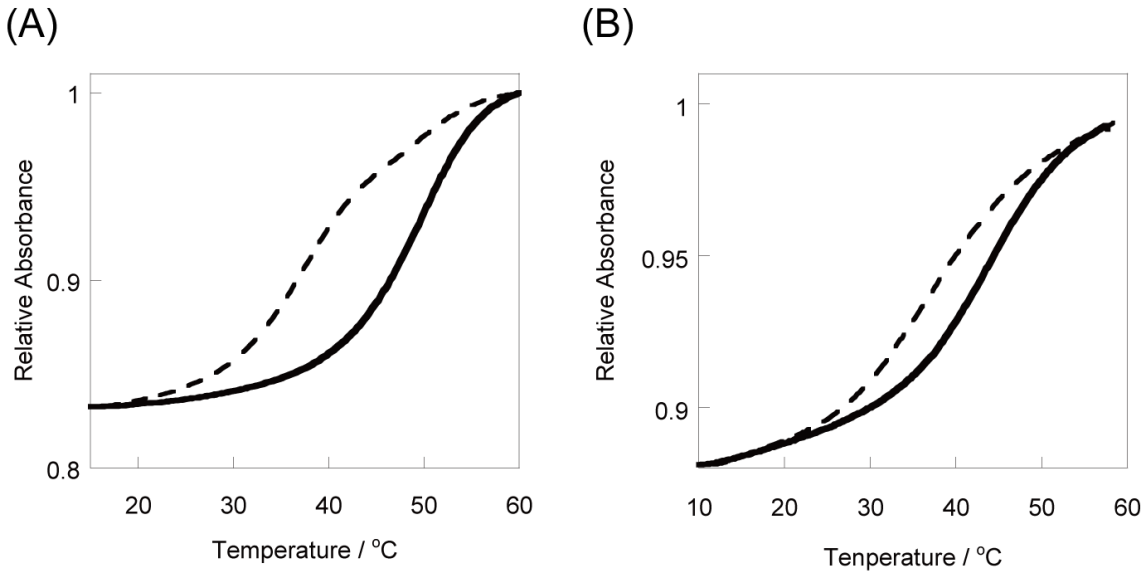

Figure 2-8. Melting curves of **R_XG/R_cC** (A) and **D_XG/D_cC** (B) with *trans*-azobenzene (solid line) and *cis*-azobenzene (dotted line).

Compared to the native RNA/RNA duplex **R_nG/R_cC** (T_m = 50.7 °C), the azobenzene-modified duplex, *trans*-**R_XG/R_cC**, showed a slightly lower T_m, indicating that *trans*-azobenzene destabilized the duplex to some extent (Table 2-1). In the case of DNA/DNA duplexes however, the T_m of *trans*-**D_XG/D_cC** (42.9 °C) was 2.0 °C higher than that of **D_nG/D_cC** (40.9 °C), demonstrating that the attached *trans*-azobenzene stabilized the DNA duplex. As described previously, this stabilization effect was

attributed to the stacking effect of the planar and hydrophobic *trans*-azobenzene with

Table 2-1. Melting temperatures (T_ms) of RNA/RNA, DNA/DNA, RNA/DNA, and DNA/RNA duplexes.

Duplex	T_m/°C [a]		
	trans	*cis*	ΔT_m [b]
R_XG/R_cC	**48.8**	**36.5**	**12.3**
D_XG/D_cC	**42.9**	**35.6**	**7.3**
$2R_X/R_cC$	**44.9**	**21.0**	**23.9**
R_XG/D_cC	**34.3**	**25.0**	**9.3**
D_XG/R_cC	**41.1**	**30.0**	**11.1**
R_nG/R_cC		**50.7** [c]	
D_nG/D_cC		**40.9** [c]	
R_nG/D_cC		**34.2** [c]	
D_nG/R_cC		**40.9** [c]	

[a] Conditions: 5 μM dsDNA or dsRNA, 100 mM NaCl, 10 mM phosphate buffer (pH7.0). [b] Change of T_m induced by *cis-trans* photoisomerization. [c] T_m values of native duplexes with only natural nucleotides. The sequences are shown in Figure 2-6. The value of the measurement error was estimated within ± 0.3 °C.

adjacent DNA base pairs.[5b, 8] In contrast, as was expected, *trans*-azobenzene cannot stabilize RNA duplex compared to native one because the azobenzene only partially stacked with the adjacent base pairs, which was confirmed in the previous section. Likewise, the slight destabilization effect of *trans*-azobenzene in RNA duplex can also be explained by the partial distortion of the duplex structure due to the insertion of azobenzene in a rigid A-form RNA duplex (Figure 2-5). However, the T_m value for the *trans*-form was still high (48.8 °C) so that RNA tethering azobenzene moiety could form stable duplex, despite the local structural change.

On the other hand, after the azobenzene was isomerized to the *cis*-form, the T_m of *cis*-**R_XG/R_cC** decreased to 36.5 °C (dotted line in Figure 2-8), demonstrating that *cis*-azobenzene significantly destabilized the RNA/RNA duplex. The T_m change (ΔT_m) by *trans-cis* photoisomerization, being used as an indicator to evaluate photoregulatory efficiency, was as large as 12.3 °C and the difference in the change of free energy between *cis*- and *trans*-form (Δ (ΔG)) was 9.8 kJ/mol (Table 2-2.). This value was much larger than that of the corresponding DNA/DNA duplex (**D_XG/D_cC**) whose ΔT_m was 7.3 °C (Table 2-1). These results indicated that RNA/RNA hybridization can be efficiently photoregulated by using azobenzene-tethered RNA.

Table 2-2. Thermodynamic parameters for the formation of RNA/RNA duplexes.

Duplex	T_m / °C [a]	ΔH^o (kJ mol^{-1})	ΔS^o (J mol^{-1} K^{-1})	ΔG^o [b] (kJ mol^{-1})
R_nG/R_cC	**50.7**	**-355**	**-987**	**-48.6**
***trans*-R_XG/R_cC**	**48.8**	**-300**	**-825**	**-44.6**
***cis*-R_XG/R_cC**	**36.5**	**-265**	**-742**	**-34.8**

[a] Conditions: 100 mM NaCl, 10 mM phosphate buffer (pH 7.0); T_m was measured at the following concentrations of RNA: 0.25, 0.5, 1.0, 2.5, and 5 μM. [b] Here the data at 37 °C (310 K) are shown.

As shown in Table 1, the T_m of *cis*-**R_XG/R_cC** was lower than that of the corresponding native RNA/RNA duplex by 14.2 °C. However, the difference in T_m between *cis*-**D_XG/D_cC** and the native DNA duplex was only 5.3 °C. Compared to DNA duplexes,

the *cis*-azobenzene might cause larger steric hindrance for RNA/RNA duplexes and more free energy lost during duplex formation by tethering nonplanar *cis*-azobenzene to the rigid A-form structure. This effect was enhanced in the case of **2R$_X$/R$_c$C**, in which two azobenzenes were introduced (Table 2-1 and see also Figure 2-1 for the sequence). The T_m of *cis*-**2R$_X$/R$_c$C** was 29.7 °C lower than that of the native RNA/RNA duplex. For the investigation on this destabilization effect of *cis*-azobenzene, molecular modeling was performed on *cis*-**R$_X$G/R$_c$C** duplex (Figure 2-9). In the case of nonplanar *cis*-azobenzene, a larger distortion occurred, especially for the two adjacent base pairs. A large steric hindrance with both base pairs and backbone may destabilize the duplex structure greatly. Thus, the rigid A-from structure of the RNA/RNA duplex seems more sensitive to steric hindrance induced by *trans*-to-*cis* isomerization of azobenzene than the B-form structure of the DNA duplex. Consequently, the large destabilization effect of *cis*-azobenzene should be the main mechanism for obtaining efficient photoregulation of RNA hybridization. For **2R$_X$/R$_c$C**, the ΔT_m between the *trans*- and *cis*-forms was as large as 23.9 °C. Accordingly, clear-cut photoregulation of RNA hybridization is attainable by introducing multiple azobenzenes.

Efficient photoregulation was also attained for an RNA/DNA duplex, which usually has an A-form structure, when azobenzene was introduced into either the RNA or DNA

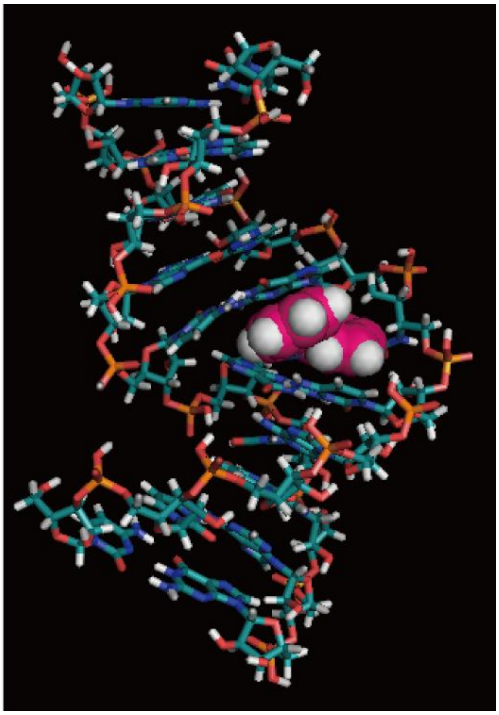

Figure 2-9. Energy-minimized structure of *cis*-$\mathbf{R_XG/R_cC}$.

strand (Table 2-1). For both cases ($\mathbf{R_XG/D_cC}$ and $\mathbf{D_XG/R_cC}$), a larger ΔT_m was obtained than for the DNA/DNA duplex, indicating again that introducing azobenzene into an A-form duplex is favourable for photoregulation. Interestingly, no destabilization effect of *trans*-azobenzene was observed in either case. Thus, introducing azobenzene into an oligonucleotide (either RNA or DNA) via D-threoninol can be used as a common, facile, and robust tool for photoregulating the functions of nucleic acids.

2-3-3 Sequence dependency of photoregulation of RNA hybridization

We also investigated the sequence dependency of photoregulatory efficiency. Assuming that the stability of an RNA/RNA duplex involving azobenzene depends

mainly on the base pairs adjacent to azobenzene,[10] we investigated four sequences in which the base at the 3′-side was systematically changed. The photoregulatory efficiency was also evaluated by the ΔT_m between the *trans* and *cis* forms. As shown in Table 2-3, for all RNA/RNA duplexes, the ΔT_m was above 9.0 °C, demonstrating that a photoresponsive RNA involving azobenzene can generally be used for efficiently photoregulating RNA hybridization. On the other hand, the ΔT_m changes to some extent with the sequence. For example, **R_XC/R_cG** showed a smaller ΔT_m (9.1 °C) than **R_XG/R_cC** by 3.2 °C, although they had the same GC content. The ΔT_m tended to be larger when a purine nucleobase, G or A, was adjacent to the azobenzene (**R_XG/R_cC**, **R_XA/R_cU**). The larger size of purines at the azobenzene-modified strand may contribute to the larger steric hindrance caused by *cis*-azobenzene.

Table 2-3 Sequence dependency of photoregulatory efficiency.

Duplex	T_m/°C [a]		
	trans	*cis*	ΔT_m
R_XG/R_cC	**48.8**	**36.5**	**12.3**
R_XA/R_cU	**41.8**	**29.4**	**12.4**
R_XU/R_cA	**41.6**	**31.2**	**10.4**
R_XC/R_cG	**46.1**	**37.0**	**9.1**

R_XG 5'-CUUAC**X**GCUGA-3'
R_cC 3'-GAAUG CGACU-5'
R_XA 5'-CUUAC**X**ACUGA-3'
R_cU 3'-GAAUG UGACU-5'
R_XU 5'-CUUAC**X**UCUGA-3'
R_cA 3'-GAAUG AGACU-5'
R_XC 5'-CUUAC**X**CCUGA-3'
R_cG 3'-GAAUG GGACU-5'

[a] Conditions: 5 μM dsRNA, 100 mM NaCl, 10 mM phosphate buffer (pH7.0). The value of the measurement error was estimated within ± 0.3 °C.

2-3-4 Effect of methyl-modification of azobenzene on photoregulation of RNA hybridization

As reported previously, by introducing methyl groups into the *ortho* positions of azobenzene (Figure 2-10), the photoregulatory efficiency of DNA hybridization is significantly improved, especially when methyl groups are introduced to both *ortho* positions on the distal benzene ring.[11] For RNA hybridization studied here, as compared with the unmodified azobenzene, the *trans*-form of modified azobenzene with methyl groups should stabilize the duplex more due to an increase of stacking interactions with the base pairs. On the other hand, remarkable destabilization can be expected in the *cis*-form because of the increase of steric hindrance. Another merit of 2′,6′-dimethylazobenzene is the high thermal stability of its *cis*-form, whose half-life is10 times longer than that of non-modified azobenzene (**X**).[9] For example the half-life

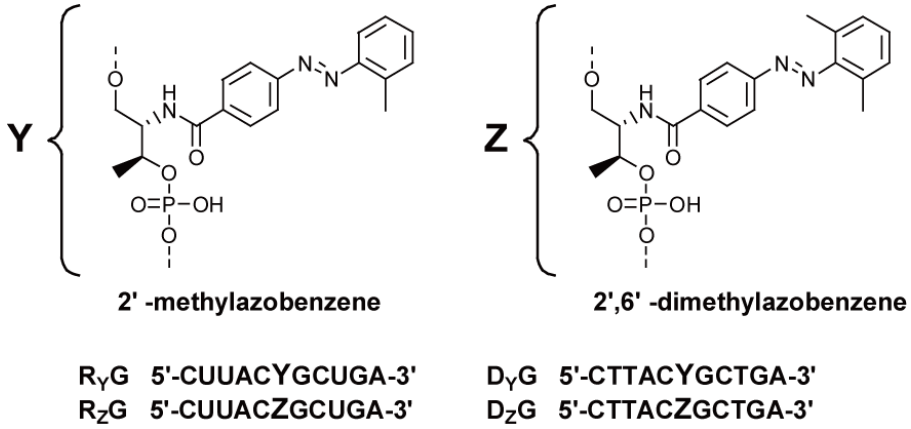

Figure 2-10. Structures of alkylated azobenzene derivatives and the DNA and RNA sequences.

of *cis*-2′,6′-dimethylazobenzene involved in DNA is about 10 days at 37 °C.[9] Assuming that a similar effect can be expected in the case of photoregulation of RNA hybridization, 2′-methylazobenzene (**Y**) and 2′,6′-dimethylazobenzene (**Z**) were also introduced into RNA. The results of T_m measurement showed that the ΔT_m of $\mathbf{R_YG/R_cC}$ and $\mathbf{R_ZG/R_cC}$ were 1.0 °C and 2.0 °C higher than that of $\mathbf{R_XG/R_cC}$, respectively. Although the improvement of photoregulatory efficiency was not as large as that of photoresponsive DNA ($\mathbf{R_YG}$ and $\mathbf{R_ZG}$), the methyl modification was still favourable for photoregulation of RNA hybridization to some extent. The smaller effect can also be explained by the difficulty of intercalation of azobenzene into base pairs of the rigid A-form RNA/RNA duplex. When a long reaction time (>24 h) is necessary, 2′,6′-dimethylazobenzene-modified RNA is promising for clear-cut photoregulation of RNA functions, and the effect of thermal isomerisation can be disregarded.

Table 2-4 Melting temperatures (T_m) of duplexes involving methyl-modified azobenzene.

Duplex	T_m/°C [a]		
	trans	*cis*	ΔT_m
$\mathbf{R_XG/R_cC}$	**48.8**	**36.5**	**12.3**
$\mathbf{R_YG/R_cC}$	**49.7**	**36.4**	**13.3**
$\mathbf{R_ZG/R_cC}$	**49.2**	**34.9**	**14.3**
$\mathbf{D_XG/D_cC}$	**42.9**	**35.6**	**7.3**
$\mathbf{D_YG/D_cC}$	**45.2**	**32.4**	**12.8**
$\mathbf{D_ZG/D_cC}$	**45.1**	**24.6**	**20.5**

[a] Conditions: 5 μM dsRNA or dsDNA, 100 mM NaCl, 10 mM phosphate buffer (pH7.0). The value of the measurement error was estimated within ± 0.3 °C.

2-4 Conclusions

(1) The intercalation of attached azobenzene into RNA duplex was confirmed by structural analysis, such as CD spectroscopy, NMR and molecular modeling.

(2) Although azobenzene cannot intercalate completely due to the rigid A-form structure, modified RNA duplex is thermodynamically stable enough to de applied as a functional RNA.

(3) We also achieved efficient photoregulation of RNA hybridization by introducing azobenzene into RNA strands via D-threoninol, irrespective of the sequence. Although *trans*-azobenzene destabilizes the RNA/RNA duplex to some extent due to the rigid A-form structure, the drastic destabilization effect of *cis*-azobenzene contributes to efficient photoregulation.

2-5 Experimental Section

Materials

Phosphoramidite monomers carrying azobenzene and its derivatives were synthesized as previously described.[7b] All conventional phosphoramidite monomers, CPG columns, the regents for DNA and RNA synthesis, and Poly-Pak cartridges were purchased from Glen Research Co. Some native DNAs (**D_nG** and **D_cC**) and RNAs (**R_cU**, **R_cA**, and **R_cG**) were purchased from Integrated DNA Technologies, Inc.

Synthesis and purification of oligonucleotides

All azobenzene-tethered oligonucleotides were synthesized on an ABI 3400 DNA/RNA Synthesizer by using typical phosphoramidite chemistry as described in a previous report.[5b] Synthesized DNA was purified by Poly-Pak cartridges and reversed-phase HPLC (Merck LiChrospher 100 RP-18(e) column). For RNA synthesis, 2′-*O*-t-butyldimethylsilyl (TBDMS) protected RNA amidite monomers were used with a Trityl-off strategy. Removal of 2′-*O*-TBDMS was accomplished using tetra-*n*-butylammonium fluoride (TBAF) and then desalted by NAP Columns (GE Healthcare NAP-10 Columns). All RNAs were finally purified by 20% polyacrylamide-8M UREA gel electrophoresis followed by reverse-phase HPLC. After purification, synthesized oligonucleotides were characterized by MALDI-TOF MS.

m/*z* calcd for $\mathbf{R_nG}$ [*M*-H^+]: 3119; found: 3120; *m*/*z* calcd for $\mathbf{R_cC}$ [*M*-H^+]: 3182; found: 3184; *m*/*z* calcd for $\mathbf{R_XG}$ [*M*-H^+]: 3495; found: 3496; *m*/*z* calcd for $\mathbf{R_YG}$ [*M*-H^+]: 3391; found: 3393; *m*/*z* calcd for $\mathbf{R_ZG}$ [*M*-H^+]: 3523; found: 3524; *m*/*z* calcd for $\mathbf{R_XA}$ [*M*-H^+]: 3789; found: 3480; *m*/*z* calcd for $\mathbf{R_XU}$ [*M*-H^+]: 3456; found: 3456; *m*/*z* calcd for $\mathbf{R_XC}$ [*M*-H^+]: 3454; found: 3456; *m*/*z* calcd for $\mathbf{D_XG}$ [*M*-H^+]: 3377; found: 3378; *m*/*z* calcd for $\mathbf{D_YG}$ [*M*-H^+]: 3391; found: 3394; *m*/*z* calcd for $\mathbf{D_ZG}$ [*M*-H^+]: 3405; found: 3406.

Photoisomerization of azobenzene and its derivatives

The light source for photoirradiation was a 150 W Xenon lamp. For the *trans* → *cis* isomerization, a UV-D36C filter (Asahi Tech. Co.) was used, and UV light (λ = 300-400 nm; 5.3 mW cm^{-2} was used to irradiate the solution of the duplex at 60 °C for 3 min. The *cis* → *trans* isomerization was carried out by irradiation with visible light (λ > 400 nm) through an L-42 filter (Asahi Tech. Co.) at 25 °C for 1 min. In both cases, a water filter was used to cut off the infrared light.

Spectroscopic measurement

UV/Vis spectra and circular dichroism (CD) spectra were measured with a JASCO model V-530 or V-550 UV/Vis and with a JASCO model V-820 CD spectrophotometer, respectively. Both instruments were equipped with programmed temperature controllers. Conditions of the sample solutions were as follows: [NaCl] = 100 mM, pH 7.0 (10 mM phosphate buffer), [DNA] = 5 μM.

Measurement of melting temperature

The melting curves of the duplexes were obtained by using the above apparatus to measure the change in absorbance at 260 nm vs. temperature, in which the temperature ramp was 1.0 °C min^{-1}. The T_m values were determined from the maximum in the first derivatives of the melting curves. Heating and cooling curves were measured, and the T_m values thus obtained coincided with each other to within 2.0 °C. The T_m values presented here are an average of 2-4 independent experiments.

Determination of thermodynamic parameters

The enthalpy change ($\Delta H°$) and the entropy change ($\Delta S°$) for duplex formation were determined according to equation 1. [12]

$$T_m^{-1} = (2.30R/\Delta H°) \log(C_t/4) + (\Delta S°/\Delta H°) \quad (1)$$

where C_t is the total concentration of both strands composing the duplex (R is the gas constant). The C_t values were varied from 1.0 to 32 μM. The change of Gibbs free energy at 37 °C ($\Delta G°$ (310 K)) was calculated from the $\Delta H°$ and the $\Delta S°$.

NMR measurements

NMR samples were prepared by dissolving three times lyophilized DNA, which contained both strands of a duplex, in a H_2O/D_2O 9:1 solution containing 10 mM sodium phosphate (pH 7.0), and the concentration of the duplex was adjusted to 1.0 mM. NaCl was added to a total sodium concentration of 200 mM. After NMR measurements in H_2O/D_2O, the samples were lyophilized again and dissolved in a D_2O solution. NMR spectra were measured by using a Varian INOVA spectrometer (700 MHz) equipped for triple resonance at a probe temperature of 280 K. 2D NOESY (mixing time of 150 ms) spectra[13] in H_2O/D_2O 9:1 were recorded by using the States-TPPI method[14] and a 3-9-19 WATERGATE pulse sequence for water suppression. FIDs (128 scans of each) of 2 K data points in the t_2 domain were collected for 512 data points in the t_1 domain. Prior to Fourier transformation, the spectra were zero-filled to give final 2 K × 1 K data points after apodization with a $\pi/2$-sifted squared sinebell function. 2D NOESY (mixing time of 100 and 200 ms), TOCSY (mixing time of 60 ms),[15] and DQF-COSY spectra[16] in D_2O were recorded by using the States-TPPI method without suppression of the H_2O signal. FIDs of the 2 K data points in the t_2 domain were collected for 512 data points in the t_1 domain. The number of scans for NOESY, TOCSY, and DQF-COSY in D_2O was 96. Prior to Fourier transformation, Gaussian window functions were applied to both dimensions.

Molecular modeling

The Insight II/Discover 98.0 program package was used for molecular modelling to obtain energy-minimized structures. The azobenzene residue was built by using the graphical program. The effects of water and counter ions were simulated by a sigmoidal, distance-dependant, dielectric function. The A-type duplex was used as the initial

structure, and AMBER force fields were used for calculation. Computations were carried out on a Silicon Graphics O2 workstation with the operating system IRIX64 Release 6.5. As an initial calculation structure, an azobenzene moiety (either *trans* or *cis* form) was placed between the base pairs.

2-6 Notes and References

[1] a) J. S. Mattick, *Bioessays.* **2003**, *25*, 930-939; b) J. S. Mattick, I.V. Makunin, *Hum. Mol. Genet.* **2006**, *15*, R17-R29.

[2] J. A. Doudna, T.R. Cech, *Nature.* **2002**, *418*, 222-228.

[3] D. P. Bartel, *Cell.* **2004**, *116*, 281-297.

[4] a) A. Fire, S. Xu, M. K. Montgomery, S.A. Kostas, S.E. Driver, and C.C. Mello *Nature* **1998**, *391*, 806-811; b) J. Kurreck, *Angew. Chem., Int. Ed.* **2009**, *48*, 1378-1398.

[5] a) H. Asanuma, X. Liang, H. Nishioka, D. Matsunaga, M. Z. Liu, M. Komiyama, *Nat.Protocols* **2007**, *2*, 203-212; b) H. Kashida, X.G. Liang, H. Asanuma, *Curr. Org. Chem*. **2009**, *13*, 1065-1084, and references cited therein.

[6] X.G. Liang, H. Nishioka, N. Takenaka, H. Asanuma, *ChemBioChem.* **2008**, *9*, 702-705.

[7] G. Reid Bishop and Jonathan B. Chaires, *Current Protocols in Nucleic Acid Chemistry* **2002**, 7.11.1-7.11.8.

[8] X.G. Liang, H. Asanuma, H. Kashida, A. Takasu, T. Sakamoto, G. Kawai, M. Komiyama, *J. Am. Chem. Soc.* **2003**, *125*, 16408-16415.

[9] a) W. D. Wilson, L. Ratmeyer, M. Zhao, L. Strekowski, D. Boykin, *Biochemistry* **1993**, *32*, 4098-4104; b) M. Nakamura, Y. Fukunaga, K. Sara, Y. Ohtoshi, K. Kanaori, H. Hayashi, H. Nakano, K. Yamana, *Nucleic Acids Res.* **2005**, ***33***, 5887–5895.

[10] J. SantaLucia, *Proc. Natl. Acad. Sci.* **1998**, *95*, 1460-1465

[11] a) H. Nishioka, X.G. Liang, H. Kashida, H. Asanuma, *Chem. Commun.* **2007**, 4354-4356. b) H. Nishioka, X.G. Liang, H. Asanuma, *Chem. Eur. J.* **2010**, *16*, 2054-2062.

[12] N. Sugimoto, Y. Shintani, M. Sasaki, *Chem. Lett.* **1991**, 1287-1290

[13] J. Jeener, B. H. Meier, P. Bachmann, R. R. Emst, *J. Chem. Phys.* **1979**, *71*, 4546-4553.

[14] D. Marion, M. Ikura, R. Tschudin, A. Bax, *J. Magen. Reson.* **1989**, *85*, 393-399.

[15] C. Griesinger, G. Otting, K. Wuthrich, R. Freeman, *J. Am. Chem. Soc.* **1988**, *110*, 7870-7872.

[16] A. J. Shaka, R. Freeman, *J. Magen. Reson.* **1983**, *51*, 169-173.

2-7 Appendix

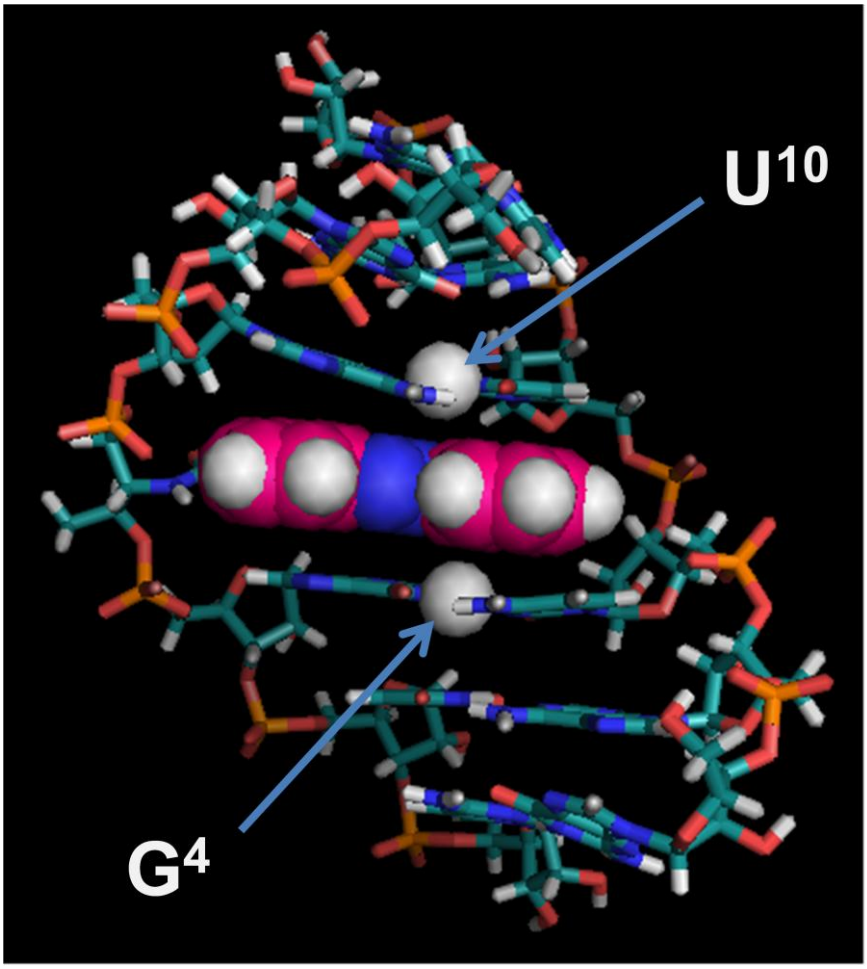

Appendix Figure 2-1. Structure of NMR-R_x/NMR-R_c duplex involving azobenzene moiety obtained from the computer modeling with the Insight II/Discover 98.0 program package. The azobenzene is highlighted in CPK (space-filling) model. The imino protons of U^{10} and G^4 are also high-lighted.

Chapter 3. Application of azobenzene-modified RNA to more effective and selective induction of RNA interference

3-1 Abstract

Although siRNA is very promising for nucleic acid drug, one of the problems of siRNA to be solved for therapeutic applications is selective RNA-induced silencing complex (RISC) formation with guide strand of siRNA. Here, we tried to use azobenzene-modified RNA to facilitate selective RISC formation, which resulted in the suppression of off-target effect in RNAi. Azobenzene was introduced to various positions on either the sense or antisense strand and the effect of introduced azobenzene on RNAi was investigated. We found that siRNA involving an azobenzene near the 5′-end of sense strand showed enhanced RNAi activity. Furthermore, it was also found out that this enhanced RNAi activity was caused by selective RISC formation with antisense strand, thus, azobenzene modification near the 5′-end of sense strand could efficiently reduce the off-target effect. In our strategy, various functional molecules can be used as RNA modifier, however, double stranded RNA with blunt ends should be needed to construct high-performance modified siRNA which can be applied to any targets. FInally, the mechanism of the improvement in RNAi efficiency caused by

modified siRNA was also investigated.

3-2 Introduction

As described in Chapter 1, RNA interference (RNAi) is a built-in system in living cells that strongly silences a specific gene through a short double-stranded RNA (siRNA).[1,2] siRNA is now commonly used as a tool for knockdown of a target gene to investigate its functional role *in vivo* due to its powerful silencing effect. However, the mis-incorporated passenger strand (sense strand) induces unexpected silencing of a non-target gene, which is one of the causes of non-specific gene silencing (off-target effects).[3] In the RNAi machinery, RISC should be formed only with the guide strand (antisense strand) for the specific targeting. Although siRNA was optimally designed to load the guide strand preferentially into RISC, it is difficult to completely avoid the unintended RISC assembly with the passenger strand. Accordingly, efforts have been made to improve the selective loading of the guide strand and increase in RNAi activity.

For the improvement of strand selectivity in RISC assembly, some groups have revealed that siRNAs with terminal mismatches[4,5] or an asymmetric terminal structure[6-8] facilitate RISC formation with the antisense strand and result in increased RNAi activity. This selective RISC assembly is principally based on the relative thermodynamic stability at the 5′-ends of siRNA.[9,10] However, it is hard to find a clear

and practical rule to design a sequence with mismatches or asymmetric structures for targeting a certain mRNA. Besides these synthetic natural siRNAs, chemical modification of siRNA is another very promising method to suppress off-target effects and increase in RNAi activity.[11-16] Furthermore, chemical modification also has other merits, such as great improvement of stability in serum and cellular uptake.[14] In particular, 2′-O-ribose methylation is effective to reduce off-target effects[15], and the introduction of a locked nucleic acid (LNA) is a typical successful means of improving selective RISC assembly.[16]

Over the last decade, we also have developed a new methodology for modification of DNA by the use of base-surrogates with D-threoninol as a scaffold for functional molecules[17]; a base-surrogate on D-threoninol is not in the form of an exchanged natural nucleotide, but is additionally inserted to the duplex (single-bulge form). This method enables the introduction of various functional molecules at any position and in any number without destroying the base-pairing of natural nucleotides and destabilizing the duplex. As shown in Chapter 2, we have demonstrated that not only DNA but also RNA tethering azobenzene on D-threoninol can also form a stable A-form duplex with a native RNA, and photoregulation of RNA hybridization has been realized.[18] All these results, as well as other successful siRNA modifications,[15,16] prompted us to introduce

an intercalator as a base-surrogate at a certain position in an siRNA to block the uptake of the passenger strand (sense strand) in order to minimize non-specific silencing and enhance RNAi efficiency.

In this chapter, we propose novel strategy for the suppression of non-specific gene silencing by use of chemically modified siRNA.

3-3 Results and Discussions

3-3-1 RNAi activity of azobenzene-modified siRNA

For evaluating the RNAi activity of chemically modified siRNA, we conducted RNAi experiment using human cells. We chose mPIASy gene (Mus musculus protein inhibitor of activated STAT 4), a mouse gene involved in the regulation of transcriptional activity, as an exogenous target gene and designed a 23-bp double-stranded RNA (dsRNA) with blunt ends as an siRNA to suppress the mPIASy expression (Figure 3-1).[19] In order to investigate the effect of a chemical modification on RNAi activity, we introduced an azobenzene moiety to various positions on either the sense or antisense strands (Figure 3-1). By mixing each azobenzene-modified 23-nt-long RNA strand with its complementary native strand, a modified dsRNA involving an azobenzene moiety can be prepared. Here, the 293FT cell line was selected

and each siRNA (with a final concentration of 33 nM) was co-transfected with an mPIASy expression vector (pCMV-SPORT6/mPIASy, see Experimental Section for details). The expressed protein was sampled at 48 h after transfection and analyzed by Western blotting (see also Experimental Section).

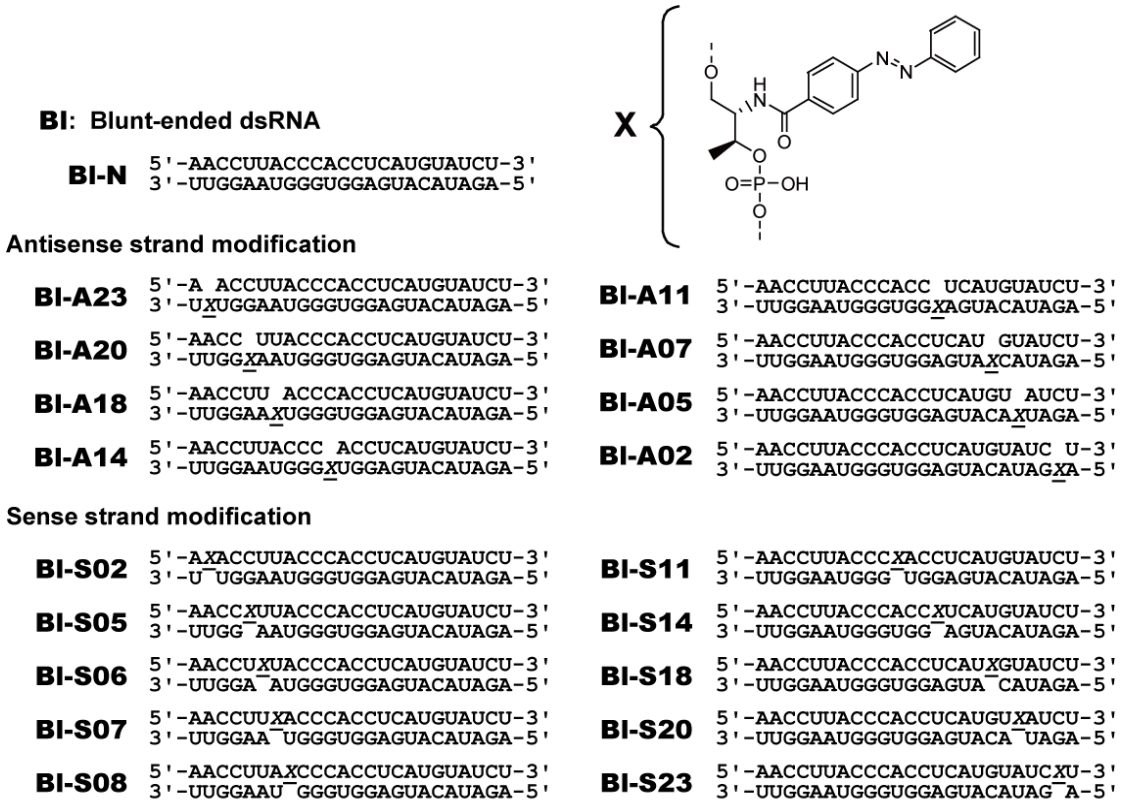

Figure 3-1. Sequences of native and modified RNA duplexes and chemical structures of azobenzene moiety introduced into RNA duplexes used in this study. The upper and lower strands depict sense and antisense strands, respectively. The number in the name of the siRNA indicates the position of an intercalator counted from the 5′-end of each strand.

Figure 3-2 shows the silencing ability of native and azobenzene-tethered siRNAs evaluated from the band intensity of expressed mPIASy. Here, β-actin was used as an

internal standard. When the mPIASy expression vector was transfected without siRNA (Control), mPIASy was efficiently expressed and a clear band of mPIASy protein was observed (compare lane 2 with 1 in Figure 3-2). In contrast, almost no mPIASy was observed in the presence of co-transfected native 23-bp blunt-ended dsRNA (Bl-N), indicating that its expression was efficiently suppressed via the RNAi pathway (compare lane Bl-N with lane Control in Figure 3-2). When an azobenzene was introduced into the antisense strand (Bl-A02 to A23 in Figure 3-1 or 3-2A), its silencing ability somewhat decreased as shown in Figure 3-2B. Deactivation was particularly severe with siRNA involving an azobenzene near the 5′-end (see Bl-A02 to A14 in Figure 3-2B). Interestingly, however, the introduction of an azobenzene moiety into the sense strand (Bl-S02 to S23) did not reduce the RNAi activity in most cases (Figure 3-2C). Rather, the RNAi activity seemed enhanced with Bl-S05 and Bl-S07, in which the azobenzene moiety was located near the 5′-end of the sense strand (see also Appendix Figure 3-1). In order to confirm the enhanced RNAi activity of siRNA, we further conducted RNAi experiments with additional BI-S06 and Bl-S08 under much lower concentrations. As shown in Figure 3-3, all these modified siRNAs exhibited much higher RNAi activity than the native one. In particular, Bl-S06 and Bl-S07 remarkably inhibited gene expression, even when only 1.0 nM of siRNA was used.

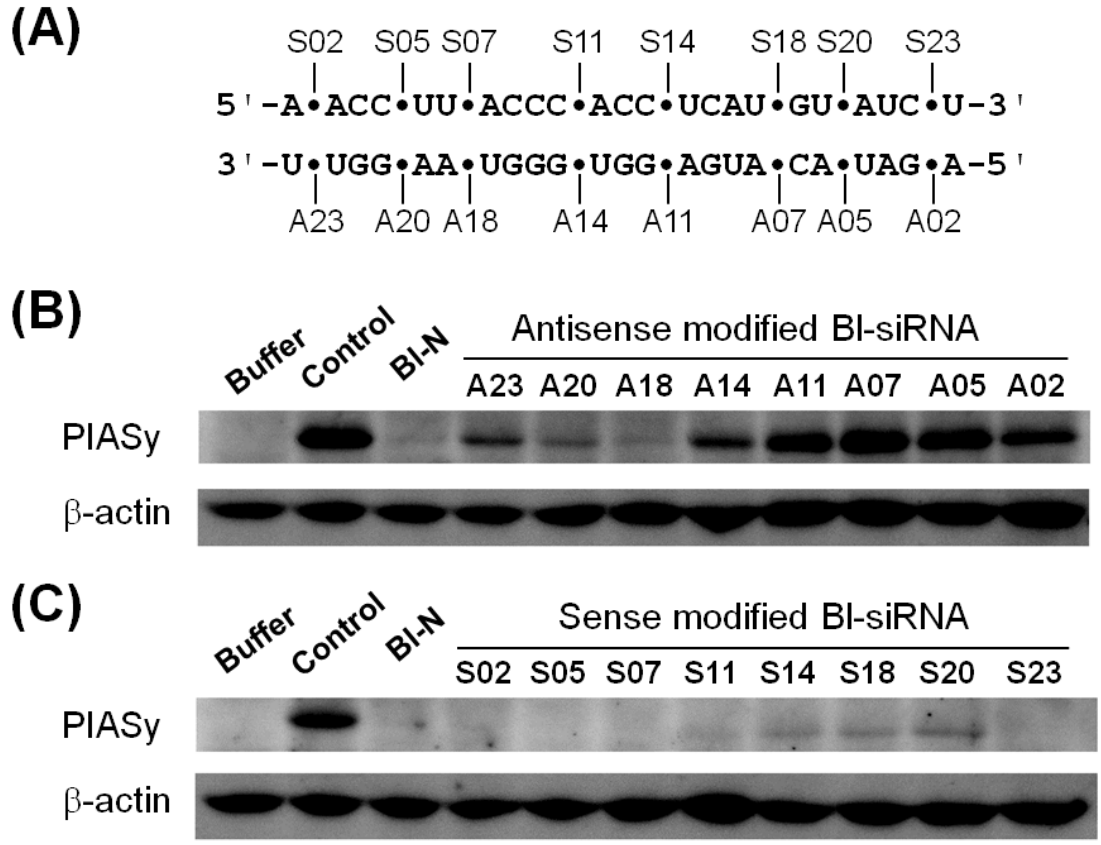

Figure 3-2. Effect of the position of azobenzene in dsRNA on RNAi activity against an exogenous mPIASy gene. A) Position of azobenzene in BI siRNA sequence. Each dot represents the position of introduced azobenzene (See Figure 3-1). An mPIASy expression plasmid and 33 nM of each siRNA modified at its antisense strand B) or sense strand C) were cotransfected into 293FT cells. After 48 h of incubation, the expression levels of mPIASy and β-actin, as an internal control, were determined by Western blot analysis.

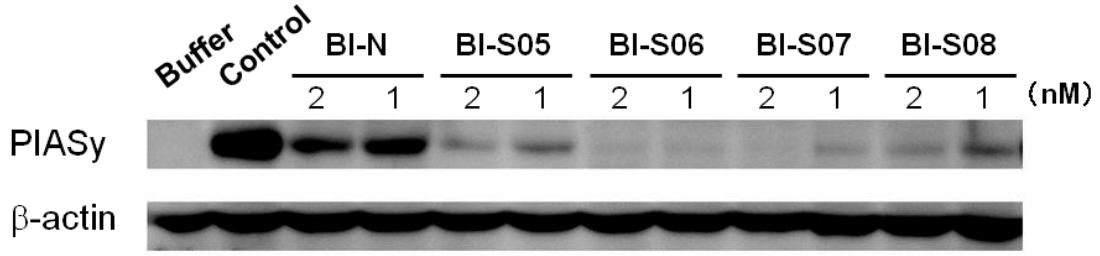

Figure 3-3. Western blot analysis after using lower concentrations (2, 1 nM) of BI-N, -S05, -S06, -S07, and -S08.

In order to confirm that reduced mRNA via the RNAi pathway contributed to the suppression of gene expression, we analyzed the amount of mPIASy mRNA by quantitative RT-PCR (qRT-PCR). As shown in Fig. 3-4, the amount of mRNA coincided well with the protein expression levels analyzed by Western blotting as shown in Figure 3-2B and 3-2C; the expressed mRNA by the presence of Bl-S05 or Bl-S07 was lower than that of native Bl-N, while Bl-A05 and Bl-A07 that strongly inhibited RNAi activity showed only a 60% reduction of mRNA expression (40% expression) compared with the control. It is noteworthy that Bl-S07, which exhibited the most efficient RNAi activity, reduced mRNA levels to nearly 5% of the control. On the basis of both Western blotting and qRT-PCR experiments, we can now conclude that the introduction of azobenzene near the 5′-end of the sense strand (Bl-S02 to Bl-S08) can enhance RNAi activity.

3-3-2 Improvement of strand selectivity of RISC formation

Although some previous studies indicate that in most cases chemical modification of RNA reduces RNAi activity[12, 20], we confirmed the enhanced RNAi activity of azobenzene-modified siRNA in the previous section. That is because, we thought, RISC assembly with antisense strand was more facilitated by introduced azobenzene.

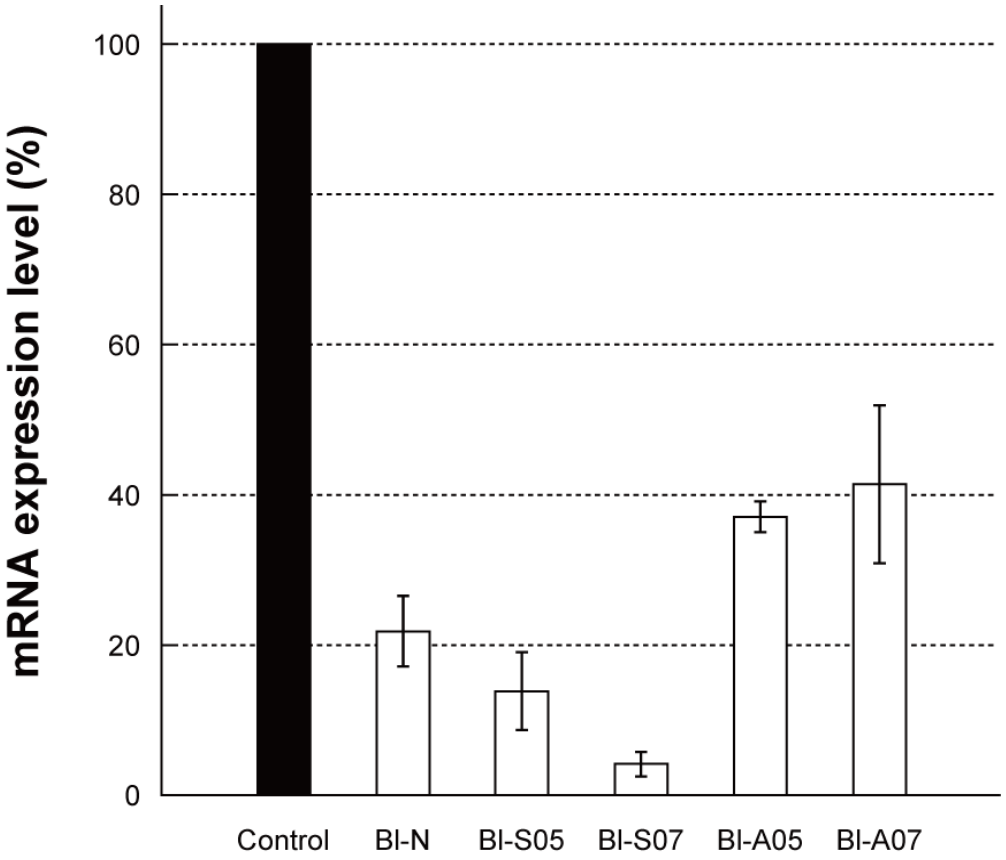

Figure 3-4. Suppression of mRNA expression by siRNA evaluated from quantitative RT-PCR experiments. The levels of mPIASy mRNA were determined by qRT-PCR and normalized by the endogenous GAPDH of 293FT. The mRNA expression level of the uninhibited control (plasmid alone) was set to 100%.

According to previous reports (Sano[6] and Sun[7]), it was reported that selective and facilitated uptake of the antisense strand can enhance RNAi activity, particularly, the introduction of a locked nucleic acid (LNA) is a typical successful means of improving selective RISC assembly.[16] Here, we hypothesized that the remarkable enhancement of RNAi activity was closely related to the selective loading of the antisense strand in RISC assembly, which was induced by the introduction of azobenzene into the sense

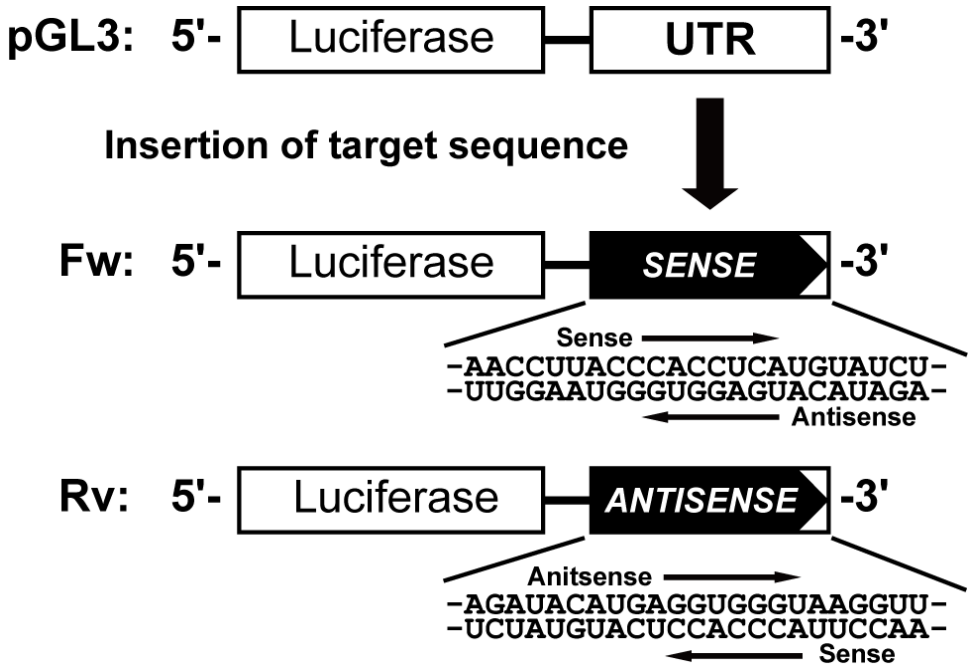

Figure 3-5. Construction of the two types of reporter plasmids (Fw and Rv) by inserting the target sequence of mPIASy (corresponding to Bl-N in Figure 3-1) into the firefly luciferase expression vector, pGL3, in different directions (*SENSE* or *ANTISENSE*). The transcripts from each plasmid contain the corresponding sequence of the sense or antisense strand in the 3′-UTR region.

strand. In order to analyze the strand selectivity and RNAi activity simultaneously, we conducted luciferase reporter assays as follows. We constructed two types of reporter plasmids, pGL3-mPIASy-Fw (abbreviated as Fw) and pGL3-mPIASy-Rv (abbreviated as Rv), involving the sequence of Bl-N in different directions (*SENSE* or *ANTISENSE*, see Figure 3-5) respectively, in the 3′-UTR region of the firefly luciferase expression vector, pGL3 plasmid-Basic with *brg1* promoter (see also Figure S3-2 in the Experimental Section). If an antisense strand of siRNA is loaded to the RISC, the *sense* sequence in mRNA transcribed from Fw is cleaved by the RNAi effect, which results in

the suppression of luciferase activity, but it does not affect Rv involving the *antisense* sequence. Similarly, the loading of the sense strand to RISC selectively suppresses the luciferase activity of Rv. Therefore, by analysing the luciferase activities of Fw and Rv with respect to *Renilla* luciferase activity as an internal control (relative luciferase activity; *firefly/Renilla*), both the strand selectivity and RNAi activity were evaluated (see also Experimental section).

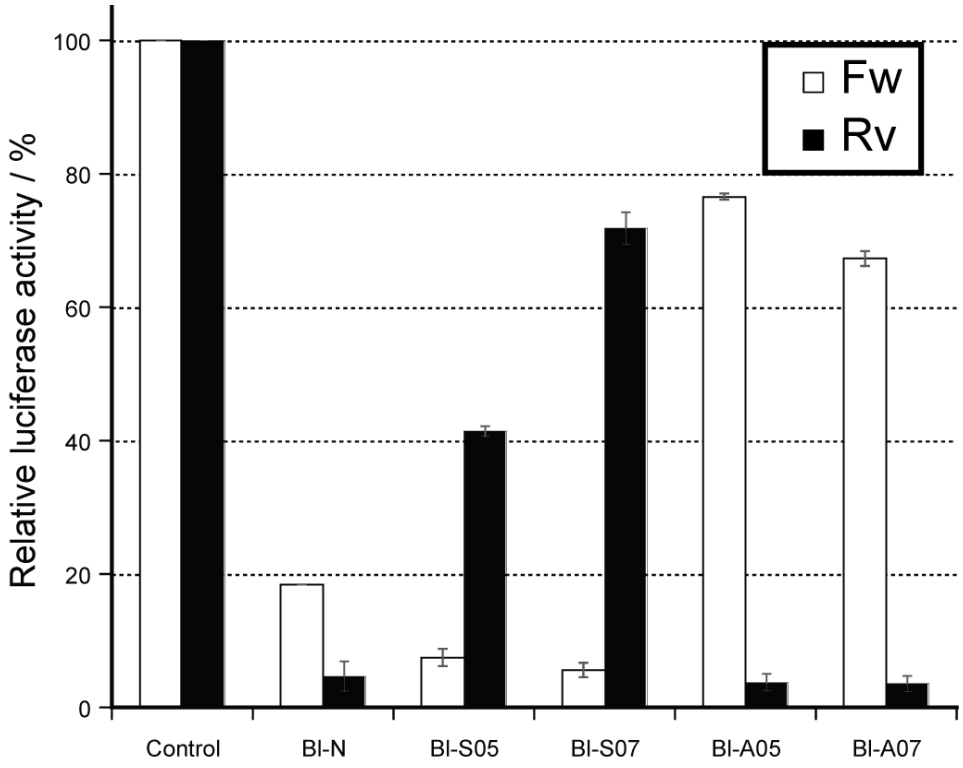

Figure 3-6. Effects of modified siRNA on the strand selection of RISC assembly. 18 nM of each siRNA (BI-N, -S05, -S07, -A05, and –A07) and reporter plasmid, pGL3-mPIASy-Fw (sense-target) or pGL3-mPIASy-Rv (antisense-target), and *Renilla* luciferase expression vector as an internal control, were cotransfected into 293FT cells. After 48 h of incubation, the relative luciferase activity (*firefly*/*Renilla)* was analyzed. The level of luciferase activity from the uninhibited control (target and control plasmids only) was set to 100%.

As depicted with white bars in Figure 3-6, RNAi activity against Fw corresponding to the target gene knockdown coincided well with the Western blot analyses (Figure 3-2); Bl-S05 and Bl-S07 inhibited luciferase activity more efficiently than native Bl-N did, whereas Bl-A05 and Bl-A07 involving an azobenzene near the 5′-end of the antisense strand lost RNAi activity. The enhanced RNAi activity was confirmed again by the IC_{50} values of Bl-N, -S05, and -S07 determined as 0.19, 0.12, and 0.09 nM, respectively, from the dose-response analyses (Figure 3-7).

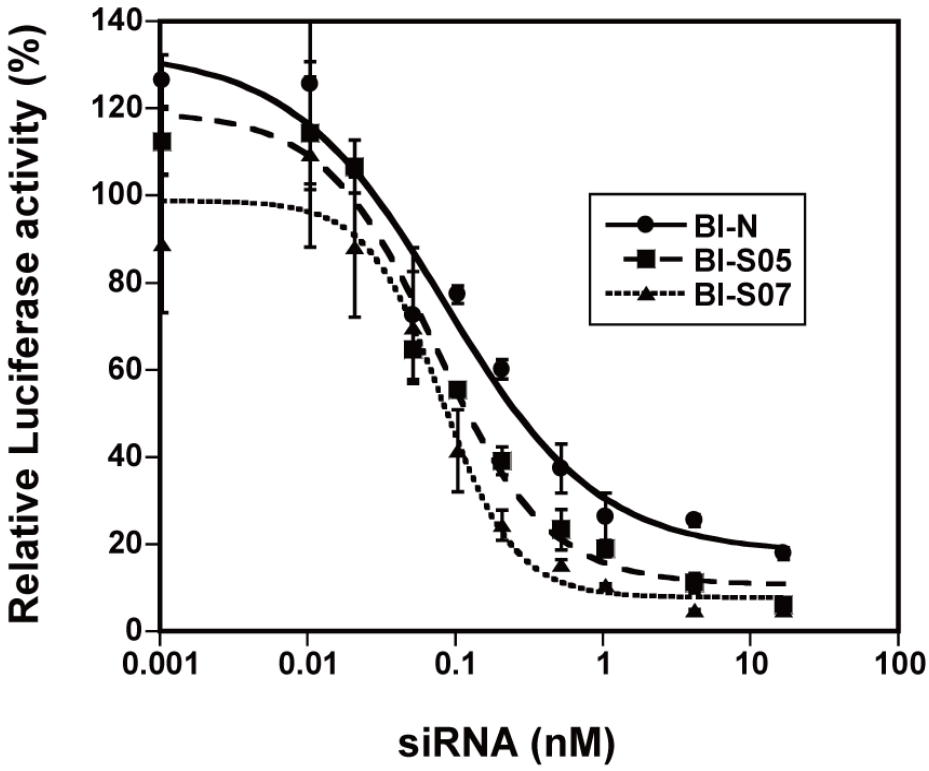

Figure 3-7. Dose-response curves on Bl-N (circles), Bl-S05 (squares), and Bl-S07 (triangles). Predetermined conc. of each siRNA (Bl-N, -S05, -S07) and reporter plasmid, pGL3-mPIASy-Fw (sense-target), and *Renilla* luciferase expression vector as an internal control, were cotransfected into 293FT cells. After 48 h of incubation, the relative luciferase activity (*firefly*/*Renilla)* was analyzed. The level of luciferase activity from the uninhibited control (target and control plasmids only) was set to 100%.

However, RNAi activity against Rv (black bars in Figure 3-6) revealed that native Bl-N efficiently suppressed Rv as well as Fw. RNAi activity of Bl-N against Rv was stronger than that against Fw, showing that the sense strand of Bl-N was more preferentially loaded into RISC than the antisense strand. This unexpected uptake of the sense strand is unfavourable for selective gene knockdown, because RISC involving an undesirable sense strand is one of the causes of off-target effects, i.e., non-specific gene silencing. However, interestingly, modification of the sense strand near the 5′-end remarkably decreased the RNAi activity against Rv (compare black bars of Bl-S05 and Bl-S07 to that of Bl-N in Figure 3-6), demonstrating that undesirable uptake of the sense strand was efficiently suppressed. On the other hand, Bl-A05 and Bl-A07, which lost RNAi activity against Fw, strongly knocked down Rv. Note that both Bl-A05 and Bl-A07 involve azobenzenes near the 5′-ends of the antisense strand, which is now used as the sense strand of siRNA for silencing expression of Rv (see Figure 3-1 for the sequence). The same phenomena as observed for Bl-S05 and Bl-S07 occurred for Bl-A05 and Bl-A07. Accordingly, the loss of their RNAi activity against mPIASy in the case of antisense modification was mainly attributed to the selective loading of the unmodified sense strand against the modified antisense strand, but not to deactivation of RISC assembled with the azobenzene-tethered antisense strand. Thus, it is now

conclusive that incorporated azobenzene promotes selective loading of the unmodified strand into RISC by strongly suppressing the uptake of the modified strand. We believe that selective RISC formation with the antisense strand by inhibiting the loading of the sense strand is one of the reasons for the enhanced RNAi activity (Figure 3-8).[6,7]

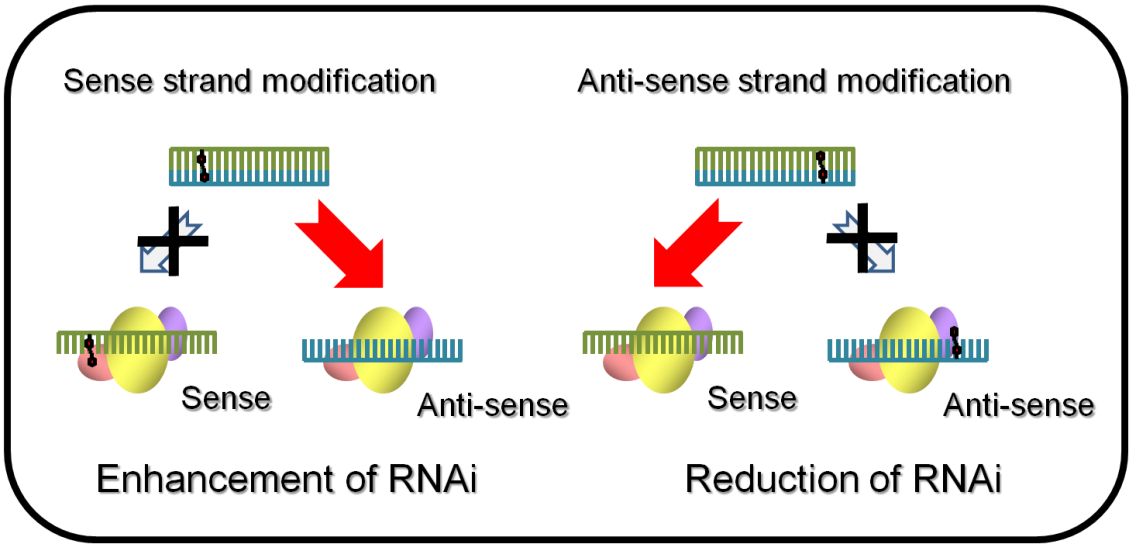

Figure 3-8. Illustration of selective RISC assembly with unmodified strands in the case of 5′-end modification.

3-3-3 Versatility of azobenzene-modified siRNA

Then, we conducted additional experiments of luciferase assay using different target plasmid and siRNA sequence to investigate the versatility of our method. We chose hPC2 gene (Human Polycomb 2) as a new target and designed native and modified siRNA that was entirely different from mPIASy siRNA (Figure 3-9). As same

as the experiment with mPIASy target, two types of reporter plasmids, pGL3-hPC2-Fw and pGL3-hPC2-Rv, involving the sequence of Bl2-N were newly constructed and RNAi activity and strand selectivity were investigated by luciferase assay.

As shown in Figure 3-10, unlike the mPIASy siRNA (Bl-N), native hPC2 siRNA (Bl2-N) efficiently suppressed Fw target (white bar), whereas it showed moderate silencing effect against Rv target (black bar), indicating that this siRNA sequence initially has high strand selectivity in RISC formation. In the case of sense strand modification, Bl2-S05 and Bl2-S07, RNAi activity against Rv was remarkably decreased although strong RNAi activity against Fw still observed. These results demonstrated that sense strand modification also efficiently and selectively inhibited RISC assembly with sense strand for hPC2 siRNA. Similarly, antisense strand modification also reduced RNAi activity against Fw by inhibiting the antisense strand loading in RISC formation. However, increase of RNAi activity was observed only in Bl2-A07, not in Bl2-A05, suggesting that the RNAi activity of modified siRNA might be affected by its sequence. That is because the relative thermodynamic stability at the 5′-ends of siRNAs is quite important for strand selection in RISC assembly.[9,10] Accordingly, since the similar effect of introduced azobenzene as observed in the case of mPIASy siRNA (see Figure 3-6) was verified in hPC2 siRNA, we believe that our

method, introduction of azobenzene near the 5′-end of sense strand, should be effective to suppress the unexpected RISC formation for any other target.

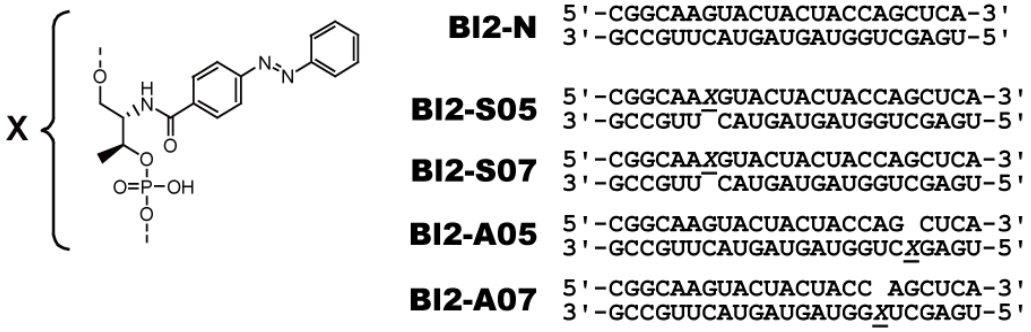

Figure 3-9. Sequences of native and modified RNA duplexes against hPC2. The upper and lower strands depict sense and antisense strands, respectively. The number in the name of the siRNA indicates the position of an intercalator counted from the 5′-end of each strand.

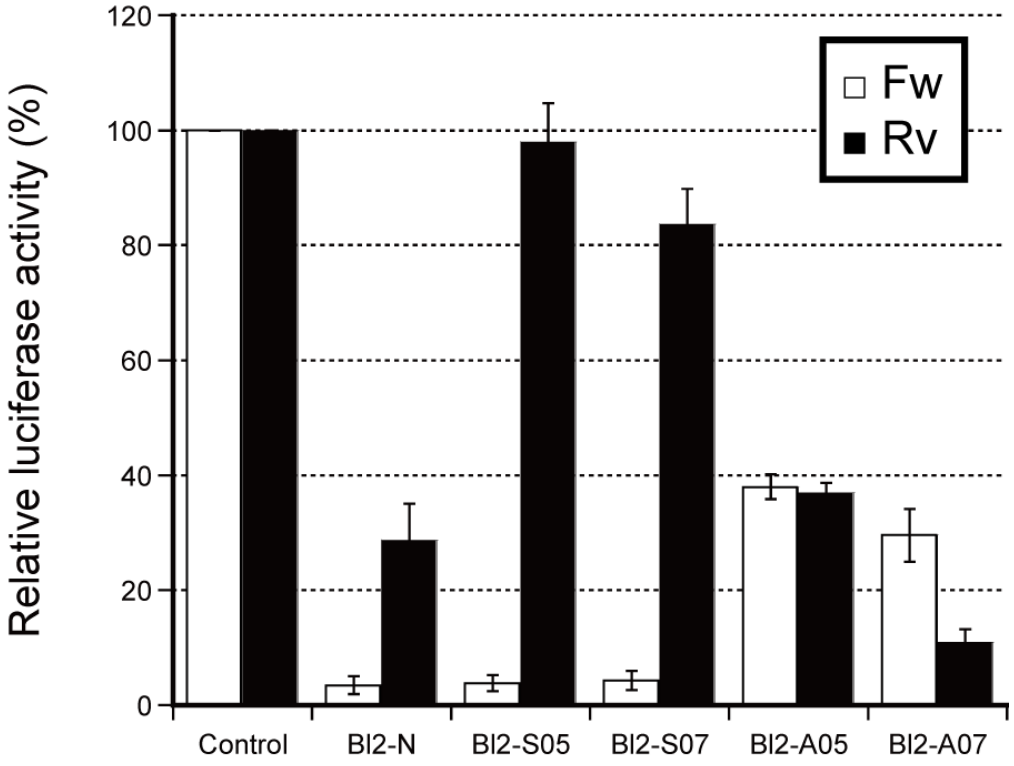

Figure 3-10. Effect of azobenzene on RNAi activity and strand selectivity for different target. Suppression of reporter plasmid, pGL3-hPC2-Fw (sense-target) or pGL3-hPC2-Rv (antisense-target) containing hPC2 siRNA (BI2-N) sequence, by modified hPC2 siRNA was analyzed by luciferase assay.

3-3-4 Effect of terminal structure of modified siRNA on RNAi activity

In general, a standard siRNA has a symmetric structure consisting of a 19-bp RNA duplex with 2-nt 3′-overhangs at both ends, which is probably the mimic of the natural siRNA produced by Dicer.[21-23] However, in this study, we used a 23-bp double-stranded RNA with blunt ends as an siRNA because recent studies have reported that RNAi activity can be enhanced using longer (~27-nt) or blunt-ended siRNA,[24] and for all these cases, the guide strand (antisense strand) should be selectively loaded to RISC to knockdown the target gene. Here, we also examined the effect of terminal structure on RNAi activity comparing blunt-ended and overhanged siRNAs. We designed native and modified siRNA consisting 19-nt duplex with 2-nt 3′-overhangs on both ends, for both mPIASy and hPC2 sequences (Figure 3-11).

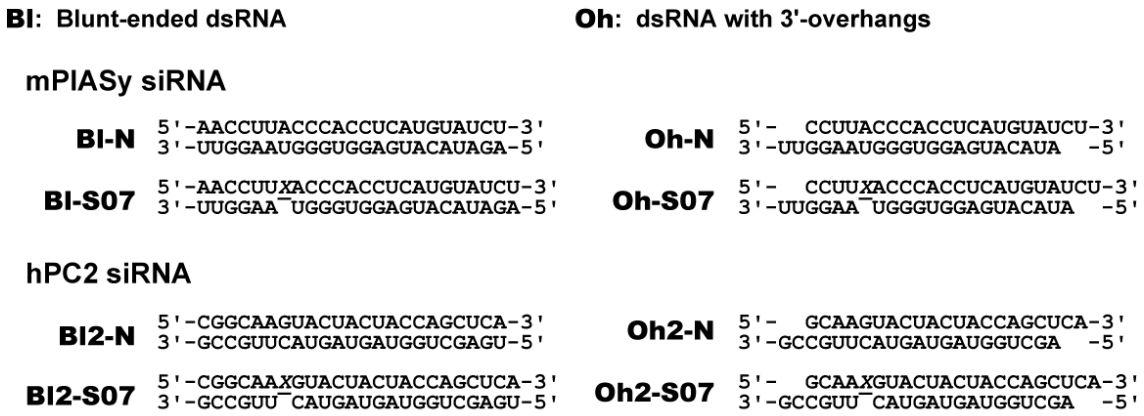

Figure 3-11. Sequences of native and modified siRNA with blunt-ends or 2-nt 3′-overhangs. Both mPIASy and hPC2 siRNA are shown.

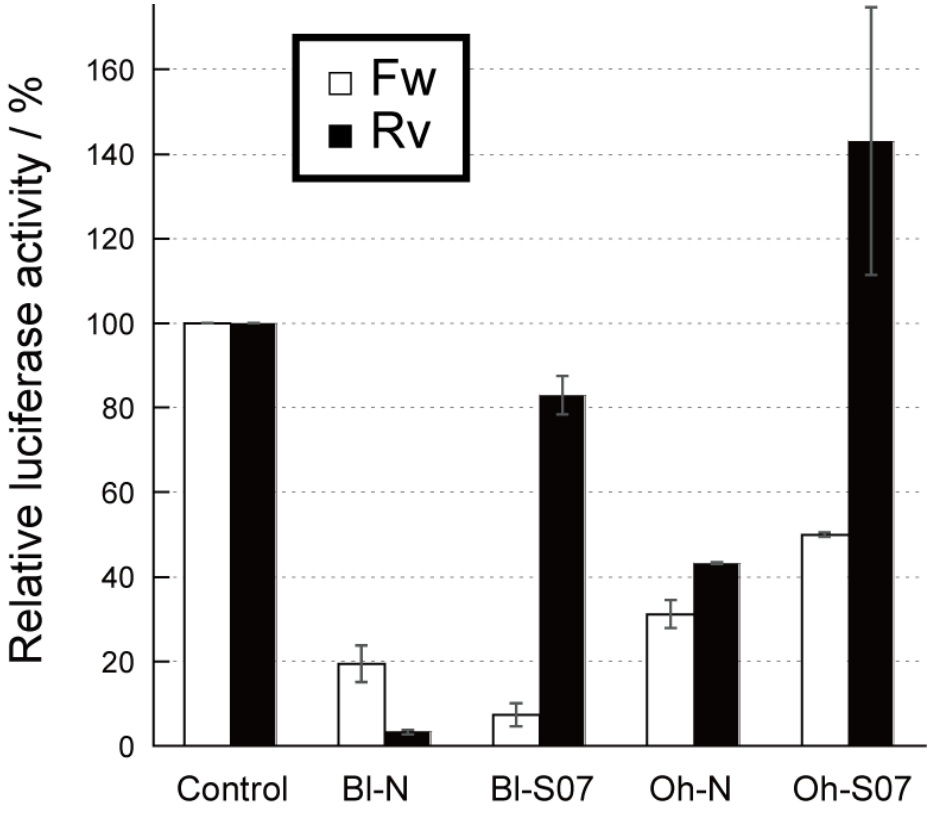

Figure 3-12. Effects of 2-nt 3′-overhangs in native or modified mPIASy siRNA on RNAi activity and strand selectivity.

As depicted in Figure 3-12, in the case of mPIASy target, we found that the RNAi activity of unmodified native Oh-N was much lower than that of Bl-N with blunt ends (compare Bl-N with Oh-N) for both Fw and Rv. These results imply that standard siRNA with 2-nt 3′-overhangs is not necessarily the best design for effective silencing of a target gene. In the case of modified siRNA, the introduction of azobenzene into the sense strand of this overhanged siRNA (Oh-S07) also improved strand selectivity as observed for modified blunt-ended siRNA (Bl-S07). However, the RNAi activity decreased greatly as compared with Bl-S07 against Fw. On the other hand, in the case of

hPC2 target (Figure 3-13), native overhanged siRNA (Oh2-N) already acquired ideal RNAi activity as compared with blunt-ended Bl2-N; remarkable suppression and high strand selectivity that was comparable to azobenzene-modified Bl2-S07. Since Oh2-N had excellent siRNA property, incorporation of azobenzene (Oh2-S07) further improved neither strand selectivity nor RNAi activity. On the basis of these results, introduction of azobenzene into overhanged siRNA could not improve RNAi efficiency although the effect of intercalator on overhanged siRNA rather depended on its sequence,. Accordingly, for our molecular design to improve RNAi activity, azobenzene should be introduced to a blunt-ended siRNA.

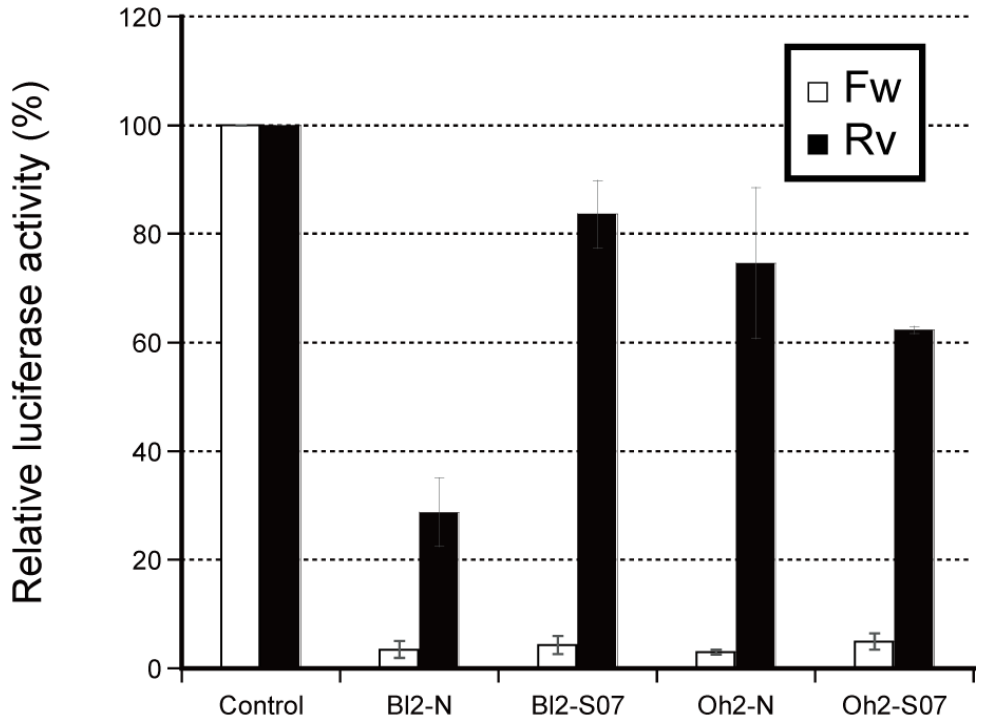

Figure 3-13. Effects of 2-nt 3′-overhangs in native or modified hPC2 siRNA on RNAi activity and strand selectivity.

3-3-5 Application of various functional molecules to siRNA modification

Then, we examined various functional molecules as candidate siRNA modifiers. Methyl red, which has a similar structure to azobenzene and is used as a quencher of fluorophores,[25] and Thiazole orange, which is a typical fluorophore used for visualizing oligonucleotides,[25] were introduced into 05 and 07 positions of sense strand as intercalators (Figure 3-14) and compared with azobenzene in terms of RNAi activity and strand selectivity. As shown in Figure 3-15, Methyl red (Bl-S05M and Bl-S07M) could also activate RNAi activity and greatly improve strand selectivity, similar to azobenzene. Similarly, Thiazole orange (Bl-S07T) remarkably improved both RNAi activity and strand selectivity even though its structure is quite different from azobenzene derivatives. These results clearly demonstrate that we can use various intercalators for improving RNAi activity and strand selectivity by tethering them on D-threoninol to a position close to the 5′-end of the sense strand.

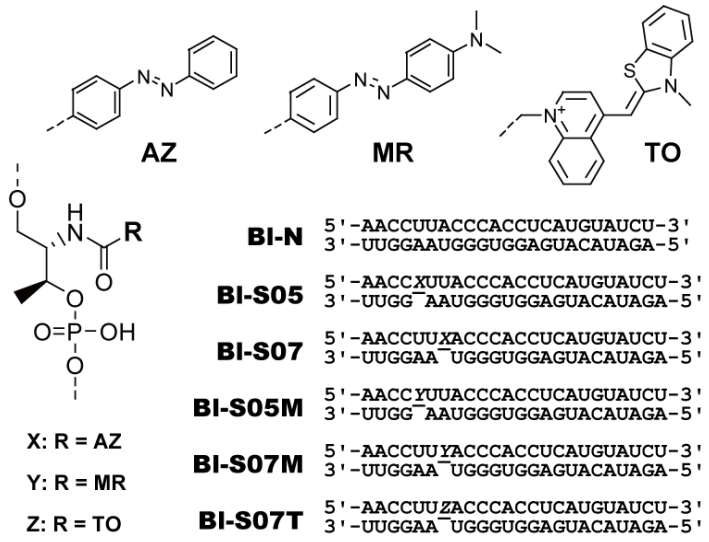

Figure 3-14. Modified mPIASy siRNAs with various functional molecules and chemical structures of intercalators introduced into siRNA.

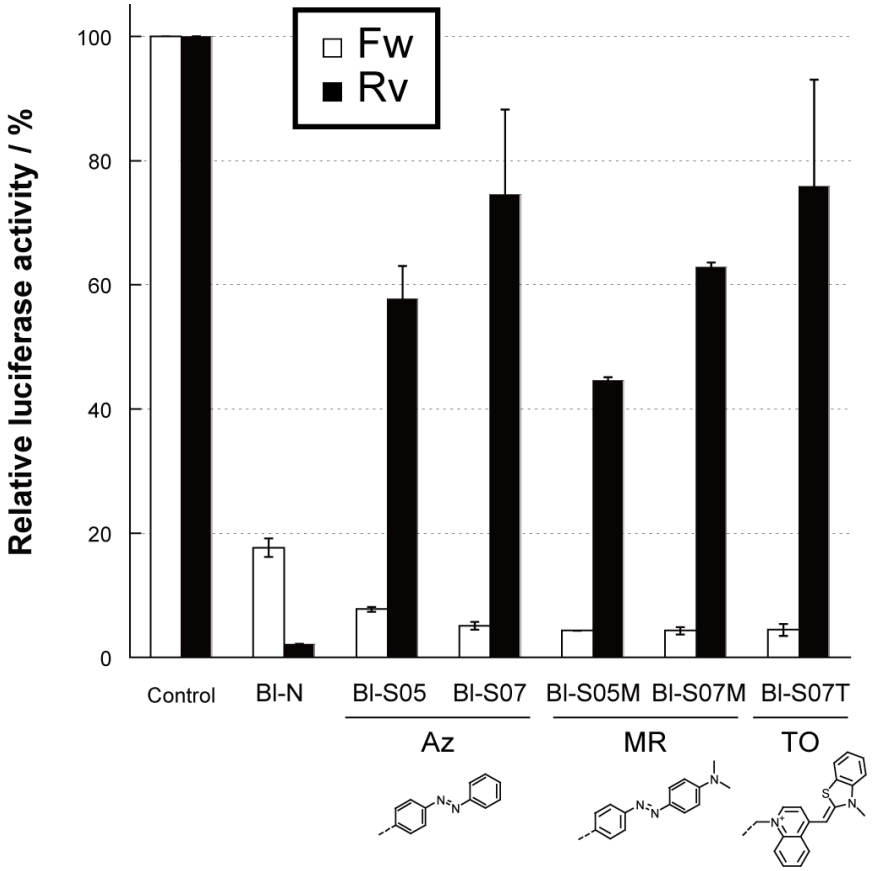

Figure 3-15. Effects of other intercalators on RNAi activity. siRNAs modified with Methyl red (BI-S05M, BI-S07M) or Thiazole orange (BI-S07T) were compared with azobenzene-modified siRNAs (BI-S05, BI-S07) in terms of their RNAi activities and strand selectivities.

3-3-6 Mechanism of selective RISC formation induced by introducing intercalators

Here, in this chapter, we succeeded in more effective and selective RNAi induction by introducing an intercalator at the 5′-end of sense strand. And the next question is how the intercalator affects RNAi machinery. It is very interesting to reveal that because the mechanism of strand selection is still unclear. So, perhaps, we can unravel the mystery of RNAi. First, we investigated the influence on the thermodynamic stability of siRNA duplex by introduced intercalator. We thought changes in relative thermodynamic stability at the 5′-ends of siRNAs should be crucial for strand selection in RISC assembly. Thus, melting temperatures (T_m) of modified siRNAs with various functional molecules (see sequences in Figure 3-14) were measured in Figure 3-16. As we examined in Chapter 2 (Table 2-1), azobenzene (Bl-S07) and Methyl red (Bl-S07M) slightly destabilize siRNA duplex, however, Thiazole orange (BL-S07T), because of larger chemical structure than azobenzene derivatives, showed strong destabilization effect. Although these differences in thermodynamic stability, each modification equally improved both RNAi activity and strand selectivity (see Figure 3-15). In addition, we also examined the effect of photoisomerization of azobenzene on RNAi activity because *trans* to *cis* isomerization of azobenzene efficiently destabilize RNA duplex (see Figure 2-8B in Chapter 2). As shown in Figure 3-17, however, any significant effect of

photo-isomerization was not observed in each siRNA modified with azobenzene (see sequences in Figure 3-1); siRNA activity of "*cis*-form" was similar to that of "*trans*-form". These results indicated that it was not a main factor for effective and selective induction of RNAi that the introduced intercalator changed the relative thermodynamic stability of siRNA.

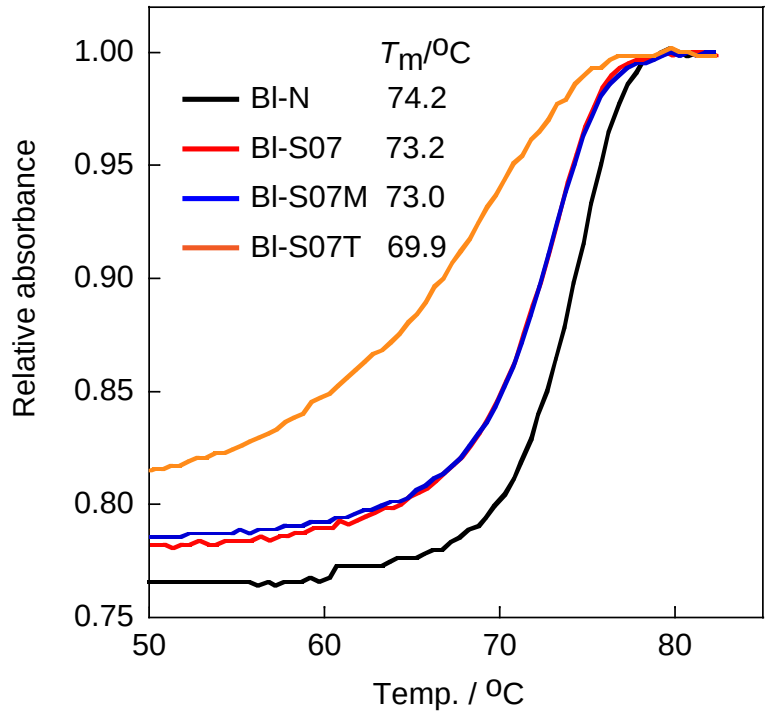

Figure 3-16. Melting curves of Bl-N (black line), Bl-S07 (red line), Bl-S07M (blue line), and Bl-S07T (orange line). [RNA] = 4□M, [NaCl] = 100 mM, pH 7.0 (10 mM phosphate buffer)

Figure 3-17. Effect of *trans*- and *cis*-azobenzene isomerized by UV irradiation on the RNAi activity.For the *trans* → *cis* isomerization, a UV-D36C filter (Asahi Tech. Co.) was used, and UV light (λ = 300-400 nm; 5.3 mW cm^{-2} was irradiated to the solution of the duplex at 60 °C for 3 min. Photo-isomerization was carried out before transfection.

The other possibility is that the introduced intercalator inhibits particular protein interaction with siRNA. According to previous reports, [6, 7] asymmetric terminal structure of siRNA can facilitate selective RISC formation and the effect of asymmetric 2-nt overhang at 3′-end of mPIASy siRNA on RNAi activity was also confirmed (Figure 3-18). Comparing blunt-ended siRNA (Bl-N), siRNA containing 3′-overhang at antisense strand (Ob-N, Overhang/blunt-end) suppressed Fw more efficiently, whereas it showed reduced activity against Rv, similar to modified siRNA tethering azobenzene near the 5′-end (Bl-S05 or Bl-S07 in Figure 3-6). Correspondingly, siRNA containing 3′-overhang at sense strand (Bo-N, Blunt-end/overhang) also behaved similarly to siRNA with antisense modification (Bl-A05 or Bl-A07 in Figure 3-6). Since the similar effect as observed in the case of modified siRNA was realized by asymmetric structure, we hypothesized that the introduced intercalator affected to form asymmetric terminal structure of siRNA. These above consideration led us to focus on an enzyme called Dicer, which is a kind of endonuclease that cleaves dsRNA with two base overhangs on 3′-end because Dicer is also said to be involved in RISC formation.[26] Thus, we thought that the intercalator might affect Dicer processing. Accordingly, in order to investigate how Dicer processes modified siRNA, we conducted Dicer cleavage assay by using native and modified siRNA with different terminal structure (Bl, Ob, Bo, and Oh)

shown in Figure 3-19 and 3-20. Each siRNA was mixed with recombinant Dicer enzyme and incubated at 37 ^{o}C for several hours, and then cleavage products were analyzed by native PAGE.

Bl-N 5'-AACCUUACCCACCUCAUGUAUCU-3'
3'-UUGGAAUGGGUGGAGUACAUAGA-5'

Bo-N 5'-AACCUUACCCACCUCAUGUAUCU-3'
3'-UUGGAAUGGGUGGAGUACAUA -5'

Ob-N 5'- CCUUACCCACCUCAUGUAUCU-3'
3'-UUGGAAUGGGUGGAGUACAUAGA-5'

Oh-N 5'- CCUUACCCACCUCAUGUAUCU-3'
3'-UUGGAAUGGGUGGAGUACAUA -5'

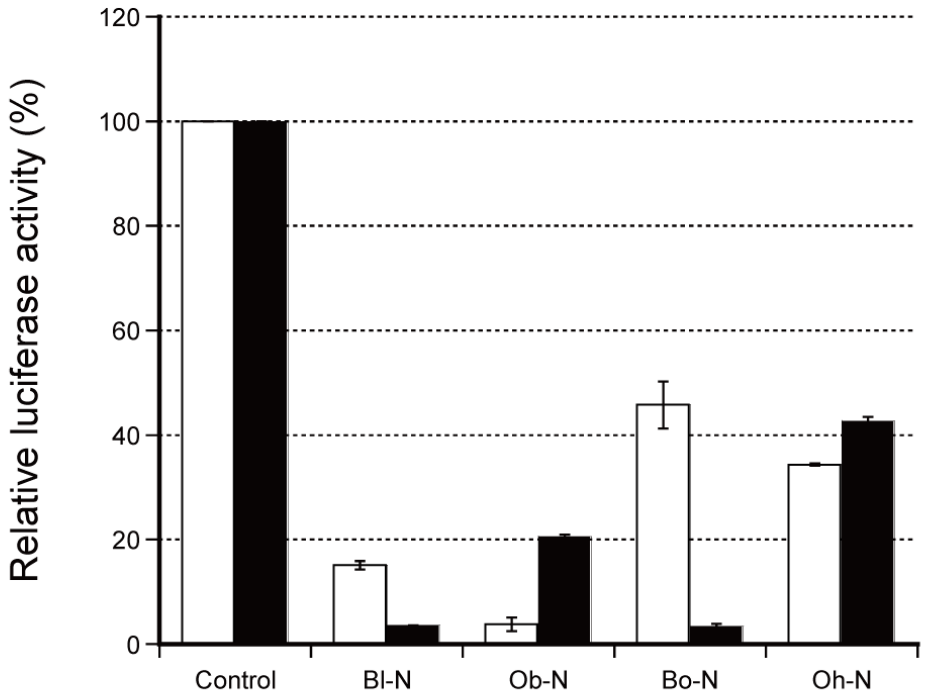

Figure 3-18. Effects of terminal structure on RNAi activity. Bl-N; blunt-ends at both termini, Ob-N; asymmetric termini with only 2-nt overhang at 3′-end of antisense strand, Bo-N; asymmetric termini with only 2-nt overhang at 3′-end of sense strand, Oh-N ; 2-nt overhangs at both termini.

In the case of native siRNA, blunt-ended siRNA (Bl-N), which is 23-bp RNA duplex, was cleaved to appear the distinct cleavage product as same size as the symmetric overhanged siRNA (Oh-N), which is 19-bp RNA duplex with 2-nt

3′-overhangs at both ends, whereas Oh-N was hardly processed by Dicer enzyme. On the other hand, siRNAs with asymmetric structure (Ob-N and Bo-N), which are 21-bp RNA duplex with 2-nt 3′-overhang at either end, were immediately processed to produce another 2-nt 3′-overhang and Oh-N were finally appeared. These results indicated that Dicer enzyme could recognize siRNA longer than 21-bp RNA duplex and produce symmetric 2-nt overhangs at both ends. Then, in the case of modified siRNA, the introduced azobenzene obviously delayed dicing for all kinds of siRNA. In particular, for Bl-S07, another cleavage product was appeared as same size as Ob-S07 and Bo-S07, indicating that Bl-S07 was processed to siRNA with asymmetric structure which resulted from Dicer processing at the only one side of blunt-ends as an intermediate of Oh-S07. Therefore, these results suggest that the production of this asymmetric terminal structure by introducing azobenzene probably affect RNAi activity and RISC formation. However, in the case of Bl-S07 and Ob-S07, of which azobenzene was introduced into the blunt-ended side, the smaller cleavage product than Oh-S07 was also observed. Namely, azobenzene also affected final product of Dicer processing and the distinct cleavage product should be clarified by additional experiments.

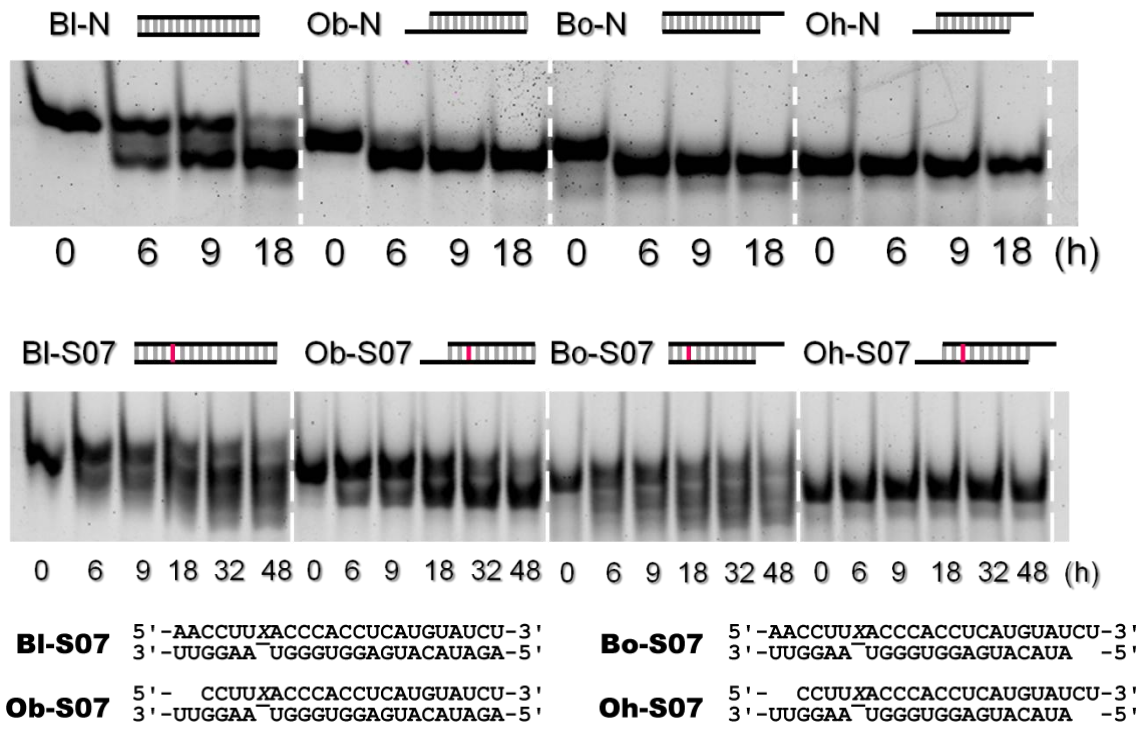

Figure 3-19. Dicer cleavage assay of native and modified siRNA with various terminal structures. Sequences of siRNA modified with azobenzene (X) are also shown here.

3-4 Conclusions

(1) We found that 23-nt blunt-end dsRNA modified with azobenzene on D-threoninol near the 5′-end of the sense strand greatly improved RNAi activity. Furthermore, by using luciferase assay, it was revealed that the incorporated azobenzene promotes selective loading of the unmodified strand into RISC by strongly suppressing the uptake of the modified strand.

(2) For the best design of modified siRNA, the intercalator should be introduced into blunt-ended RNA duplex. It will enable that our method can be applied to target

any gene.

(3) We also demonstrated that other functional molecules, such as Methyl red and Thiazole orange, could enhance RNAi activity and strand selectivity in RISC formation.

(4) From the result of Dicer cleavage assay, the introduced intercalator could disturb Dicer processing and facilitate the production of siRNA with asymmetric terminal structure. We concluded that this asymmetric terminal structure might probably affect strand selectivity in RISC formation.

3-5 Experimental Section

Synthetic siRNAs and duplex formation

The phosphoramidite monomers carrying Methyl red and Thiazole orange were synthesized as previously described.[27,28] All the conventional phosphoramidite monomers, CPG columns, the reagents for RNA synthesis, and Poly-Pak cartridges were purchased from Glen Research Co. Non-modified RNA strands were supplied by Integrated DNA Technologies (IDT) and azobenzene-modified RNA were purchased from Nihon Techno Service Co., Ltd.

RNA strands containing Methyl red and Thiazole Orange were synthesized on an ABI 3400 DNA/RNA Synthesizer by using typical phosphoramidite chemistry as described in a previous report.[27-29] For RNA synthesis, 2′-*O*-t-butyldimethylsilyl (TBDMS) protected RNA phosphoramidite monomers were used with Trityl-off

strategy. Removal of 2′-*O*-TBDMS was accomplished using tetra-*n*-butylammonium fluoride (TBAF) and then desalted by NAP Columns (GE Healthcare NAP-10 Columns). All RNAs were finally purified by 20% polyacrylamide-8M UREA gel electrophoresis followed by reverse-phase HPLC (Merck LiChrospher 100 RP-18(e) column). All RNA strands used in this study were characterized by MALDI-TOF MAS.

Table S3-1. Results of MALDI-TOF MAS:

Sense strand	[*M*-H$^+$]	Found
Bl-N (native 23 mer)	7145	7146
Oh-N (native 21 mer)	6487	6483
Bl-S02	7520	7520
Bl-S05	7520	7520
Bl-S06	7520	7517
Bl-S07	7520	7519
Bl-S08	7520	7516
Bl-S11	7520	7518
Bl-S14	7520	7522
Bl-S18	7520	7516
Bl-S20	7520	7520
Bl-S23	7520	7521
Bl-S05M	7564	7568
Bl-S07M	7564	7562
Bl-S07T	7644	7646
Oh-S07	6862	6861

Antisense strand	[*M*-H$^+$]	Found
Bl-N (native 23 mer)	7489	7489
Oh-N (native 21 mer)	6814	6817
Bl-A23	7864	7862
Bl-A20	7864	7861
Bl-A18	7864	7862
Bl-A14	7864	7865
Bl-A11	7864	7862
Bl-A07	7864	7864
Bl-A05	7864	7860
Bl-A02	7864	7861

siRNA preparation

RNA duplexes were prepared by mixing 20 μM each sense and antisense strand in annealing buffer (10 mM TAE, 0.25 mM EDTA, pH 8.3), and incubated for 5 min at 95°C, followed by cooling to room temperature for 0.5- 1h.

Plasmid construction

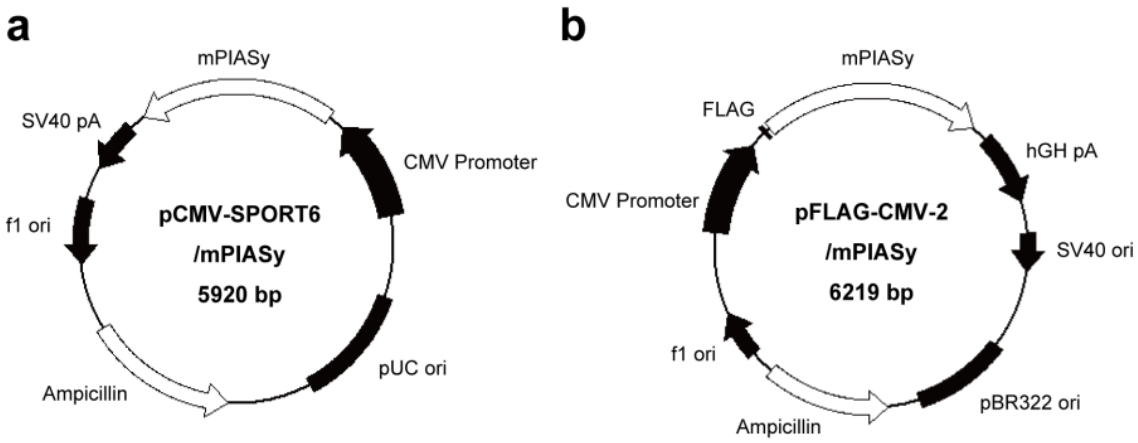

Figure S3-1. Vector maps of mPIASy expression vectors

Plasmid vector (a) pCMV-SPORT6/mPIASy (Invitrogen Clone ID: 4236082) and (b) pFLAG-CMV-2/mPIASy used as the mPIASy (Mus musculus Protein Inhibitor of Activated STAT 4) expression vector for western blot analysis (a) and qRT-PCR. (b), respectively. To create pFLAG-CMV-2/mPIASy, mPIASy coding region was amplified from pCMV-SPORT6/mPIASy by PCR using following forward primer: CATGAATTCGGCGGCAGAGCTGGTGGAG (*Eco*R I site is underlined) and reverse primer: CATAGATCTTCAGCACGCGGGCACCAG (*Bgl* II site is underlined). The amplified DNA fragments were introduced into Multi Cloning site (MCS) in pFLAG-CMV-2 (Sigma-Ardrich).

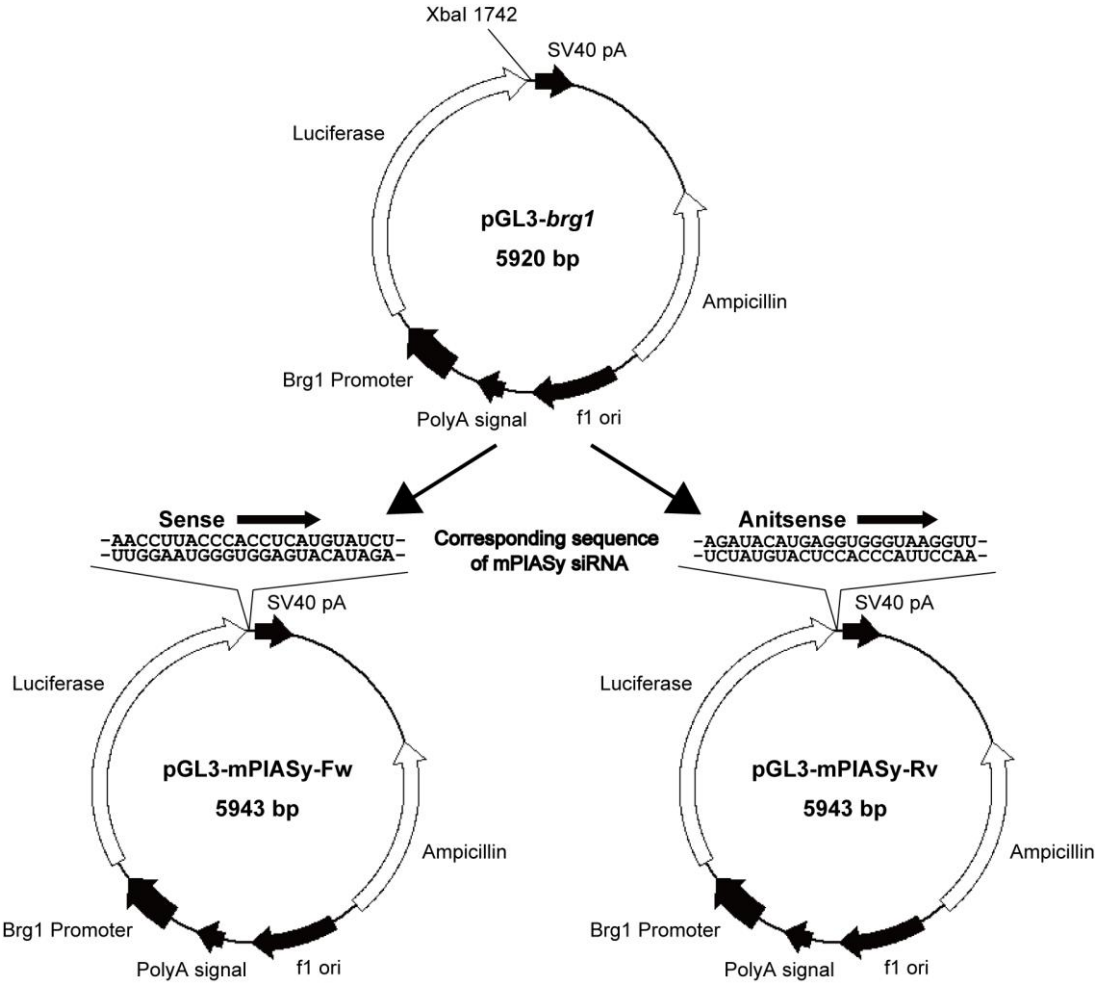

Figure S3-2. Vector maps of luciferase reporter plasmids containig mPIASy target sequence.

Plasmid vector pGL3-mPIASy-Fw (abbreviated as Fw) and pGL3-mPIASy-Rv (abbreviated as Rv) were used for luciferase reporter assay. For the construction of Fw and Rv, DNA fragments containing corresponding sequence of mPIASy siRNA (Bl-N, Scheme 1 in main article) with *Xba* I restriction site was prepared as follows: Sense fragment: 5′-CTAGAACCTTACCCACCTCATGTATCT-3′ and Antisense fragment: 5′-CTAGAGATACATGAGGTGGGTAAGGTT-3′ (*Xba* I sites are underlined. The sequence on the dash line and dotted line represents sense and antisense sequence of mPIASy siRNA (Bl-N), respectively.). The DNA fragments were introduced into the 3′-UTR region of pGL3-*brg1* in different directions and the direction of the insert (Fw

or Rv) was confirmed by sequencing using sequencing primer, RVprimer4: GACGATAGTCATGCCCCGC. Plasmid pGL3-*brg1* which contains the promoter region of the mouse *brg1* gene into MCS in pGL3-Basic vector (Promega)[30] and *Renilla* luciferase expression vector containing the promoter region of the elongation factor Iα gene (vector map and sequence are not shown) were generously provided by Prof. Shinji Iijima (Department of Biotechnology, Nagoya Univ., Nagoya, Japan).

Cell culture

293 FT cells (Invitrogen) were cultured in Dulbecco's modified Eagle's medium (DMEM) supplemented with 10% fetal bovine serum, 80 μg/ml penicillin, 90 μg/ml streptomycin.

Transfection and Western blot analysis

293 FT cells were cultured in 24-well plates and reached to 70-90% confluent at the time of transfection. Cells were cotransfected with 1-33 nM of siRNA and 100 ng mPIASy expression vector (pCMV-SPORT6/mPIASy, Fig. S1a) by using Lipofectamine™ 2000 (Invitrogen) according to the manufacturer's instructions. After incubation at 37°C for 48 h, cells were washed with PBS and lysed in 100 μl SDS sample buffer (0.2 M Tris-HCl, pH 6.8, 3% SDS, 5% 2-Mercaptoethanol, 10% Glycerol and BPB). Protein samples were incubated for 5 min at 95°C, and separated by 7.5% SDS-PAGE, followed by electric transfer to the Hybond-P membrane (GE healthcare). The mPIASy and β-actin (as an internal control) were detected by using anti-mPIASy (sc-18247, Santa Cruz), anti-β-actin (AC-15, SIGMA) primary antibodies, and anti-goat (sc-2020, Santa Cruz), anti-mouse (sc-2005, Santa Cruz) horseradish

peroxidase-conjugated secondary antibodies, respectively. Each protein was visualized with Western lightning Plus reagent (Perkin Elmer).

qRT-PCR (related to Fig. 2 in main article)

293 FT cells were cotransfected with 18 nM of siRNA and 100 ng mPIASy expression vector (pFLAG-CMV-2/mPIASy, Fig. S1b) by using Lipofectamine^{TM} 2000. After incubation at 37^{o}C for 48 h, total RNA was isolated from transfected cells by using RNAiso reagent (TAKARA) and purified by ethanol precipitation according to the manufacturer's instructions. An amount of 1 -3 μg of total RNA was reverse-transcribed with reverse transcriptase (ReverTra Ace, Toyobo) to generate cDNA by using random primer pd(N)9. To quantify mRNA levels of mPIASy and GAPDH (as an internal control), real-time PCR was carried out on Light Cycler (Roche Applied Science) by using LightCycler® FastStart DNA MasterPLUS SYBR Green I kit (Roche Applied Science) and PCR primers as follows: mPIASy-F: 5′-AAGGTCAACCACAGCTACTG CTCA-3′ and mPIASy-R: 5′-AGCCACAGAGTAGCTCTTGCCATA-3′ for mPIASy, hGAPDH-F: 5′-TCGACAGTCAGCCG CATCTTCTTT-3′ and hGAPDH-R: 5′-ACCA AATCCGTTGACTCCGACCTT-3′ for GAPDH. Data were obtained from two independent experiments and the threshold cycle (C_t) was calculated with LightCycler® software.

Dual Luciferase reporter assay

Two types of reporter plasmids, pGL3-mPIASy-Fw (Fw) and pGL3-mPIASy-Rv (Rv), containing target sequence in the 3′-UTR region of the pGL3 plasmid (Fig S2) were used for luciferase reporter assay. Fw contains the code sequence of

5′-…AACCTTACCCACC TCATGTATCT…-3′, which will be transcribed to an mRNA containing the same sequence as the sense strand (5′-AACCUUACCCA CCUCAUGUAUCU-3′) in mPIASy siRNA (Bl-N, Scheme 1 in main article). On the other hand, Rv contains 5′-…AGATACATGAGGTGGGTAAGGTT…-3′ as the code sequence, which is complementary to the code sequence in Fw, and the transcribed mRNA contains the same sequence as the antisense strand in Bl-N (5′-AGAUACAUGAGGUGGGUAAGGU U-3′). If the antisense strand of siRNA is loaded to RISC, sense sequence in mRNA transcribed from Fw but not Rv is cleaved by RNAi, which results in the suppression of luciferase activity (*SENSE*-target). Similarly, loading of sense strand to RISC selectively suppresses the luciferase activity of Rv but not Fw (*ANTISENSE*-target). 293 FT cells seeded in 24-well plates were transfected with 18 nM of siRNA, 100 ng of firefly luciferase expression vector, pGL3-mPIASy-Fw or pGL3-mPIASy-Rv, and 2 ng of *Renilla* luciferase expression vector by using Lipofectamine^{TM} 2000. After incubation at 37^{o}C for 48 h, cells were washed with PBS and lysed in 1× Passive Lysis Buffer (Promega). Each 20 μl of lysate sample were transferred to 96-well plate and luciferase activity was measured by using Dual-Luciferase Reporter Assay System kit (Promega) according to the manufacturer's instructions with Multilabel Plate Reader (ARVO^{TM}X3, Perkin Elmer).

Dicer cleavage assay

Each siRNA (5 μM) was mixed with recombinant Dicer enzyme (Genlantis) in reaction buffer and incubated at 37 ^{o}C for several hours. At each time point, reaction was stopped by addition of stop solution and samples were collected to be analyzed by 20% native PAGE. Gels were stained with SYBR Green II (Takara) and cleavage products

were detected by FLA 300 (Fujifilm).

3-6 Notes and References

[1] A. Fire, S. Xu, M. K. Montgomery, S. A. Kostas, S. E. Driver, C.C. Mello, *Nature* **1998**, *391*, 806-811.

[2] S. M. Elbashir, J. Harborth, W. Lendeckel, A. Yalcin, K. Weber, T. Tuschl, *Nature* **2001**, *411*, 494-498.

[3] P. R. Clark, J. S. Pober, M. S. Kluger, *Nucleic Acids Res.***2008**, *36*, 1081-1097.

[4] H. Hohjoh, *FEBS Lett.* **2004**, *557*, 193-198.

[5] Y. Ohnishi, K. Tokunaga, H. Honjoh, *Biochem. Biophys. Res. Commun.* **2005**, *329*, 516-521.

[6] M. Sano, M. Sierant, M. Miyagishi, M. Nakanishi, Y. Takagi, S. Sutou, *Nucleic Acids Res.* **2008**, *36*, 5812-5821.

[7] X. Sun, H. A. Rogoff, C. J. Li, *Nat. Biotechnol.***2008**, *26*, 1379-1382.

[8] C. I. Chang, J. W. Yoo, S. W. Hong, S. E. Lee, H. S. Kang, X. Sun, H.A. Rogoff, C. Ban, S. Kim, C. J. Li, D. K. Lee, *Mol. Ther.* **2009**, *17*, 725-732.

[9] D. S. Schwarz, G. Hutvagner, T. Du, Z. Xu, N. Aronin, P. D. Zamore, *Cell* **2003**, *115*, 199-208.

[10] A. Khvorova, A. Reynolds, S. D. Jayasena, *Cell* **2003**, *115*, 209-216.

[11] Y. L. Chiu, T. M. Rana, *RNA* **2003**, *9*, 1034-1048.

[12] N. M. Bell, J. Micklefield, *ChemBioChem* **2009**, *10*, 2691-2703.

[13] Y. Li, C. He, P. Jin, *Chem. Biol.* **2010**, *17*, 584-589.

[14] T. Kubo, Z. Zhelev, H. Ohba, R. Bakalova, *Biochem. Biophys. Res. Commun.* **2008**, *365*, 54-61.

[15] A. L. Jackson, J. Burchard, D. Leake, *RNA* **2006**, *12*, 1197-1205.

[16] J. Elmen, H. Thonberg, K. Ljungberg, M. Frieden, M. Westergaard, Y. Xu, B. Wahren, Z. Liang, H. Ørum, T. Koch, C. Wahlestedt, *Nucleic Acids Res.* **2005**, *33*, 439-447.

[17] a) H. Asanuma, X. G. Liang, H. Nishioka, D. Matsunaga, M. Liu, M. Komiyama, *Nat.Protocols* **2007**, *2*, 203-212. b) H. Kashida, X. G. Liang, H. Asanuma, *Curr. Org. Chem.* **2009**, *13*, 1065-1084.

[18] H. Ito, X. G. Liang, H. Nishioka, H. Asanuma, *Org. Biomol. Chem.* **2010**, *8*, 5519-5524.

[19] Y. Sato, K. Miyake, H. Kaneoka, S. Iijima, *J. Biol. Chem.* **2006**, *281*, 21629-21639.

[20] J. Kurreck, *Angew. Chem., Int. Ed.* **2009**, *48*, 1378-1398.

[21] P. D. Zamore, T. Tuschl, P. A. Sharp, D. P. Bartel, *Cell* **2000**, *101*, 25-33.

[22] S. M. Elbashir, J. Martinez, A. Patkaniowska, W. Lendeckel, T. Tuschl, *EMBO J.* **2001**, *20*, 6877-6888.

[23] J. Martinez, A. Patkaniowska, H. Urlaub, R. Luhrmann, T. Tuschl, *Cell* **2002**, *110*, 563-574.

[24] D. H. Kim, M. A. Behlke, S. D. Rose, M. S. Chang, S. Choi, J. J. Rossi, *Nat. Biotechnol.* **2005**, *23*, 222-226.

[25] Y. Hara, T. Fujii, H. Kashida, K. Sekiguchi, X. G. Liang, K. Niwa, T. Takase, Y. Yoshida, H. Asanuma, *Angew. Chem. Int. Ed.* **2010**, *49*, 5502-5506.

[26] a) I. J. MacRae, K. Zhou, J. A. Doudna, *Nat. Struct. Mol. Biol.* **2007**, *10*, 934-940. b) W. F. Lima, H. Murray, J. G. Nichols, H. Wu, H Sun, T. P. Prakash, A.R. Berdeja, H. J. Gaus, S. T. Crooke, *J. Biol. Chem.* **2009**, *23*, 2535-2548.

[27] H. Kashida, T. Fujii, H. Asanuma, *Org. Biomol. Chem.* **2008**, *6*, 2892-2899.

[28] Y. Hara, T. Fujii, H. Kashida, K. Sekiguchi, X. G. Liang, K. Niwa, T. Takase, Y. Yoshida, H. Asanuma, *Angew. Chem. Int. Ed.*, **2010**, *49*, 5502-5506.

[29] H. Asanuma et al., *Nat.Protocols* **2007**, *2*, 203-212.

[30] T. Itoh, K.Miyake, T. Yamaguchi, M. Tsuge, H. Kaneoke, S. Iijima, *J. Biochem.*, **2010**, *149*, 301-309.

3-7 Appendix

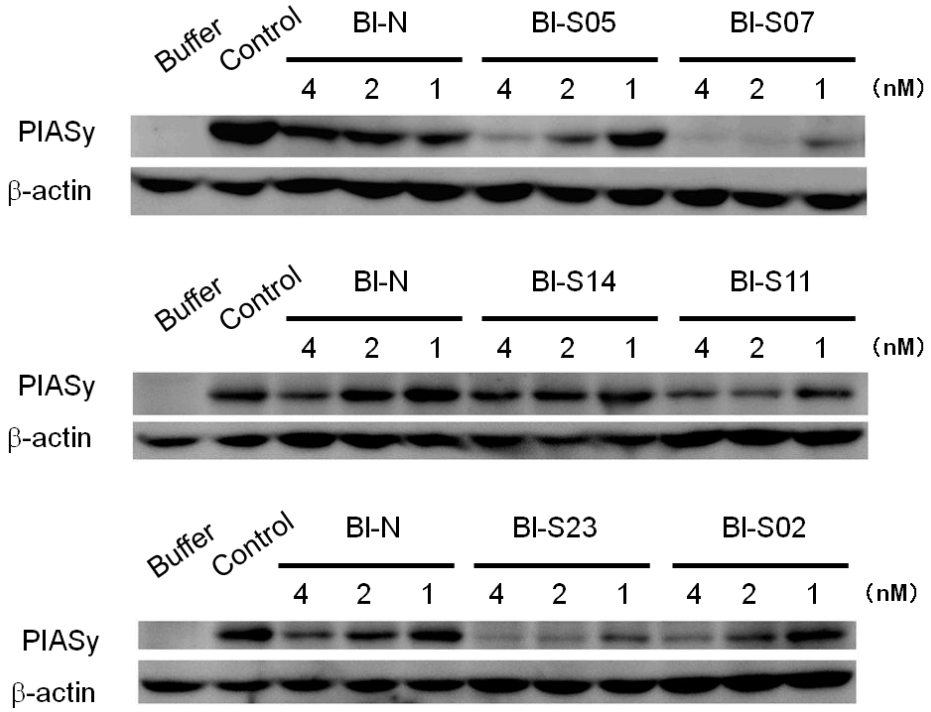

Appendix Figure 3-1. RNAi activity of siRNA with sense strand modification. Western blot analysis was carried out in the case of using lower concentration (4, 2, 1 nM) of BI-S02, -S05, -S07, -S11, -S14 and -S23 comparing with BI-N.

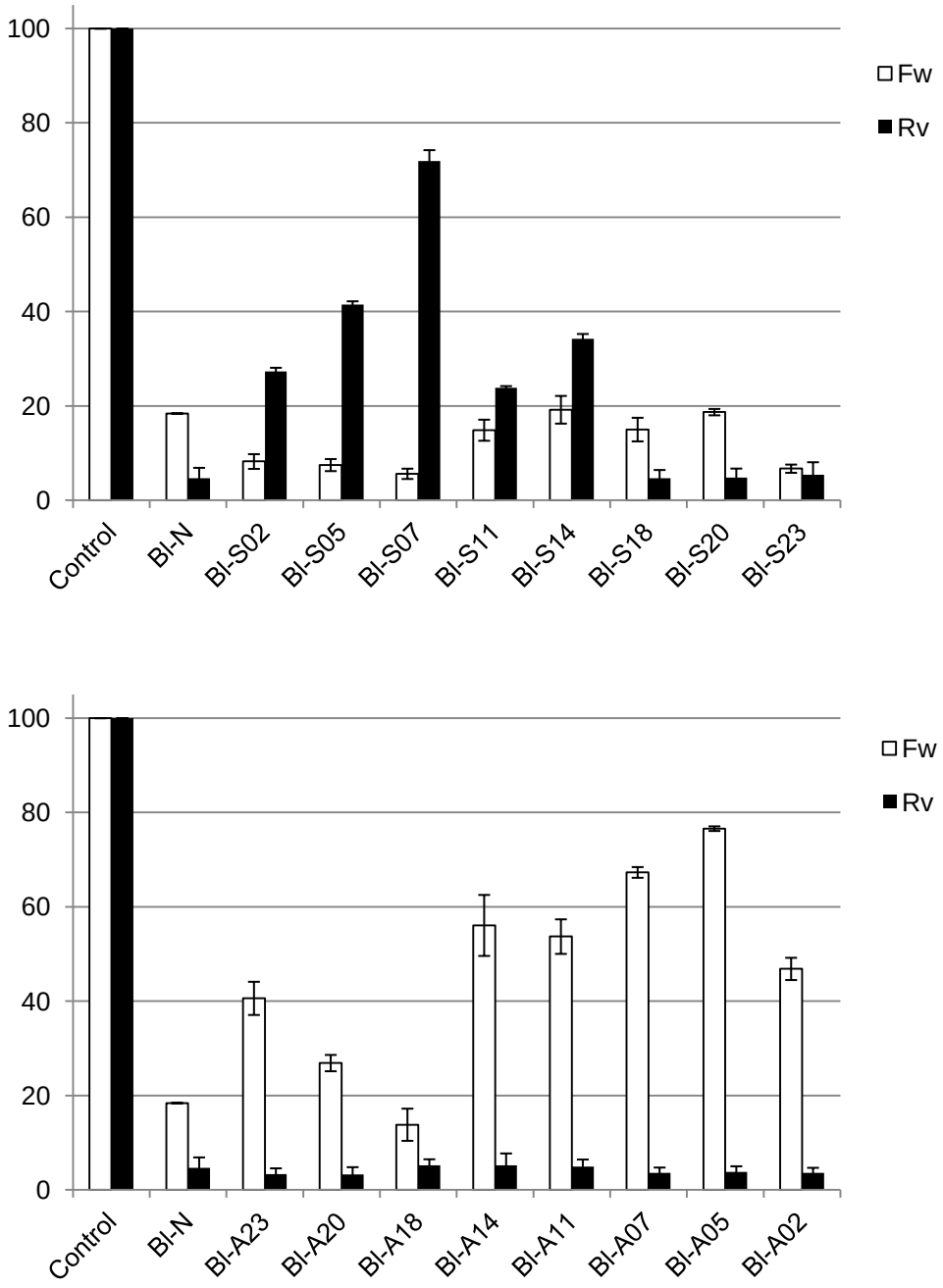

Appendix Figure 3-2. Results of luciferase assay using each modified mPIASy siRNA used in this study. pGL3-PIASy-Fw and pGL3-PIASy-Rv plasmids were used as Fw and Rv target, respectively.

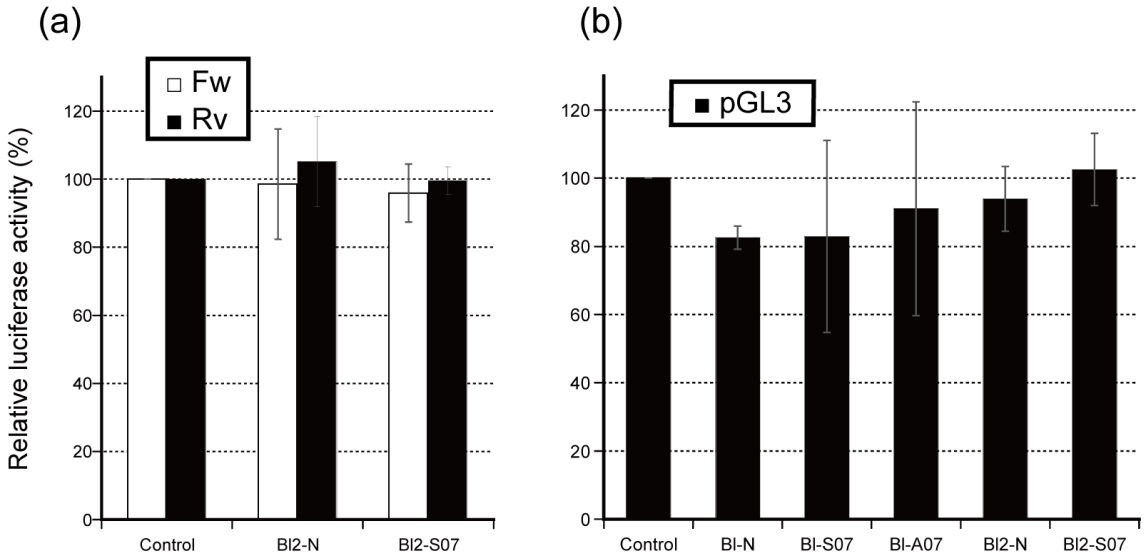

Appendix Figure 3-3. Effect of addition of non-target RNA duplex on the luciferase activity. (a) hPC2 siRNA (Bl2-N and Bl2-S07) that is not related to mPIASy was added to pGL3-PIASy-Fw and pGL3-PIASy-Rv plasmids. (b) siRNA that does not target pGL3 was added to original pGL3 plasmid, which contained neither mPIASy nor hPC2 target sequence.

Chapter 4. Construction of siRNA probe for real-time monitoring of RISC formation

4-1 Abstract

A couple of fluorophore and quencher was introduced to siRNA to construct siRNA probe. Thiazole orange and Methyl red were selected as a fluorophore and a quencher, respectively, and they were introduced to the either strand as they faced each other to form the cluster. The results of luciferase assay revealed that siRNA tethering the fluorophore-quencher cluster near the 5′-end of sense strand showed sufficient RNAi activity and strand selectivity. Because of the efficient quenching effect, the siRNA probe can visualize the dissociation of RNA duplex by the drastic changes in fluorescence intensity. We applied this siRNA probe to the real-time monitoring of RISC formation.

4-2 Introduction

As described in Chapter 1, details of RNAi machinery, especially strand selection in RISC loading, are still unclear. The uncovering this mystery of RNAi should be necessary for further application of RNAi, such as therapeutic treatment. For the investigation of RNAi machinery, some groups have used dye-labeled siRNA.[1, 2] Helm

et al. reported a FRET-based visualization method by introducing a pair of fluorescein and tetramethlyrhodamin (TMR) to the end of each strand of siRNA.[3] However, these terminal modifications should be exposed possible risks to be eliminated from siRNA because of the enzymatic degradation of labeled RNA. Accordingly, the fluorescence from eliminated dyes must be the crucial noise for the precise imaging of target siRNA.

On the other hand, in our previous work, we have prepared several types of dye-clusters in DNA duplex by using the same base-surrogate strategy as developed in intercalator conjugation.[4] In DNA duplex, dyes are adjacent to each other between base-pairs and they can form the stable dye-cluster due to its large stacking interaction, therefore, this clustering in DNA duplex is quite effective for the quenching of fluorophores by appropriate quenchers.[5] Based on this technique, we also succeeded in construction of functional DNA probes,[6] and fluorescent label agents.[7] for specific detection of target DNA or RNA.

Recently, we found that this clustering effect was also available in RNA duplex. Consequently, we thought that we can investigate the RNAi machinery by using cluster-conjugated siRNA as a siRNA probe. For example, as shown in Figure 4-1, selective loading of fluorophore-label antisense strand enable to trace RISC, whereas in the duplex, fluorophore is quenched by fluorophore-quencher interaction, therefore, by

observing the changes in fluorescence intensity, we can realize real-time monitoring of RISC formation and get some key information to clarify the mechanism of RISC assembly. Furthermore, our inter-stranded modification will be hardly be eliminated from siRNA by RNA digestion.

In this chapter, we tried to construct siRNA probe for real-time monitoring of RISC formation by introducing fluorophore-quencher cluster motif to siRNA.

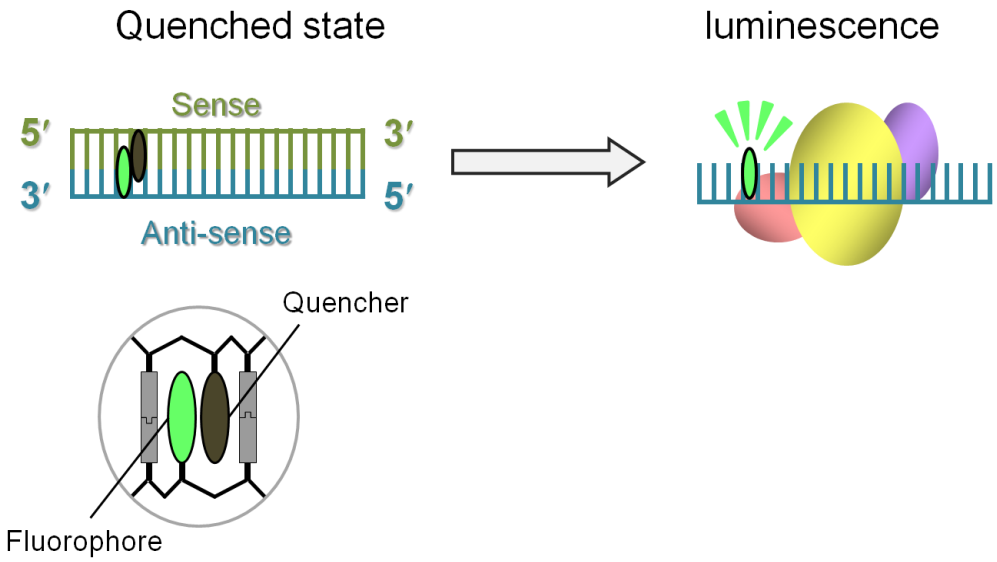

Figure 4-1. Illustration of RISC tracing by using siRNA tethering fluorophore-quencher cluster motif.

4-3 Results and Discussions

4-3-1 Construction of siRNA probe with fluorophore-quencher cluster and investigation of their RNAi activity

In order to design siRNA probe with fluorophore-quencher assembly for real-time monitoring of RISC assembly in living cells, Thiazole orange and Methyl red were selected as a fluorophore and a quencher, respectively because Methyl Red effectively quenches the emission of Thiazole orange in a DNA duplex.[6]. Methyl red was introduced into 05, 07, and 09 position of sense strand, and Thiazole orange was also introduced at corresponding position of antisense strand to construct "TO-MR" siRNA probe (Figure 4-2). The same sequence as mPIASy siRNA (Bl-N) was used for siRNA probe construction (see Figure 3-1 in Chapter 3).

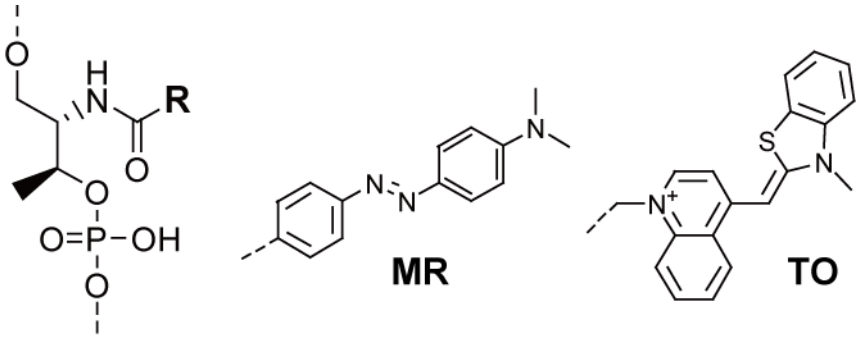

BI-N	5'-AACCUUACCCACCUCAUGUAUCU-3' 3'-UUGGAAUGGGUGGAGUACAUAGA-5'
TO-MR05	5'-AACC-MR-UUACCCACCUCAUGUAUCU-3' 3'-UUGG-TO-AAUGGGUGGAGUACAUAGA-5'
TO-MR07	5'-AACCUU-MR-ACCCACCUCAUGUAUCU-3' 3'-UUGGAA-TO-UGGGUGGAGUACAUAGA-5'
TO-MR09	5'-AACCUUAC-MR-CCACCUCAUGUAUCU-3' 3'-UUGGAAUG-TO-GGUGGAGUACAUAGA-5'

Figure 4-2. Sequences of modified siRNA for siRNA probe and chemical structures of dye molecules introduced into siRNA. Methyl red (MR) and Thiazole orange (TO) were used in this study.

At first, we investigated RNAi activity of siRNA probe by luciferase assay. Each

siRNA were cotransfected with pGL3-mPIASy-Fw (Fw target) and pGL3-mPIASy-Rv (Rv target) into 293FT cells and RNAi activity and strand selectivity were analyzed (see also Experimental section in Chapter 3). As shown in Figure 4-3, TO-MR09 showed reduced RNAi activity against both Fw and Rv, indicating that both sense and antisense strands were inhibited to be loaded into RISC. This result well coincided with the case of single azobenzene molecule introduction at center of sense strand (11 or 14 position) shown in Chapter 3 (Appendix Figure 3-2). On the contrary, TO-MR05 and TO-MR07 showed silencing effect against Fw as well as to native Bl-N, whereas their RNAi activity against Rv were greatly decreased. These results indicated that RISC assembly with antisense strand was facilitated by siRNA probe even if fluorophore was introduced near the 3′-end of antisense strand. Now, we concluded that the fluorophore-labeled antisense strand could be selectively loaded into RISC by introducing fluorophore-quencher assembly near the 5′-end of sense strand, and siRNA probe should be available for tracing of RISC formation.

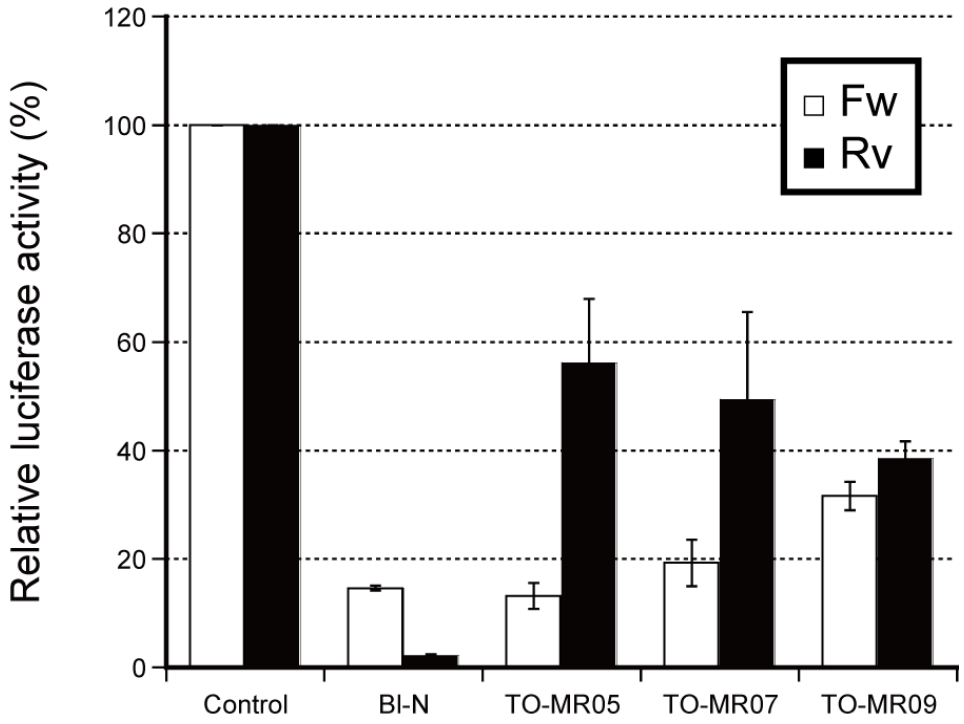

Figure 4-3. RNAi activity of siRNA probe which tethers fluorophore-quencher cluster.

4-3-2 Spectroscopic properties of siRNA prove

In previous section, we found that TO-MR05 was the most effective in RNAi activity and strand selectivity. Thus, we next investigated spectroscopic properties of TO-MR05 as a siRNA probe. First, we evaluated the quenching efficiency of the Thiazole orange and Methyl red cluster in siRNA comparing single- and double-stranded fluorophore labeled RNA (ssTO-05 and dsTO-05). As shown in Figure 4-4, single-stranded ssTO-05 (blue line) excited at 510 nm gave strong fluorescence at around 533 nm, which was slightly quenched in the case of double-stranded dsTO-05 (red line). That is because interactions between Thiazole orange and the adjacent

base-pairs showed quenching effect. On the other hand, TO-MR05 (green line) remarkably quenched the fluorescence of Thiazole orange, and the ratio of the emission intensity of ssTO-05 at 533 nm with respect to that of TO-MR05 was as great as 144 (i.e., signal/background (S/B) ratio = 144) due to the close stacking of the fluorophore and quencher. This quite large S/B ratio between the single- and double-stranded states proved that TO-MR05 has enough capability as a siRNA probe.

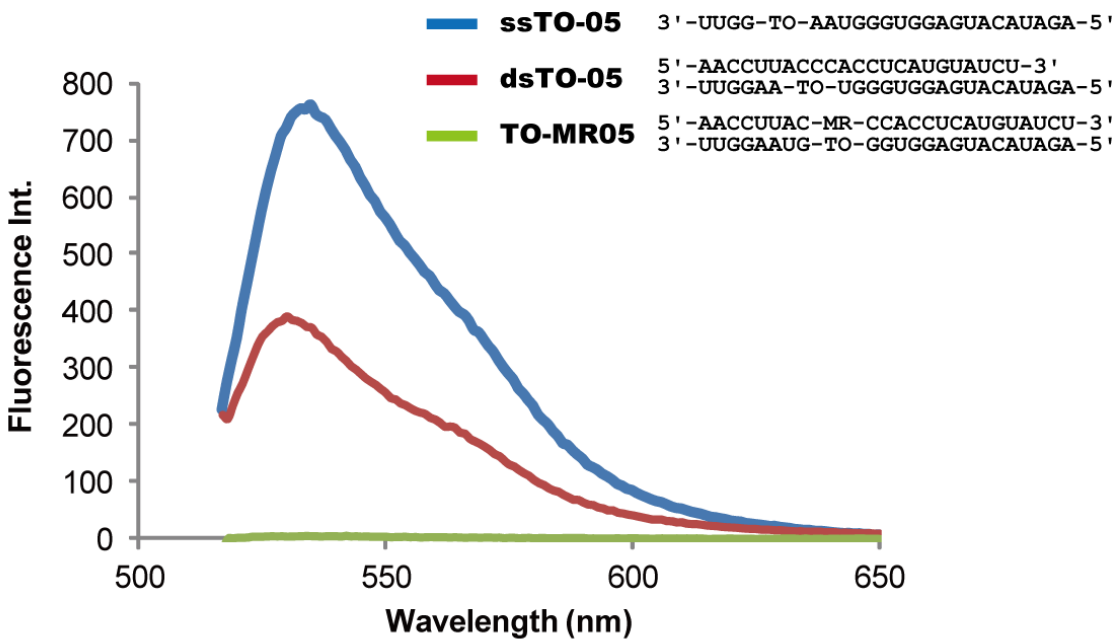

Figure 4-4. Fluorescence emission spectra of ssTO-05 (blue line), dsTO-05 (red line) and TO-MR05 (green line) excited at 510 nm. Solution conditions were as follows: 20 °C, [Antisense strand] = 0.4 μM, [Sense strand] = 0.2 μM, [NaCl] = 100 mM, pH 7.0 (10 mM phosphate buffer).

Then, we also investigated the influence of siRNA degradation on fluorescence intensity. As we mentioned in introduction, siRNA is exposed to some ribonucleases

after introduction into inside cells and very likely to be digested. If siRNA probe is degraded and fluorophore is eliminated from siRNA, the eliminated fluorophore must be fateful noise to the precise monitoring of RISC assembly. However, our design of siRNA probe which retains fluorophore inside of the RNA duplex can probably avoid fluorophore elimination caused by siRNA digestion. Therefore, we examined the change in the fluorescence intensity of siRNA probe after incubation in Hela cell lysate. Each siRNA, dsTO-05 and TO-MR05, was incubated in Hela cell lysate at 37^{o}C and their fluorescence intensity were measured at each time points (Figure 4-5). Interestingly, far from emitting Thiazole orange by siRNA digestion, fluorescence from dsTO-05 was gradually decreased according to the incubation time, indicating that siRNA degradation by ribonuclease quenched Thiazole orange. This phenomenon is thought to be due to the property of Thiazole orange itself, and this finding is very favorable to the precise monitoring. On the other hand, TO-MR05 efficiently quenched fluorescence from Thiazole orange after 24 h incubation in Hela cell lysate. Namely, quenching efficiency of TO-MR05 is not affected by siRNA digestion. These results indicated that our siRNA probe, TO-MR05, could efficiently and precisely be emitted only when siRNA duplex was dissociated to single strands.

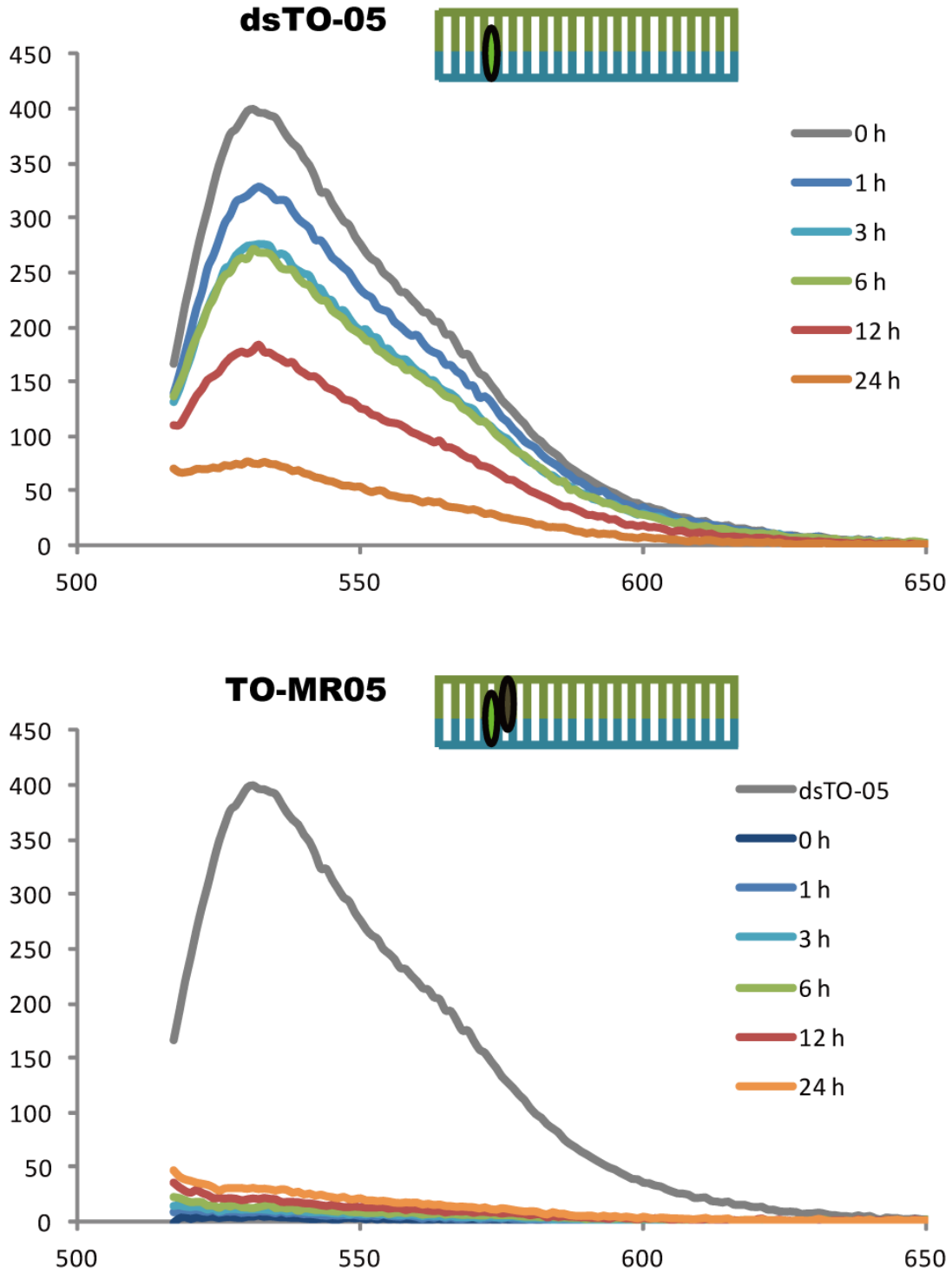

Figure 4-5. Fluorescence emission spectra of dsTO-05 and TO-MR05 incubated in Hela cell lysate. Every spectrum was measured at each time point of incubation.

4-3-3 Fluorescence monitoring of RISC formation in living cells

Finally we actually applied TO-MR05 as asiRNA probe to monitor RISC assembly in living cells. By simply observing the increase in fluorescence according to RISC assembly with fluorophore labeled antisense strand, we thought that it was possible to find out when RISC assembly would be begun after siRNA transfection. Therefore, siRNAs were transfected into Hela cells by using Lipofectamine 2000 and changes in fluorescence intensity at each time points were observed by fluorescence microscope (Figure 4-6). In the case of dsTO-05, as a control, strong fluorescence from Thiazole orange was clearly observed inside cells in only 5 hours after transfection. The result indicates that siRNA is successfully transfected and accumulated in Hela cells in 5 hours. By contrast, only a very weak fluorescence was observed from cells transfected with TO-MR-05, however, the increase of fluorescence intensity according to the incubation time was hardly observed even in after 2 days incubation. Our results showed that remarkable rise in RISC assembly could not be observed by changes in fluorescence intensity although TO-MR05 could also efficiently quench Thiazole orange inside the living cells. However, from the fact that TO-MR05 efficiently suppressed target gene (white bar in Figure 4-3), RISC must be formed with fluorophore labeled antisense strand correctly. In fact, fluorescence of Thiazole orange,

though it was very weak, was also observed from cells transfected with TO-MR05 in 5 hours after transfection. Combining above these findings, we can infer that RISC formation will be started within 5 hours after transfection and most of siRNA probe still form duplex, not to be used for RISC assembly. Namely, because only a few of them were involved in RISC formation, increase in fluorescence was hardly observed. Therefore, in our conclusion, RISC will be formed immediately after siRNA transfection and only a few of transfected siRNA are used for RISC assembly.

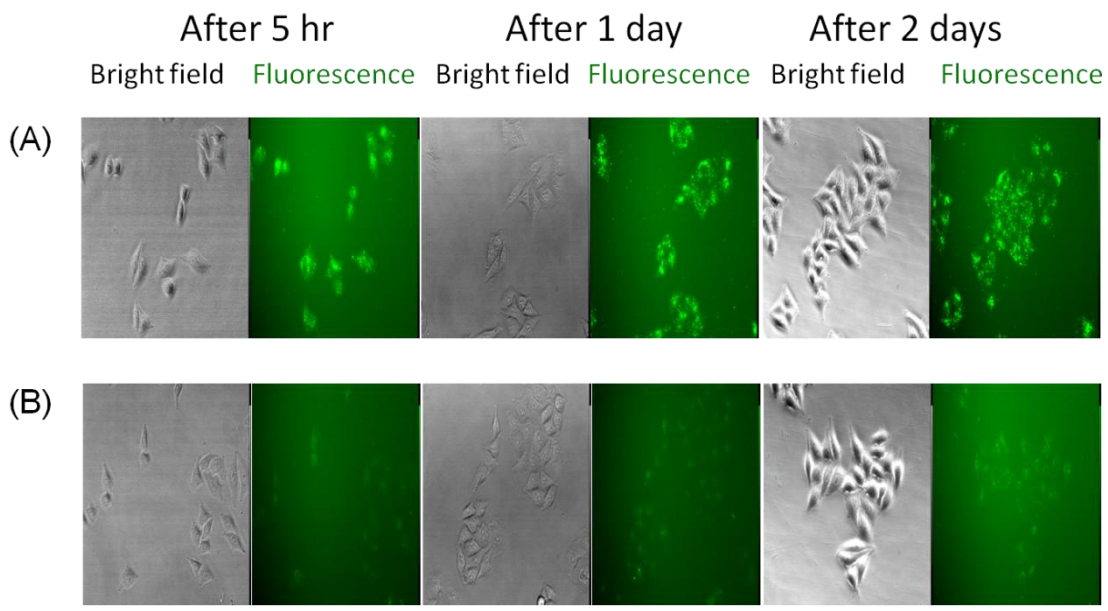

Figure 4-6. Fluorescence microscope images of transfected Hela cells with (A) ssTO-05 or (B) TO-MR05. Each image was acquired at 5h, 24 h and 48h after transfection.

4-4 Conclusions

(1) We found that siRNA probe, TO-MR05, showed sufficient RNAi activity and strand selectivity and efficient quenching effect against Thiazole orange.

(2) From the result of fluorescence monitoring in living cells by using siRNA probe, we found that RISC would be formed immediately after siRNA transfection and only a few of transfected siRNA were involved in RISC formation.

4-5 Experimental Section

Synthetic siRNAs and preparation

All RNA strands were synthesized in the same manner as described in Chapter 3. For transfection, RNA duplexes were prepared by mixing 20 μM each sense and antisense strand in annealing buffer (10 mM TAE, 0.25 mM EDTA, pH 8.3), and incubated for 5 min at 95°C, followed by cooling to room temperature for 0.5- 1h.

Cell culture

Both Hela cells (for living cells imaging) and 293FT cells (for luciferase assay) were cultured in Dulbecco's modified Eagle's medium (DMEM) supplemented with 10% fetal bovine serum, 80 μg/ml penicillin, 90 μg/ml streptomycin.

Transfection and Dual Luciferase reporter assay

See Chapter 3

Fluorescence measurements in standard buffer

Fluorescent spectra were measured with with a microcell. The excitation wavelength was 510 nm for Thiazole orange. The conditions of the sample solutions were as follows (unless otherwise noted): [NaCl] = 100 mM, pH 7.0 (10 mM phosphate buffer). The concentration of RNA tethered with was 0.2 μM or 0.4 μM, respectively. All samples were heated at 80 °C for 5 min in the dark before the measurement.

Fluorescence measurement in Hela cell lysate

siRNA was prepared by mixing 2.0 μM and 3.0 μM of siRNA strand tethering a fluorophore or quencher, respectively in 100 μl of Hela cell lysate. Samples were incubated at 37^{o}C in a JASCO model FP-6500, and fluorescence intensity was measured at each time points.

Microscopic analysis

Hela cells were cultured in 24-well plate and reached to 30% confluent at the time of transfection. Cells were transfected with 66 nM of siRNA and incubated at 37^{o}C. For the imaging of transfected cells, media were replaced with PBS and cells were excited between 450-490 nm to acquire the images by using a fluorescence microscope, ECLIPSE (Nicon).

4-6 Notes and References

[1] J. Cheng, S. M. Sagan, Z. J. Jakubek, J. P. Pezacki, *Biochemistry* **2008**, *47*, 8130-8138.

[2] Z. Medarova, W. Pham, C. Farrar, V. Petkova, A. Moore, *Nat. Med.* **2007**, *13*,

372-377.

[3] M. Helm *et al*., *Nucleic Acids Res.***2007**, *35*, e124.

[4] H. Asanuma, X. G. Liang, H. Nishioka, D. Matsunaga, M. Liu, M. Komiyama, *Nat.Protocols* **2007**, *2*, 203-212.

[5] H. Kashida, T. Fujii and H. Asanuma, *Org. Biomol. Chem.*, 2008, **6**, 2892

[6] Y. Hara, T. Fujii, H. Kashida, K. Sekiguchi, X. Liang, K. Niwa, T. Takase, Y. Yoshida and H. Asanuma, *Angew. Chem. Int. Ed*, 2010, **49**, 5502.

[7] H. Kashida, K. Sekiguchi, X. Liang and H. Asanuma, *J. Am. Chem. Soc.*, 2010, **132**, 6223.

Chapter 5. Investigation on photoregulatory efficiency of azobenzene modified DNA in gene expression

5-1 Abstract

In order to photoregulate gene expression by using photoresponsive DNA which contains azobenzene moieties at T7 promoter region, first of all, we tried to construct T7 expression system available in human cells. By combining T7 RNA polymerase expression vector with firefly luciferase gene linked to T7 promoter, T7 driven-luciferase expression in human cells was realized. Then, we constructed linear template DNA, not plasmid, tethering azobenzene moieties and investigated its photoregulatory efficiency. As a result, photoregulation of gene expression could not be succeeded. Further study revealed that the linear template DNA might be unavailable for gene expression in human cells, thus circulated template with azobenzene modifications should be needed for photoregulation.

5-2 Introduction

Recently, artificial control of gene expression has gained attention because of its promising applications in cell biology, pharmacology, and bionanotechnology.[1, 2] Especially, photoregulation of biological functions, which can be used as a robust tool

for investigating the mechanism of particular biological phenomena in living cells, aroused much interest [3, 4]. In our previous work, we have developed a photoresponsive DNA by introducing azobenzene moieties that can be reversibly photoisomerized between *trans* and *cis* forms [4]. Furthermore, we also designed a photoswitch of gene expression by attaching azobenzene moieties to T7 promoter and DNA transcription by T7 RNA polymerase were successfully photoregulated *in vitro* (Figure 5-1).[5]

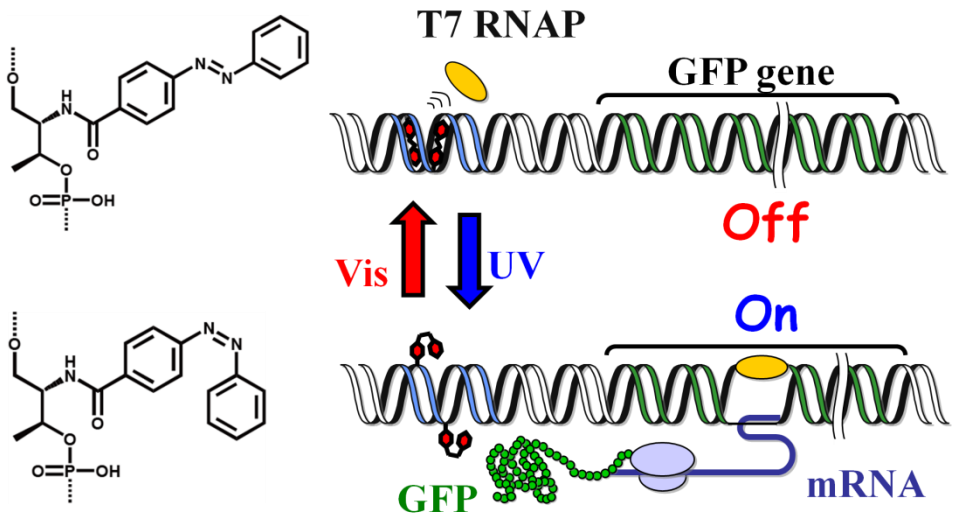

Figure 5-1. Illustration of *in vitro* photoregulation of gene expression with GFP gene linked to azobenzene-modified T7 promoter.

In this Chapter, we tried to apply this photoswitch to photoregulation of gene expression in human cells. However, T7 promoter should not work well in mammalian cells because they don't have T7 RNA polymerase. Therefore, we established an expression system involving T7 promoter and T7 RNA polymerase in human cells

(Figure 5-2). Additionally, we also investigated photoregulation of target gene expression by using photoresponsive DNA.

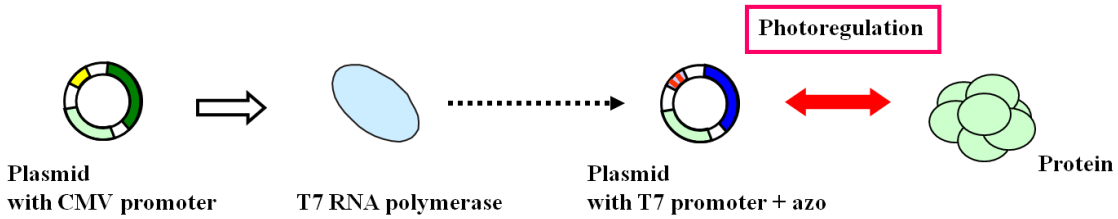

Figure 5-2. Our strategy for photoregulation of gene expression in human cells.

5-3 Results and Discussions

5-3-1 Construction of T7 expression system available in human cells

In order to realize photoregulation of gene expression in human cells, we tried to establish T7 expression system which can be used in human cells. We chose AcGFP, a kind of GFP variant, as a target gene and constructed a template plasmid coding AcGFP gene with internal ribosome entry site (IRES) under T7 promoter, pT7-AcGFP. (see also Experimental section) In the case of transcription by T7 RNA polymerase, transcripts might not have the 5′-cap, therefore, IRES sequence should be needed for ribosome binding.[4, 7] For the expression of T7 RNA polymerase, we used also constructed vectors harboring T7 RNA polymerase with/without nuclear localization signal (NLS) under CMV promoter, pRNP-NLS(+) and pRNP-NLS(-), respectively. (see also

Experimental section) If T7 polymerase contains NLS, it can be transferred to inside the nucleus.[8] Then, both template DNA and T7 expression vector were transfected to 293FT cells and additionally, AcGFP expression vector, pAcGFP, was also transfected as a positive control. After 48 hours incubation, AcGFP expression was confirmed by fluorescence microscope. As shown in Figure 5-3A, cells transfected with pAcGFP efficiently expressed AcGFP. However, the level of expression with combination of T7

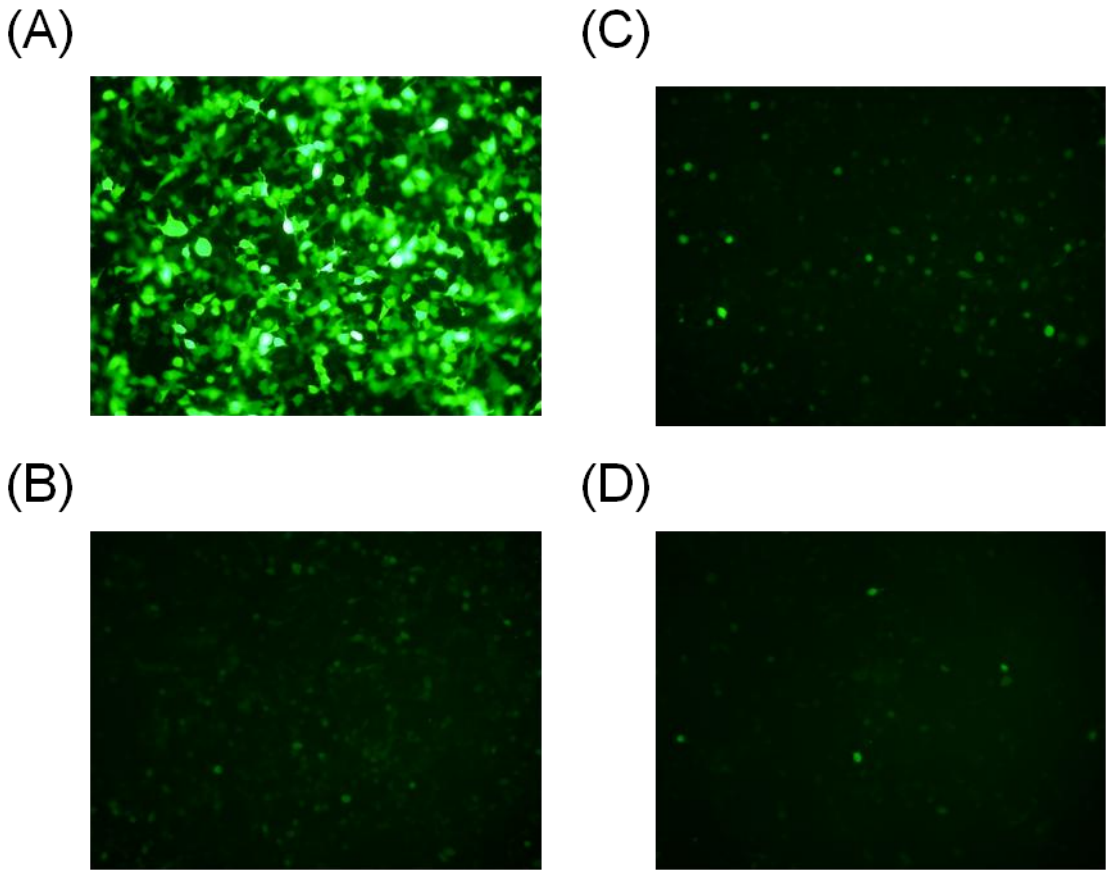

Figure 5-3. Fluorescence microscope images of transfected 293FT cells with (A) pAcGFP (Positive control), (B) pT7-AcGFP only (Negative control), (C) pT7-AcGFP and pRNAP-NLS(-) or (D) pT7-AcGFP and pRNAP-NLS(+). Each image was acquired at 48h after transfection.

promoter and T7 RNA polymerase (Figure 5-3C and D) was almost equal to that of negative control (Figure 5-3B). T7 polymerase expression and localization was also confirmed by immunostaining (Appendix Figure 5-1), namely, both T7 RNA polymerase expression vector properly worked. Therefore, from these facts, we concluded that there were some problems in template DNA.

In the paper published by Deiters et al.[4], they succeeded in photoregulation of firefly luciferase expression by using caged T7 polymerase. Hence, we tried to use this firefly luciferase template plasmid, pT7Luc, and T7 RNA polymerase expression vector, pG31, which were generously provided by Prof. A. Deiters. pT7luc codes firefly luciferase gene with IRES sequence under T7 promoter (see also Experimental section), whereas pG31 is almost same as pRNAP-NLS(-) (the vector map and sequence are not shown). Then, we conducted luciferase reporter assay by transfecting pT7Luc and pG31 to HEK293 cells and analyzed the level of luciferase expression. As shown in Figure 5-4, cotransfection of both pG31 and pT7Luc induced significantly strong luminescence of firefly luciferase, whereas transfection of pG31 alone (Negative control) showed only a background level of luciferase expression. Therefore, we confirmed T7 driven-luciferase expression by combining both template DNA plasmid and T7 RNA polymerase expression vector.

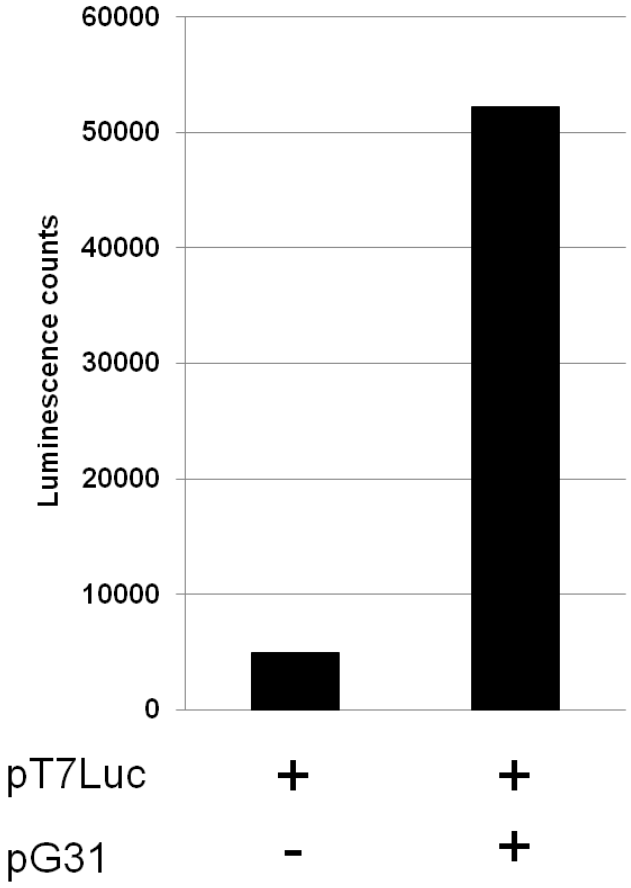

Figure 5-4. Expression of firefly luciferase with T7 promoter. HEK293 cells were cotransfected with pT7Luc (template) and no other plasmid or pG31 (T7 RNA polymerase expression vector). Luciferase activity was measured by luciferase assay system after 48 h.

5-3-2 Usage of linear templates and azobenzene-modified DNA for gene expression

In this section, we tried to construct azobenzene-modified template DNA for photoregulation of gene expression. However, as shown in Figure 5-5, our strategy of modified DNA production is optimized for producing linear template DNA. Thus, we constructed linear template DNA, not plasmid, and introduced azobenzene moieties at the T7 promoter region. We also made unmodified linear template (NL), not containing

azobenzene, for the comparison of azobenzene-modified linear template (AzL).

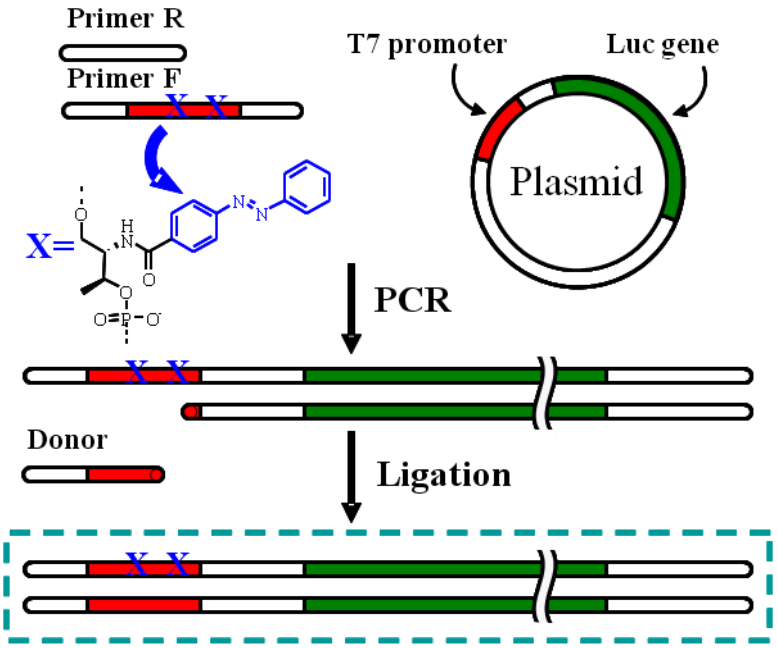

Figure 5-5. Schematic illustration of the approach to construct photoresposive DNA template for luciferase expression by introducing azobenzene moieties into T7 promoter region.

Then, we investigated photoregulatory efficiency of azobenzene-modified linear template DNA as a photoswitch of gene expression in human cells. 150 ng of each template DNA, pT7Luc, NL, AzL was cotransfected with pG31 to HEK293 cells and after transfection, cells were either irradiated with UV light (365 nm, 2 min) or kept in the dark, and the effect of UV light irradiation on their luciferase activity was investigated (Figure 5-6). No negative effect on luciferase expression due to UV light exposure was observed (Control). However, in the case of linear template, intensity of luminescence was quite weak regardless of UV light exposure, even by using

unmodified linear template (NL and AzL in Figure 5-6). These results implied that the our linear template DNA was unsuitable for gene expression in human cells.

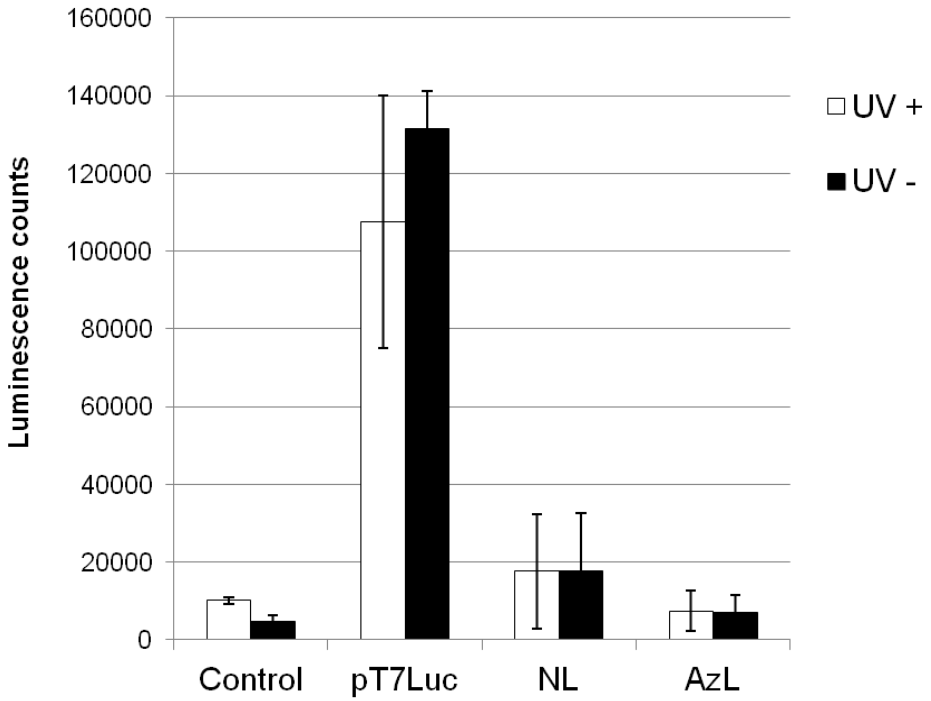

Figure 5-6. Investigation of photoregulatory efficiency of azobenzene-modified template DNA. HEK293 cells were cotransfected with pG31 and pT7luc, unmodified linear template (NL) or azobenzene modified linear template (AzL). Control indicated cells transfected with only pT7Luc. After transfection, cells were either irradiated with UV light (+ UV) or kept in the dark (-UV). Luciferase activity was measured by luciferase assay system after 48 h.

In order to improve expression level, we tested much longer linear template made by one-site digestion of pT7Luc using restriction enzyme, *Aat* II, because the length of linear DNA template might affect transfection efficiency. In addition, we also examined whether the increased amount of NL (300 ng or 450 ng) would be effective for enhancement of expression. As shown in Figure 5-7, the digested pT7Luc which

contained the full-length sequence of pT7Luc showed only a background level of expression almost equal to Control. Similarly, increased amount of NL could not enhance luciferase expression. These results indicated that linear template might be unavailable for T7-driven luciferase expression in human cells. Therefore, we concluded that azobenzene-modified plasmid template should be necessary for photoregulation of gene expression.

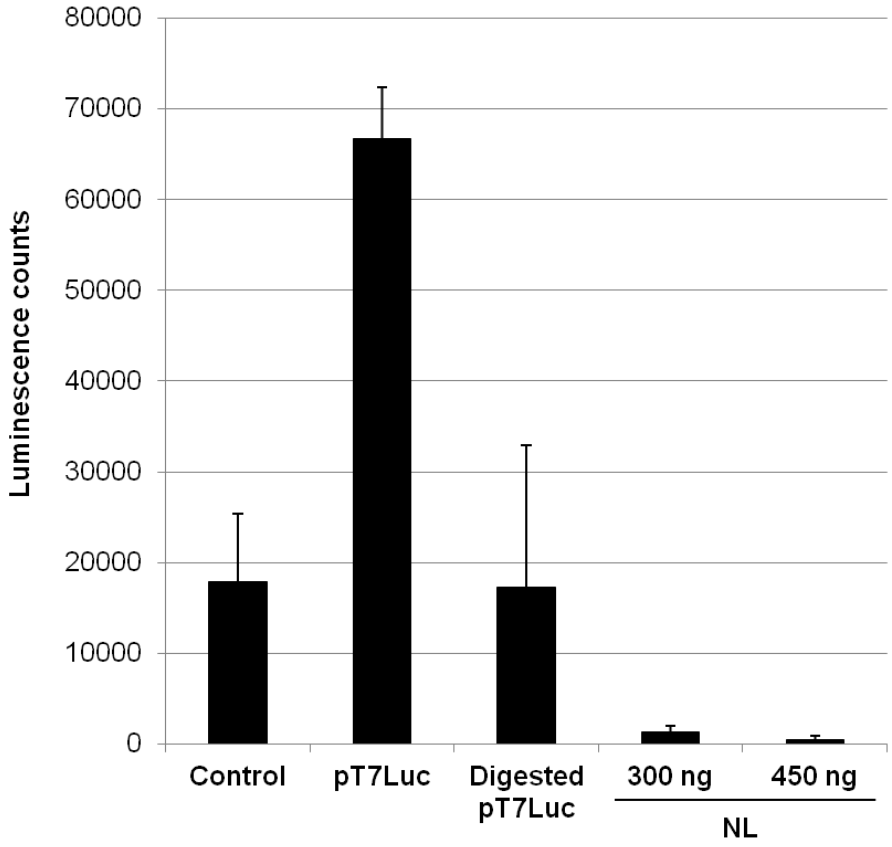

Figure 5-7. Expression of ludiferase using several linear template DNA.

5-4 Summary and prospects

In this study, we succeeded T7-driven expression of firefly luciferase in human

cells by using template plasmid with T7 promoter and T7 RNA polymerase expression vector. Then, we also examined photoregulation of gene expression with azobenzene-modified linear template. However, instead of photoregulation, unmodified linear template could not work in human cells. Further experiments with linear template in different conditions revealed that linear template might be unavailable for T7 expression system in human cells, and we concluded that plasmid template should be necessary. Therefore, we will attempt to construct azobenzene-modified circular template. The linear template with/without azobenzene moieties used in this study has restriction sites of *Pst* I at both ends. Thus, we can circulate the linear template by self-ligation with T4 DNA ligase after digestion by *Pst* I. Then, we will investigate photoregulatory efficiency of the circulated template with azobenzene moieties in human cells.

5-5 Experimental section

Plasmid construction

Plasmids used for AcGFP expression are shown in Figure S5-1. pT7-AcGFP contains AcGFP gene attached with IRES sequence under T7 promoter. In addition, it also contains SV40 polyA site next to terminator region. pACGFP was used as a positive control for AcGFP expression in 293FT cells. pRNAP –NLS(-)/(+) were also used for

T7 RNA polymerase expression.

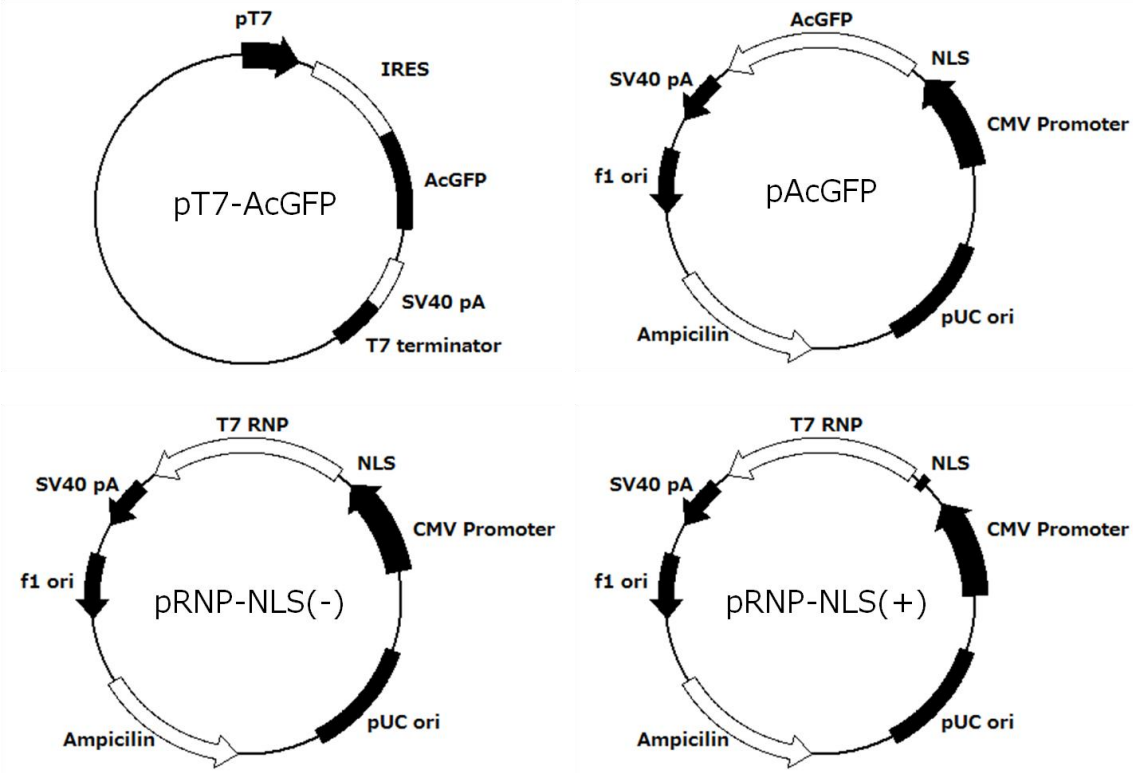

Figure S5-1. Plasmids used for AcGFP expression.

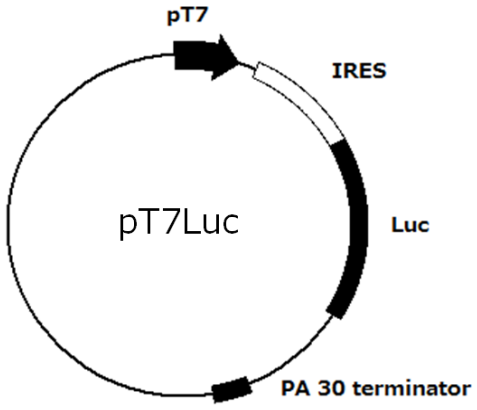

Figure S5-2. Vector map of T7Luc used as a template of firefly luciferase.

Plasmid pT7Luc coding firefly luciferase with IRES sequence under T7 promoter was used as a template DNA for luciferase expression (Figure S5-2). pG31 harboring T7

RNA polymerase under CMV promoter was also used for expressing T7 RNA polymerase in human cells (the vector map and sequence are not shown).

We also constructed linear template with/without azobenzene moieties. The template region from T7 promoter to terminator in pT7Luc was amplified by PCR using primers as follows: Luc-F, a forward primer for native linear template: 5′-CGATCTGCAGTAATACGACTCACTATAG-3′, AzLuc-F, a forward primer containing two azobenzenes: 5′-CGATCTGCAGTAATACGA**X**CTCACT**X**ATA GGATCCGCCCCTCTCC-3′ (**X** represented an azobenzene) and Luc-R, a reverse primer: 5′-CGATCTGCAGCGGTGATGTCGGCGATA-3′. All these primers have *pst* I recognition site (underlined). PCR products amplified with native primer (Luc-F and Luc-R) were used as native linear template after column purification. For completion of azobenzene-modified template construction, lacked portion (Donor) was supplied and ligated with T4-ligase to make a full duplex having azobenzenes.

Cell culture, transfection and Luciferase assay

For AcGFP expression, 293 FT cells were cultured in 24-well plates and reached to 70-90% confluent at the time of transfection. Cells were cotransfected with 100-600 ng of pT7-AcGFP and 50 ng of polymerase expression vector (pRNAP –NLS(-) or pRNAP –NLS(+)) by using Lipofectamine^{TM} 2000 (Invitrogen) according to the manufacturer's

instructions. After incubation at 37°C for 48 h, cells were washed with PBS and observed by fluorescence microscope.

For luciferase assay, HEK293 cells were cultured in 96-well plates and reached to 70-90% confluent at the time of transfection. 150-450 ng of each plasmid of luciferase template and T7 RNA polymerase expression vector was cotransfected by using X-tremeGENE (Roche) according to the manufacturer's instructions.

After incubation at 37°C for 48 h, luciferin substrates were added into the media and luciferase activity was measured with Plate Reader.

5-6 Notes and References

[1] Z. Zhang, J. Gildersleeve, Y. Y. Yang, R. Xu, J. A. Loo, S. Uryu, C. H. Wong, P. G. Schultz, *Science* **2004**, *303* 371-373.

[2] Y. Benenson, B. Gil, U. Ben-Dor, R. Adar, E. Shapiro, *Nature*. **2004**, *429*, 423-429.

[3] V. Mikat, A. Heckel, *RNA*, **2007**, *13*, 2341-2347.

[4] C. Chou, D. D. Young, A. Deiters, *ChemBioChem*, **2010**, 11, 972-977.

[5] H. Asanuma, T. Ito, T. Yoshida, X. G. Liang, M. Komiyama, *Angew Chem Int Ed*, **1999**, *38*, 2393–2395.

[6] X.G. Liang, R. Wakuda, K. Fujioka, H. Asanuma, *FEBS J*., **2010**, *277*, 1551-1561.

[7] M. L. Meyer-Ficca, R. G. Meyer, H. Kaiser, A. R. Brack, R. Kandolf, J. H. Kupper, Anal. Biochem., **2004**, *334*, 9-19.

[8] A. Lieber, U. Kiessling, M. Strauss, *Nucleic Acids Res.* **1989**, ***17***, 5887–5895.

5-6 Appendix

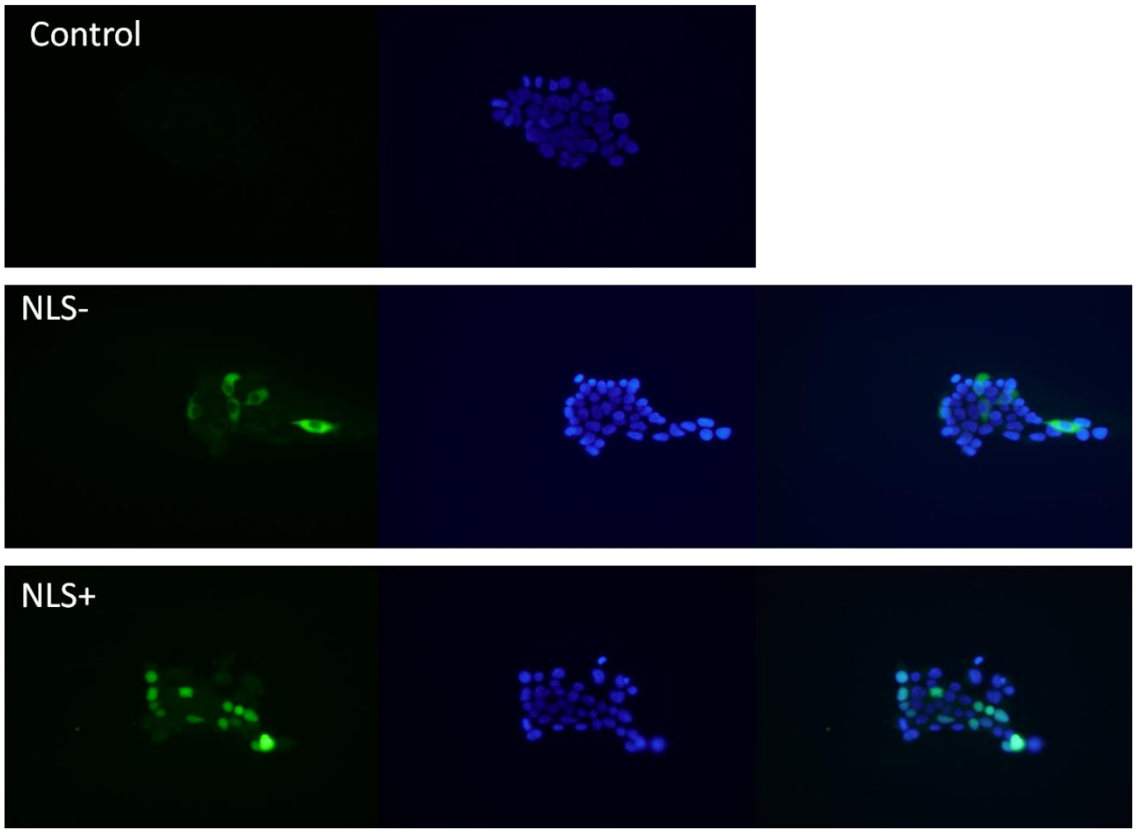

Appendix Figure 5-1. Confirmation of T7 RNA polymerase expression and localization. Cells were treated with fluorophore-labeled antibody to detect T7 RNA polymerase. Nucleus was alos stained by DAPI.

Publication List

1. "Improvement of RNAi activity and strand-selectivity of RISC formation by modified siRNA involving intercalators near 5'-termini"
   Ito, H.; Urushihara, M.; Liang, X. G.; Asanuma, H.
   ChemBioChem, *accepted*.

2. "Construction of photoresponsive RNA for photoswitching RNA hybridization."
   Ito, H.; Liang, X.G.; Nishioka, H.; Asanuma, H.
   Org. Biomol. Chem.,**2010**, *8*, 5519-5524.

3. "Development of photoresponsive RNA towards photoswitching of RNA functions."
   Ito, H.; Nishioka, H.; Liang, X. G.; Asanuma, H.
   Nucleic Acids Symp. Ser., **2007**, *51*, 171-172.

List of Oral Presentations

1. "The construction of azobenzene-modified siRNA for high silencing activity in RNA interference"
   Hiroshi Ito, Hidenori Nishioka, Xingguo Liang, Hiroyuki Asanuma
   2010 International Chemical Congress of Pacific Basin Societies, Hawaii, USA, 2010.

2. "Construction of azobenzene-modified siRNA for more effective and selective induction of RNA interference"
   Hiroshi Ito, Xingguo Liang, Hiroyuki Asanuma
   Nagoya University Global COE in Chemistry 4th Annual Symposium, Nagoya, Japan, 2011

3. "Selective RISC formation and the enhancement of RNAi activity by modified dsRNA"
   Hiroshi Ito, Xingguo Liang, Hiroyuki Asanuma
   5th Joint Symposium on Biorelevant Chemistry, Tsukuba, Japan, 2011

Acknowledgment

The present article is a thesis for application of doctoral degree at the Department of Molecular Design and Engineering, Graduate School of Engineering, Nagoya University. All the study work was carried out under direction of Professor Hiroyuki Asanuma from April 2006 to March 2012.

I would like to express my deepest gratitude to Prof. Hiroyuki Asanuma who provided helpful comments and suggestions. I am also indebt to Associate Professor Hiromu Kashida for his advice and valuable discussions. I would also like to thank Prof. Shinji Iijma and Prof. Toshiya Endo whose comments made enormous contribution to my work. I would also especially thank Prof. Xingguo Liang who provided carefully considered feedback and valuable comments.

I would also like to say thanks for co-worker Dr. Hidenori Nishioka, Mr. Kenta Fujioka, Mr. Masaaki Urushihara, Mr. Toshiki Takagi, Mr. Junya Takai and other members of Asanuma Laboratory for their contribution and advice for this study. I would also like to express my gratitude to members of Iijima Laboratory for their contribution and advice for this study.

I am also greatly indebted to “Nagoya University Global COE Program” for their financial support to me.

Finally, I would like to express my gratitude my family for their moral support and warm encouragements.